A MORPHOLOGICAL STUDY OF THE INITIAL COLD DRAWING DEFORMATION IN THE SUPERSTRUCTURE OF BULK CRYSTALLIZED LINEAR POLYETHYLENE

A THESIS

Presented to

The Faculty of the Division of Graduate

Studies and Research

by

Roger David Hester

In Partial Fulfillment

of the Requirements for the Degree

Doctor of Philosophy

in the School of Chemical Engineering

Georgia Institute of Technology

July, 1974

A MORPHOLOGICAL STUDY OF THE INITIAL COLD DRAWING DEFORMATION IN THE SUPERSTRUCTURE OF BULK CRYSTALLIZED LINEAR POLYETHYLENE

Approved:

J. D. Muzzy, Chairman

E. A. Starke

John L. Lundberg

Date approved by Chairman: Aug. 9, 1974

DEDICATION

To all those young Atlanta ladies

whom this bachelor has known,

especially Sandra, Kris, Ellie,

Barbara, Carol, Cheryl, Kathy, and Rita.

ACKNOWLEDGMENTS

I am grateful to the National Science Foundation (NSF Grant GK-27851) and the Union Camp Corporation for their financial sponsorship of this work.

I am deeply indebted for the efficient assistance of the Chemical Engineering staff during the course of my research, especially Messrs. H. Conners, S. A. Bloom, C. R. Blackwood, and J. A. Nabors.

Also I would like to acknowledge all those past instructors who have patiently guided my formal education, one of whom, last but not least, has been my thesis advisor, Dr. John D. Muzzy.

TABLE OF CONTENTS

TABLE OF CONTENTS (Concluded)

LIST OF TABLES

LIST OF FIGURES

LIST OF FIGURES (Concluded)

NOMENCLATURE

A	area, rate constant
Å	Angstrom
BDR	bulk draw ratio
b_o	molecular thickness on a crystal face
C	molecular flexibility factor
^oC	degrees Centigrade
CR	compression ratio
cm	centimeters
D	self diffusivity
DD	draw direction
DSC	differential scanning calorimeter
d	diameter, distance
E	nucleation activation constant
e	2.717 ...
F	function of
f	microtoming distortion factor
G	growth rate
G_o	growth rate constant
g	grams
H	enthalph
HDPE	high density polyethylene
h	Planck constant
^oK	degrees Kelvin

k	Boltzmann constant
L	intercept length
LD	normal to draw direction
LDPE	low density polyethylene
Ln	natural logarithm
l	lamellar thickness
M	molar
MN	molecular weight (number average)
MW	molecular weight (weight average)
mc	millicalories
mg	milligrams
No	Avogadro number
n	number of molecular chain segments
PP	polypropylene
R	gas constant
RT	room temperature
SEM	scanning electron micrograph (microscope)
T	temperature
TGC	thermal gradient crystallizer
TLM	transmissions light micrograph (microscope)
V	volume
W	sample weight

Subscripts:

a	amorphous
b	bulk
c	crystallization, crystal

e	fold surface
f	fusion
i	impingement
m	melting
s	lateral surface

Greek Letters

β	spherulite growth structural factor
γ	shear rate
Δ	incremental quantity
δ	lamellar width
ϵ	Eyring activation energy for viscous flow
η	viscosity
θ	time
μ	micron unit
ν	number of primary nuclei
π	3.1416 ...
ρ	density
σ	surface energy
χ	degree of crystallinity

Other Indices:

*,**, †,‡,	footnotes
$\bar{}$	average
$\perp$	perpendicular
//	parallel
$^{o}_{or}{}^{\circ}$	perfect, ideal, degrees
~	approximately

SUMMARY

The usefulness of a polymer material usually depends upon its response to stress. Depending upon fabrication and deformation conditions, a polymeric solid may be brittle or ductile. Ductile rather than brittle deformation is usually desired. The semicrystalline polymers can exhibit both types of deformation response. In ductile deformation, some semicrystalline polymers undergo a morphological transition to a fibrous structure. An understanding of the influence of initial morphology on a polymer's response to stress and the structural changes occurring with strain is needed to establish crystallization conditions which will improve the mechanical properties of polymer solids.

High density polyethylene, MARLEX 6050, served as a model for study on the initial morphological changes occurring in a semicrystalline polymer under stress. Large tensile samples of this material were crystallized from the melt by using isothermal or air quench cooling conditions. These samples, when deformed by uniaxial extension at 60^{o}C, were ductile or brittle depending upon crystallization conditions. The isothermally crystallized tensile samples were brittle. However, the quenched cooled samples were sufficiently ductile to be transformed into a fibrous structure.

The polymer properties and structural changes occurring with deformation of the tensile samples were measured or observed by using phase contrast light microscopy, scanning electron microscopy, differential scanning calorimetry and densitometry.

A chromic acid surface etching technique was developed and used to reveal the morphological features of the polyethylene surfaces formed from cryogenic sectioning of the bulk samples. After etching, the polymer structures were observed by using a scanning electron microscope. Etching was found to enhance surface structural features by more rapidly oxidizing areas of less crystallinity and regions containing structural discontinuities such as cracks.

Morphological examination of the predrawn bulk samples showed that the isothermally crystallized samples had a uniform splayed spherulitic superstructure. Quenched samples had ringed spherulites at or near their surfaces and splayed spherulites in their interiors. This superstructure gradient with sample thickness formed during crystallization and was caused by an increase in thermal insulation with sample depth. Because of this effect, ringed spherulites, formed at the quenched sample surfaces, were crystallized at lower melt temperatures than the splayed spherulites found within the sample.

As shown by heats of melting and density measurements, the splayed spherulite superstructures were more crystalline than the ringed spherulites. Also large cracks were observed between and through the predrawn, splayed spherulites of the isothermally crystallized samples. These cracks were due to a volume reduction accompanying high structural crystallinity.

No cracks were observed before or after initial deformation of the ringed spherulites. However, density measurements showed that sample density decreased slightly after limited drawing. This volume increase may be caused by the formation of unobserved submicroscopic voids in or between the ringed spherulites. Initial deformation within individual

ringed spherulites was homogeneous, but deformation was not uniform among neighboring ringed spherulites. This implies that some slip in shear was occurring between spherulites.

All spherulites formed during quenched crystallization had nearly equal diameters of about 60 microns. Thus as an approximation, melt crystallized polyethylene is constructed of many small perfectly packed spherical superstructures. Using this structure model, spherulitic growth rates during primary crystallization were calculated from differential scanning calorimeter thermograms. These growth rate data and estimates of molecular mobility in the melt were used to estimate the number of molecular tie links providing strength to the solid superstructures. Polyethylene melt, crystallized at lower temperatures, contained many more tie links within a ringed spherulite superstructure than splayed spherulite superstructure crystallized at higher temperatures.

In summary, the ductile draw behavior of high density polyethylene depends strongly upon the melt crystallization conditions. Slow cooling or use of high isothermal temperature conditions produce highly crystalline solids. These solids contained large cracks caused by unrelieved volume contractions. These crystallization conditions produced superstructures which contained few molecular tie links to blunt the growth of these cracks when these samples were extended. Therefore sample fracture occurred. In contrast, rapid cooling of polyethylene melts forms solids with spherulite superstructures composed of closely packed lamellar bundles which are connected by many molecular tie links. These tie links redistribute stress concentrations imposed in the initial stages of drawing and thereby blunt

any crack propagation. This allows these superstructures to rearrange themselves without brittle fracture and begin a ductile draw transformation into a fibrous material.

CHAPTER I

INTRODUCTION

Polymeric materials are important because of their low manufacturing cost, ease of fabrication, strength, and toughness. Films, adhesives, elastomers, and fibers are produced from synthetic polymers. For almost every plastic product, man has engineered a polymer system to respond in a specific environment to physical and chemical forces in a manner suitable to meet his needs. The environment can be as simple as standard room conditions or as exotic as conditions in outer space or the interspace of our own bodies.

Although man uses polymer materials, his ability to engineer their properties is usually crude and empirical. Fundamental knowledge of even simple polymer systems is inadequate. Much work must be done before man can understand the true nature of long chain molecules and more adequately engineer polymer materials.

A linear polymer molecule's dimension in length is usually very much greater than its diameter. For polyethylene, the diameter is only a few angstroms, whereas the molecular length may be thousands to millions of angstroms.

Most plastics are composed of polymer molecules of the same type which have a large distribution of lengths. Each molecule, because of its length, interacts with itself and many of its neighboring molecules. The attractive forces of molecular interaction and the freedom of

molecular movement in these force fields determine the response characteristics of a plastic to stress. These response characteristics, e.g. impact resistance, stiffness, and hardness, are measured by various standard mechanical tests. Molecular mobility and intermolecular forces and therefore plastic properties are critically dependent upon the temperature and the ability of the polymer molecules to pack together.

In the melt state, van der Waals and polar attractive forces between atoms of polymer molecules are great, but less than in crystalline solids. Molecular volume and mobility are greater than the crystalline solid and the plastic's response to stress is that of a viscoelastic fluid. Molecules are arranged with much less order than in a crystal.

As the temperature of a polymer system is reduced, molecular mobility decreases and the molecules may rearrange themselves to decrease their free energy. Molecules in arranging themselves develop a greater degree of order. If after this process of ordering an imperfect crystal state exists, then the polymer has crystallized. Other polymers solidify without sufficient order to be crystalline. The amount of molecular ordering after a crystallization process is dependent ultimately upon the atomic composition of the polymer, but more directly upon its molecular length distribution, and the rate at which the system temperature is reduced. The polymer systems with limited or no molecular ordering after solidification are supercooled viscoelastic fluids which may become glassy at lower temperatures. Usually perfect molecular ordering with a complete thermodynamic decrease in the system's free energy is not possible due to kinetic restrictions, i.e., viscous retardation. These are the semicrystalline or partially crystalline polymers.

In research on semicrystalline polymer systems, high density polyethylene frequently is selected for study because it is a commercially important and relatively simple, linear polymer. This polymer has served as a model of study by many investigators. Most investigators have used solution or melt cast thin films or single crystals because of the difficulty of analyzing bulk crystallized samples. These past studies are indicative of what is present in bulk polyethylene; never-the-less, confirmation by duplicating and studying the true commercial bulk crystallization and deformation situations is required.

In this work, large high-density polyethylene samples were crystallized from the melt at rates approximating commercial practice and deformed by uniaxial extension at a relatively low temperature, viz., cold drawn. The morphology and the initial structural changes that occurred in the solid polymers were analyzed using light microscopy, scanning electron microscopy, differential scanning calorimetry, and densitometry. The results obtained from the bulk samples were compared and found compatible with the interconnected multi-phase semi-crystalline theories of morphology, crystallization mechanism, and deformation response which have been formulated from results of studies by previous investigators on thin films and single crystals.

CHAPTER II

REVIEW OF THE LITERATURE

Polyethylene often has been selected for polymer science studies because of its relatively simple molecular structure. The properties of polyethylene molecules have been studied in dilute solvent solutions, in the melt phase,[29] and in the solid phase as single crystals or thin films crystallized from solutions or melts.[58] From this work it has been established that polyethylene crystallizes from dilute solutions and melts in the form of crystallites of approximately 100 Å in thickness and several microns in width and length. The polymer molecules are folded at the surfaces of the crystallites and lie parallel to one another in the plane normal to these surfaces. The crystal unit cell is orthorhombic with the molecules in a planar zig-zag conformation. Each molecular fold can be formed with four or five gauche carbon to carbon bonds.

Crystallization of polyethylene from melts or concentrated solutions is never complete due to the collection of molecules in a partially oriented and constrained amorphous phase between lamellar crystallites. An interconnected multi-phase polymer system is formed which has a continuously alternating imperfect crystal phase--constrained amorphous phase construction.[45,80,82] When this system is stressed, the strain that results is from the interaction of the phases to the applied stress. The amount of order in the phases and the connectedness[54,55] between phase units greatly affect the mechanical properties of semicrystalline polymer

systems.

Obviously, control over the solid structure would enable better engineering design of the polymer systems to meet specific mechanical needs. Some of the techniques used for structure control include: 1) introduction of fillers or plasticizers, 2) blending in different types of polymer into the structure, 3) increasing molecular branching, 4) changing the average molecular length and/or the molecular length distribution, 5) regulation of the process of molecular crystallization, and 6) orientation of the molecular structure during or after crystallization. Two methods of control, 1) regulation of the process of bulk crystallization from the melt state, and 2) orientation by cold drawing, will be reviewed with emphasis on application to the high density polyethylene system studied in this work, MARLEX* 6050.

MARLEX 6050 is a typical unfilled commercial plastic made of medium molecular weight, highly linear polyethylene molecules having a broad molecular weight distribution. Because of chain regularity, i.e., a small degree of branching and suitable atomic profile, molecular folding is easily accomplished; consequently, the degree of crystallinity and bulk density are high. Therefore the name, high density polyethylene (HDPE). Medium density and low density polyethylenes (MDPE, LDPE) contain molecules that are branched which limits the degree of crystallinity, and hence the maximum density they can develop.

---

*Trademark, Phillips Petroleum Company, Bartlesville, Oklahoma.

Bulk Crystallization of High Density Polyethylene

HDPE bulk crystallization is usually accomplished at low pressures by lowering the melt temperature below the polyethylene crystallization temperature. In the less common pressure crystallization process, solidification is obtained by the sudden release of a large compression force on the melt. This lowers the crystallization temperature below the melt temperature.

Most commercial crystallization processes are of the low pressure type. The melt temperature is either lowered to a constant value below the crystallization temperature, isothermal crystallization, or is continuously decreased, dynamic crystallization. The dynamic crystallization process is the more common industrial practice, while the isothermal crystallization process mainly is used for laboratory studies on crystallization kinetics.

In all thermal crystallization processes, the phase change from the viscous melt to the solid state does not occur instantaneously, but is controlled by the kinetics of primary and secondary nucleation, i.e., the mechanism of attaining the first molecular fold onto a "seed" structure and the subsequent continuation of molecular folding on the then existing polymer crystal surface.

Primary Nucleation

Provided the melt temperature is sufficiently low, either heterogeneous and/or homogeneous primary nucleation occurs to initiate molecular crystallization. In both nucleation types, crystallization is initiated by "seed" structures which may be foreign objects, e.g., dirt or catalyst

particles; or organic agents, e.g., remains of previous crystal structures or gel particles. The "seed" structures must contain regions of chemical affinity and geometrical shape which are of appropriate size and length to accommodate and hold a polymer molecular segment. This action probably provides the polymer anchor needed to establish the first molecular fold.[11] If the number of active "seeds" varies both with time and melt temperature, homogeneous primary nucleation is occurring. If the number of active "seeds" varies only with temperature, heterogeneous primary nucleation is occurring. Combinations of homogeneous and heterogeneous nucleation can also occur.

Cormia, Price, and Turnbull[19] have shown that when bulk samples of MARLEX 6050 HDPE are melt crystallized, primary nucleation is always heterogeneous. They suggested that the "seeds" of nucleation are heterogeneities because freezing sites were always initiated at the same points in the melt after repeated sample freezing and melting.

Pennings, Van der Mark, and Kiel[81] have shown that primary heterogeneous nucleation of MARLEX 6050 HDPE in solvent solutions can be induced by hydrodynamic shear. During crystallization of these solutions, shish-kebab crystal structures form around nuclei of elongated polymer molecules. These primary nucleation "seeds" probably are generated by unidirectional stretching and alignment of entangled molecules, i.e., an unraveling of the molecular coils in the laminar flow regions of the stirred solution. For polypropylene samples crystallized immediately after injection molding, Fitchman and Mencik[26] have observed morphological features which are due to the hydrodynamically induced primary nucleation caused by the melt

flow occurring during the injection molding operation. Thus hydrodynamically induced heterogeneous nucleation is common to both solution and melt crystallization processes.

Secondary Nucleation

In the secondary nucleation stage of bulk crystallization, polymer molecules continuously fold onto the growth surface established during primary nucleation. Although each molecular fold increases the molecule's free energy, the act of folding increases the cohesive interaction between molecules to provide the thermodynamically required total decrease in the polymer system's free energy.

If the polymer system is slowly crystallized in a manner which allows an approach to thermodynamic equilibrium, the molecular chains will become extended.[1,2] For the more common rapid crystallization processes, equilibrium is not closely attained because of rate and viscous effects. Rapid crystallization conditions require the system to select the solidification path that will most rapidly decrease its free energy. This effect dictates that a definite average molecular length between folds be established for each crystallization condition. This maximizes the rate of molecular addition to the crystal surface.

Hoffman and co-workers[38-40] have shown that this kinetic effect is one of growth by coherent secondary nucleation. The correct temperature dependence of crystal thickness and growth rates normal to the folded molecular chains is predicted by this model. In this model, crystal growth is the result of the probability that a certain number of thermally induced, segmental, molecular jumps toward the crystal growth surface will have the energy necessary to overcome both a viscous energy barrier of

motion and also have the energy needed for aligning and folding onto the crystal surface. The energy of the viscous barrier is a function of the polymer's chemical structure and the system temperature. The energy needed for molecular attachment to the crystal surface is a function of melt temperature and its supercooling. For both HDPE and LDPE, the kinetics of crystal growth is similar at the same relative melt supercooling.[14]

The viscous energy barrier varies with the amount and degree of molecular entanglements in the melt or solution phase, i.e., the molecular lengths and distribution, solvent concentration, and temperature.[105] The nucleation barrier is a strong function of the polymer molecule's stereoregularity.

Because of length differences, each molecule has its own particular susceptibility for solidification from the melt or solution, and therefore some molecular segregation must occur during crystallization.[50,94] The extent of this segregation probably depends upon the amount and rate of melt supercooling.

Secondary Crystallization

During the secondary nucleation process, the polymer molecules that are fully or partially rejected from the growth surfaces collect between the lamellar crystallites. These molecules, which account for approximately half of the polymer material[38] may later crystallize at a slower rate or when temperature conditions are more agreeable for crystallization.[47] This post or secondary crystallization continues for a long period of time after primary crystallization is completed,[66] and is probably controlled by molecular diffusion.[40] The exact mechanism of secondary crystallization is

obscure, but it is probably from the actual formation of additional crystallites rather than an increase in perfection of existing crystallites.[93]

Matsuoka[69] suggested that secondary crystallization could produce voids between the crystallites formed by primary crystallization. This effect probably was observed from sample fracture surfaces of annealed MARLEX HDPE.[72]

Morphology of Bulk Crystallized Polyethylene

In bulk crystallization of polyethylene from the melt, primary nucleation occurs at many sites. From each site, lamellar crystallites expand to fill space by the process of secondary nucleation and branching. The structures formed are called spherulites. Each spherulite expands by radial growth of the lamellar crystallites acting in concert until it impinges with other spherulites. After impingement, rapid primary crystallization is completed. Before and after impingement, slower secondary crystallization is occurring.[53] The steps of primary nucleation, lamellar growth and branching by secondary nucleation and the spherulite structure after impingement, are schematically depicted in Figures 1, 2, and 3, respectively.

Lamellar Structure

After primary nucleation and during secondary nucleation the lamellar crystallites grow outward as molecules are "reeled in" from the melt to the growth fronts.[51] Neighboring melt molecules become aligned normal to the growth fronts. In primary crystallization of melts, the lamellar crystallites are discrete units but in densely packed arrays. Because of the

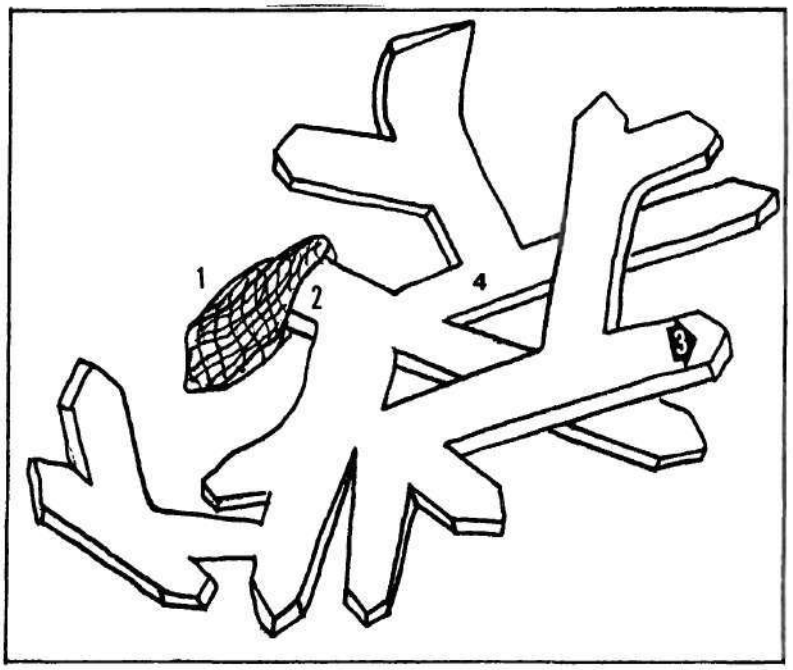

Figure 1. Schematic of Heterogeneous Nucleus and Lamellar Branching [1) Heterogeneity, 2) Surface of a Primary Lamalla, 3) Lamellar Growth Direction, 4) Surface of a Branched Lamella]

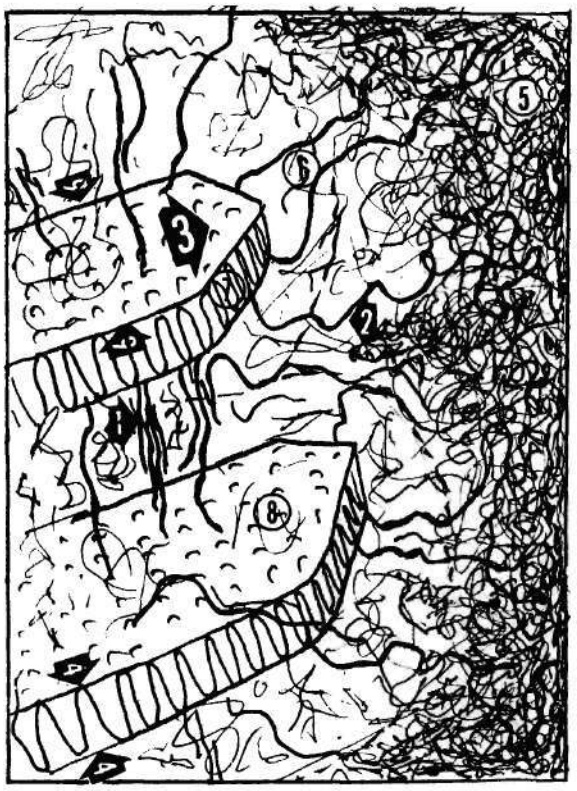

Figure 2. Schematic of Lamellae During Primary Growth [1) Interlamella tie links, 2) Direction of Molecular Movement, 3) Lamallar Growth Direction, 4) Lamellar Thickness, 5) Unperturbed Melt, 6) Perturbed Melt, 7) Secondary Nucleii Growth Surface, 8) Molecular Fold Surface, 9) Lamellar Width]

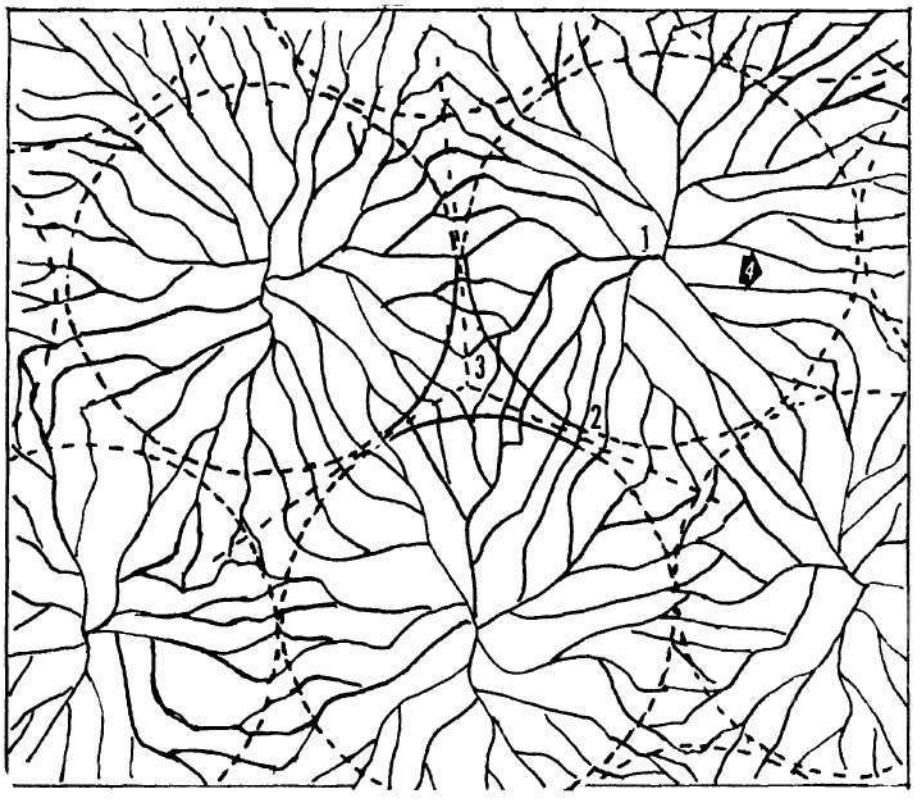

Figure 3. Schematic of Melt Crystallized Polyethylene Spherulites Showing Lamellar Branching [1) Nucleus, 2) Impingment Boundary, 3) Constrained Growth Volume, 4) Primary Growth Direction]

closeness of growth fronts and molecular alignment in the melt, some of the intervening molecules in the melt phase between crystallites may be partially crystallized within two adjacent lamellae. This action constrains the melt phase between crystallites and links lamellae together. Keith and Padden[47] and others[8,102] believe this forces a coordination of lamellar orientation during crystallization. This phenomena could explain the co-operative radial twist[30] among lamellae during growth. This can be observed from polarized light microscopic views of spherulites in thin polymer films.

Schultz and Kinloch[101] proposed that the direction of lamella twisting is due to transverse screw dislocations of the same sign which are spaced along the lamellar radial axis. This model predicts the correct temperature dependence of the degree of twist, viz., larger supercooling produces greater lamellae twist.[56] However, Keller and Sawada[57] have questioned the ability of completely twisted lamellae to pack and efficiently fill space. This objection has been eliminated by the recent observations of Breedon, et al.[12,13] Their electron micrographs of melt crystallized MARLEX 6050 showed that lamellar rotation is probably due to alternating right and left-handed partial twist. This geometry would enable closer lamella packing and provide the efficient space filling requirements needed.

To fill space, the twisting lamellae must also branch during growth. Keith and Padden[48] have theorized that the frequency of noncrystallographic branching during melt crystallization is inversely proportional to the width of the growing lamellae, i.e., a larger lamellar width decreases branching. They proposed that the lamellar width is proportional to the

ratio of molecular self-diffusivity in the melt to the crystallite growth rate. In their analysis any singularity in the form of a misoriented region on the lamellar surface, e.g., a screw dislocation, is a potential source of noncrystallographic branching. Branching will occur if the misorientation is approximately equal to the size of the lamellar width forming in the system crystallizing. Generally, in bulk crystallization, lamellar width and separation, i.e., coarseness, increases with decreasing melt viscosity and decreasing supercooling. This effect appears to be confirmed by Krueger and Yeh[62] in their work on crystallization of polyethylene films under high shear flow and rapid cooling conditions, i.e., large supercooling. They have produced samples with lamellae having width and length dimensions much less than the wave length of visible light, i.e., transparent crystallized polyethylene. Normal crystallization conditions produce larger anisotropic lamellae which scatter light.

Keith and Padden's analysis also suggests that the distance maintained between lamellar crystallites during primary crystallization is approximately equal to the thickness dimension of the forming lamellae. The material collected between the lamellae is a constrained, amorphous phase of shorter molecules which contains the longer tie molecules connecting lamellae. Of course, some of the amorphous phase molecules will solidify during secondary crystallization. The small angle x-ray studies of Kavesh and Schultz[44] on melt crystallized MARLEX HDPE appear to confirm the existence of this multi-phase structure. In their work, lamellar thickness and constrained, amorphous interlamellar thickness varied with crystallization conditions, but maintained a thickness ratio of approximately one to one.

Spherulite Structure

From the above discussion it was shown that spherulite structure is the result of coordinated lamellar twisting, branching, and growth in a radial direction from a primary nucleus into a polymer melt. This system of spherulites defines the bulk structure of many semicrystalline polymers including HDPE.

As spherulites grow, very low molecular weight impurities, because of their high mobility, tend to diffuse radially away from each of the advancing lamellar growth fronts. Higher molecular weight impurities with less mobility together with interlamellar molecular tie links collect between the radiating, lamellar branches.[49] It is believed that the low molecular weight impurities which collect between spherulite boundaries reduces interspherulitic cohesion.[18,46,86,91] These impurities probably decrease the number of tie links formed between impinging spherulites, the interspherulitic tie links, and therefore weaken the bulk superstructure.

Kasatkin, et al.,[42] in their work with thin solution cast films of polyethylene, showed that increased end contact between the growing lamellar ribbons of impinging spherulites would improve the strength of the spherulite superstructure. End contact provides the geometry which enables more molecules to tie together growing lamellar ribbons of different spherulites in the borders between spherulites.

In summary, polyethylene bulk macrostructure is formed from the union of many spherulitic superstructures each of which is in turn formed from many lamellar substructures made from the molecular crystalline

microstructure. Apparently each structural unit is connected to other units by some form of molecular tie link.

Deformation of Polyethylene

With regard to the multi-phase theory of semicrystalline polymer structure, polyethylene bulk deformation can be considered as the direct and combined interactive response of each structural unit within the polymer system to an applied stress. Each structural unit ranging from the largest level of spherulite superstructure to the smallest crystalline microstructure is connected by molecular bonds in the form of tie groups.[52,54] Therefore any semicrystalline polymer, including polyethylene, is structurally inhomogeneous and contains mechanical defects, voids,[69] and crystalline dislocations,[17,90] which are introduced into and between structural units during crystallization. Any large stress acting on a mechanically inhomogeneous structure will have concentrated stresses at its flaws.[31] If the polymer structure is sufficiently mobile at these flaw points, then deformation energy can be dissipated by local inelastic flow in which only a few molecular bonds are broken. If the rate of strain is large at these points and low temperature conditions restrict molecular mobility such that the energy absorbed by flow exceeds the energy needed to create new surfaces, then the largest flaws will propagate preferentially along structural paths of least resistance, i.e., along spherulite boundaries and between lamellae.[24] As these cracks propagate more rapidly, less molecular flow is possible at the crack growth tips because of molecular flow rate limitations. Therefore energy is absorbed more and more by breaking molecular bonds until finally rapid catastrophic bulk fracture occurs at the weakest flaw.

Therefore , bulk ductile deformation occurs only if temperature and strain rate conditions exist that favor the required molecular flow at each level of the polymer's structure. Otherwise brittle fracture will result.

Polymer ductile deformation by uniaxial extension below the polymer's crystallization temperature, the cold draw process, is critically important industrially. This draw process provides the high speed medium needed to transform a relatively unoriented spherulitic polymer structure into the fibrous, high strength oriented structure which produces a synthetic fiber. For this draw process, a pre-drawn polymer structure must be formed in crystallization which insures that ductile transformation occurs over possible brittle fracture.

Polyethylene has been used extensively to study the cold draw process. The results of major studies on the molecular mechanics of bulk polyethylene cold draw deformation are outlined below.

Structural Criterion Necessary for Cold Draw Deformation

Many investigators have detected submicroscopic and microscopic fissures developing during the initial cold draw deformation of polyethylene. Bettelheim and Stein[9] using penetrating and nonpenetrating liquids measured increases in the specific volume of MARLEX 6050 film during stretching, and concluded that submicroscopic holes appear before twenty-five percent elongation. Keith and Padden[46] observed that voids are formed at the center of spherulites and at interspherulite boundaries during initial stretching of thin spherulitic films of linear polyethylene. They suggested that this caused the opalescence and the low densities of drawn polyethylene.

Zhurkov and co-workers,[113,114] using x-ray, EPR, and IR techniques,

found that submicroscopic fissures developed in the amorphous regions of room temperature stressed polyethylene film. These microvoids result from molecular bond rupture and have disk like shape (spanning ~ 150 Å). These disks are oriented normal to the induced stresses. They also found that during ductile deformation the size of these disks remain unchanged, but that their concentration within the sample increases continuously to a limiting value. Peterlin[83] explains that these fissures are the rupture of tie molecules in the polyethylene structure. He concludes that the large number of fissures in drawn HDPE is a consequence of high stress concentrations on the shortest, most unfavorably located tie molecules which are irregularly distributed throughout the sample superstructure.

If a sufficient number of molecular tie links at any microfissure are broken during sample straining and permit the microfissure to reach a critical crack size, then by self-propagation through the crystalline microstructure, a microcrack would appear in the spherulite superstructure. This has been observed in bulk samples by Muzzy.[74,75] Indeed if these microcracks continue to grow and are not blunted or stopped by the molecular tie groups in the superstructure, then catastrophic bulk fracture will occur. Smith[104] also observed these microscale, inhomogeneous deformations in his studies of polyethylene film fracture under multiaxially applied loads.

In summary, when stressing a bulk sample of polyethylene, initial deformation probably occurs in the interlamellar constrained amorphous layer[43] where voids exist due to crystallization and where short tie links are strained and broken. If these microcracks, either existing or formed from the broken tie links, do not propagate through the structure but are

contained and only serve to absorb the severe local stress energy, then spherulitic polymer structure reorganization into a fibrous structure will begin without catastrophic fracture.

Ductile Deformation by Cold Drawing

Peterlin has recently proposed a molecular model which apparently explains the polyethylene drawing process.[84,85,87] A brief description of this model and the major studies which have guided to its formulation are outlined below.

Three stages of deformation exist during cold drawing of semi-crystalline polymers such as HDPE: 1) plastic deformation of the original spherulitic structure in the bulk sample pre-neck region, 2) discontinuous transformation of the spherulitic structure into a fiber structure by micronecking in the bulk sample neck region, and 3) plastic deformation of the fiber structure in the bulk sample post-neck region.

In the first stage, lamellae are initially in parallel stacks within the spherulite superstructure and are interconnected by molecular tie links in the amorphous interlayer between lamellae. The number of these tie links increases with molecular weight and rate of crystallization.[41,52] During the initial strain, because the lamellar crystalline structures are stronger than the tie links connecting them, the lamellae rotate, slip and/or tilt until each lamella reaches an optimum position where it can deform by longitudinal molecular chain slip within its lattice. This optimum position exists when lamellae are tilted approximately 45^{o} to the stress axis. Lamellae are positioned differently within the spherulite superstructure and therefore the amount of lamellar tilt will vary depending upon its position in the spherulite relative to the stress axis.[60]

Therefore, this stage of deformation is not micro or macro uniform. However, the individuality of the spherulites remain preserved and almost all the induced strain is accommodated in the interlamellar, amorphous interlayer. From x-ray studies of HDPE, Kaufman and Schultz[43] indicate that during this stage some molecules are pulled out of the lamellae to destroy some of their crystallinity and some tie molecules in the amorphous interlayers extend. Also from x-ray studies, Keller and Pope[59] indicate that some microvoids are also formed in the amorphous interlayers during this stage.

In the second stage, every lamella transforms into a microfibril by a process of micronecking. In micronecking, blocks of folded molecular chains are pulled off of the lamellar ribbons by shear slip at the weak planes within the lamellar lattice. The folded chain blocks are attached to each other by the previously existing tie molecules and the tie molecules which are formed when the blocks are pulled from the lamellar ribbons. Cracks or microvoids appear during this process. Many tie molecules bridge the cracks formed normal to the stress axis, but very few tie molecules bridge the cracks parallel to the stress axis. Therefore lateral cohesion between blocks is weak and the longitudinal cracks coalesce and elongate during addition straining This is especially noticeable at spherulite boundaries.[98]

The crystalline blocks pulled from the lamellar ribbons are attached to one another by tie molecules and form a "string of pearls" structure that is very thin, a few hundred angstroms, but very long, ten or more microns.[84,89] The thickness of each crystalline block depends upon its draw temperature, i.e., the temperature in the micro lamellar destruction

zone, and not upon the bulk temperature or the original lamellar thickness. The long structural unit which forms is a microfibril and the transformed spherulite structure has become fibrous.

In the final stage of deformation, the microfibrils slide past one another, and thus extend the interfibrillar tie molecules and also unfold some molecular chain sections from their anchor on the crystalline blocks. Due to this plastic deformation, there is a rapid increase in bulk sample length by alignment of interfibrillar tie molecules with the stress axis. With progressive strain, the resistance to elongation or strain hardening increases due to the alignment of these tie molecules. An elongation value is eventually reached where additional post-neck extension is not favored. Tensile stresses are then transmitted through the post-neck region to the neck region where lamellar transformation continued.

Summary

From the studies on polyethylene crystallization, deformation, and morphology, general molecular theories of polymer structure formation and mechanical deformation have been established which probably apply to all semicrystalline polymers. Of course, depending upon the polymer's chemical structure,[105] deformation rate,[24] and phase state,[59] some of these molecular theories may need slight adjustments, but they explain most of the structure and deformation observations made on more complicated polymer systems such as nylon.[21,88,106]

Crystallization conditions affect the number and orientation of tie molecules within a polymer solid. Extreme crystallization conditions can produce almost no molecular tie links, e.g., an extended crystalline

chain structure[22]; or many oriented tie molecules, e.g., transparent polyethylene structures.[62] When a polymer system is stressed, if the number of tie molecules is large, they act to keep the stress distribution uniform so that ductile deformation can occur even though microvoids or cracks are forming.[108] If the number of tie molecules is small, localized stresses occur which may produce a sufficiently large Griffith[31] type flaw, and bulk rupture may take place. Ductile cold draw deformation produces a fibrous product whose strength is due to the formation and alignment of tie molecules in the stress direction.[99] Therefore, the toughness and strength of a polymer in an environment is dependent upon the number of tie links in its structure, and their ability to resist brittle deformation by crack formation and propagation.

The above theories have been almost exclusively formulated from experimental observations made on thin films or single crystals. Very little experimental work on large polymer samples has been done and some uncertainty exists concerning the applicability of these theories to the three dimensional situation existing within large samples.[5,104] This work was undertaken to study the deformation response of large bulk crystallized HDPE samples and to relate the structural changes occurring to that previously observed in thin films.

CHAPTER III

EXPERIMENTAL TECHNIQUES

Sample Preparation

General Considerations

In order to simulate polymer melt-crystallized morphology and bulk size deformation response, thick sheet samples of MARLEX 6050 high density polyethylene were needed. The use of films or thin sheets was rejected because this would introduce undesired surface effects into the polymer's structure. It was previously concluded from other studies that thin film structures do not simulate bulk structures[5] or their deformation response.[104] The use of these large samples also enabled the observation of structure morphology at all the various stages of bulk deformation and also provided sufficient sample material for structure analysis by several characterization techniques.

Material Selection

MARLEX 6050 HDPE is an ethylene homopolymer produced by the Phillips Petroleum Company. The resin properties are listed in Table 1. MARLEX 6050 is a typical unfilled linear polyethylene having a broad molecular weight distribution. It was selected for study because it has a relatively simple crystalline structure, and can be deformed by cold drawing under uniaxial extension. Also it has been extensively characterized in the drawn and undrawn state from past studies on thin films[82] and rods.[75]

Table 1. Nominal Physical Properties of MARLEX 6050

Property	ASTM Test	Value
Molecular Weight (Weight Average)		$< 1.1 \times 10^5$
Density, gms/cc	D1505-63T	0.964
Melt Index, gms/10 min	D1238-65T	5.0
Molecular Weight Distribution (MW/MN)		10 to 20
Environmental Stress Cracking Resistance, hrs @ F_{50}	D1693-60T	< 1
Tensile Strength, psi (kg/cm^2)		
20 in/min (508mm/min)	D638-64T Die "C" of	4400 (310)
2 in/min (50.8mm/min)	D412-64	4000 (282)
Elongation, %		
20 in/min (508mm/min)	D638-64T, Die "C" of	12
2 in/min (50.8mm/min)	D412-64	120
Impact Strength, ft lbs/in. notch (cm kg/cm)	D256-56	.8 (4.3)
Vicat Softening Temperature, °F (°C)	D1525-65T	257 (125)
Brittleness Temperature, °F (°C)	D746-64T	-110 (-79)
Flexural Modulus, psi (kg/cm^2)	D790-66	220,000 (15,400)
Hardness, Shore D	D1706-61	68

Sample Preforming

To eliminate gas entrapment in the large polyethylene samples needed for study, a vacuum sheet forming operation was required. The MARLEX polyethylene resin in fluff form was placed uniformly into a flat three sided mold, 10" × 16" × 1". The mold containing the polyethylene fluff was heated in an over to 170°C under 28 inches Hg vacuum. A small nitrogen gas bleed was purged through the oven to remove oxygen and thereby inhibit polyethylene oxidative degradation. After slow cooling (~ 15°C/hr) from 170°C to 50°C, the 1/4 inch thick polyethylene sheet was removed from the vacuum oven.

Four samples having a dog-bone shape, 4" × 10" × 2" gauge width, were cut from each sheet to dimensions closely conforming to ASTM test method D638-64T (Tensile Properties of Plastics). See Figure 4 for sample dimensions. Any defective samples containing holes or cracks were discarded.

Thermal Crystallization

The purpose of the thermal crystallization step was to form the polyethylene sheet samples into uniform thickness tensile samples having structures which are typical of those produced in commercial crystallization operations. A thermal gradient crystallizer (TGC) was built to accomplish this task. See Figure 5.

The TGC in a cross-sectional view appears as a sandwich. From the center containing the dog-bone shaped polyethylene sample, it was outwardly constructed of a 1/8 inch aluminum support plate, a 1/4 inch air channel, and a 1 inch block of asbestos insulation. The polyethylene sample was surrounded on its periphery by a 0.22 inch thick Teflon spacer. The aluminum-Teflon-polyethylene sample sandwich structure was held together

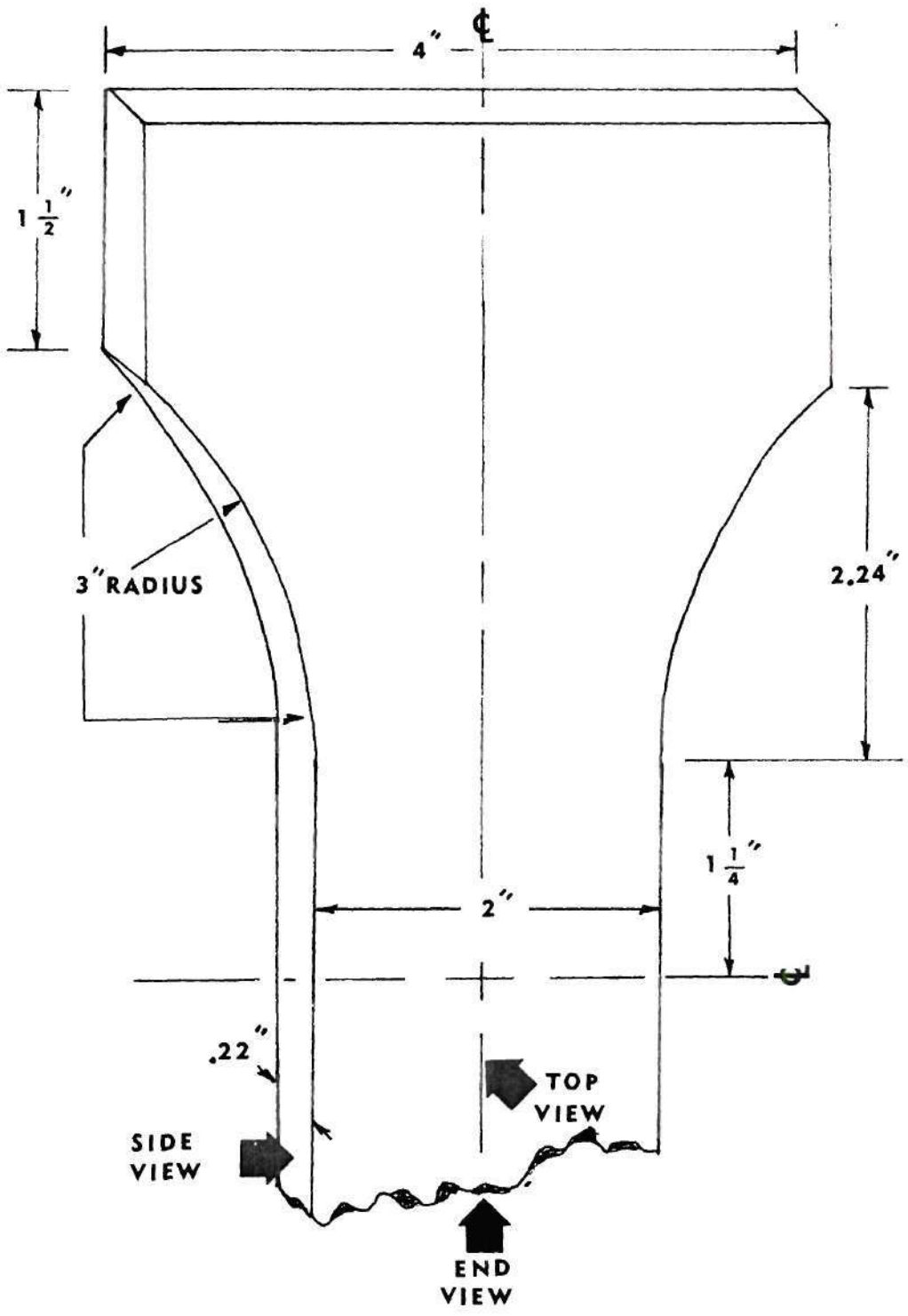

Figure 4. Tensile Test Specimen Dimensions

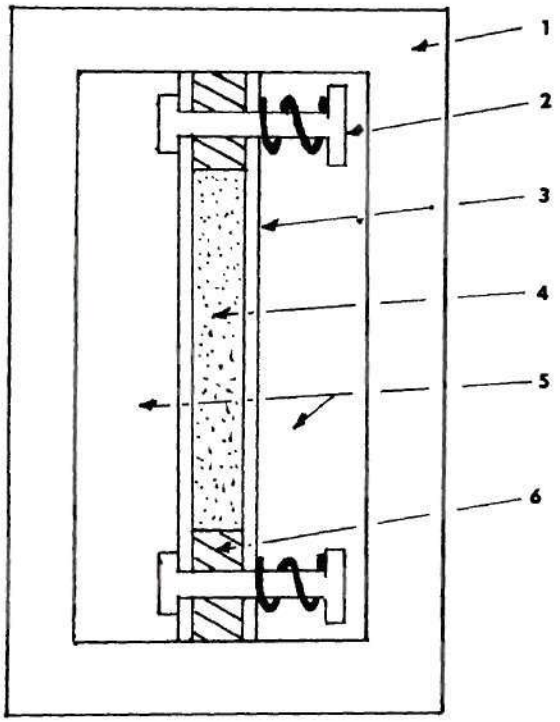

Figure 5. Cross Sectional Schematic of Thermal Crystallizer [1) Insulation, 2) Spring Clamp, 3) Aluminum Support, 4) Polyethylene Sample, 5) Air Channels, 6) Teflon Support]

by six force spring clamps. When the oversized 1/4 inch thick polyethylene samples melted in the TGC, they were compressed to a uniform 0.22 inch thickness and a small polymer flash formed around their periphery. This action produced an air tight contact between the polyethylene sample and the other sandwich members. This prevented sample oxidation, decreased heat transfer resistance between the sample and aluminum support plates, and insured sample to sample thickness uniformity.

During the crystallization operation, heated air was forced at a high velocity (~ 100 ft/sec) through both air channels without recycling. This once through high velocity flow design enabled a fast cooling or heating control response on air temperature (~ 100^{o}C/min.). This also lowered the air film heat transfer resistance at the aluminum support plate surfaces. Air temperature in both channels was independently controlled to ± 2^{o}C. The polyethylene sample cooling and heating rates were limited by the thermal resistance of the polymer sample and the air film boundary. Maximum heating and cooling rates at the centerline of the polyethylene sample were measured to be approximately 1^{o}C/min. during a sample phase change and 18^{o}C/min. otherwise. See Figure 6 for the TGC cooling characteristic during quench crystallization.

After the polyethylene sheet samples were installed in the TGC, the samples were heated to 170^{o}C and maintained at this temperature for a minimum time of one hour. The air temperature was then decreased to a value below the polyethylene's crystallization temperature. This simulated isothermal crystallization techniques. For other samples, the air temperature was continuously reduced from 170^{o}C to simulate air quench crystallization techniques. After sample crystallization and cooling to room temperature,

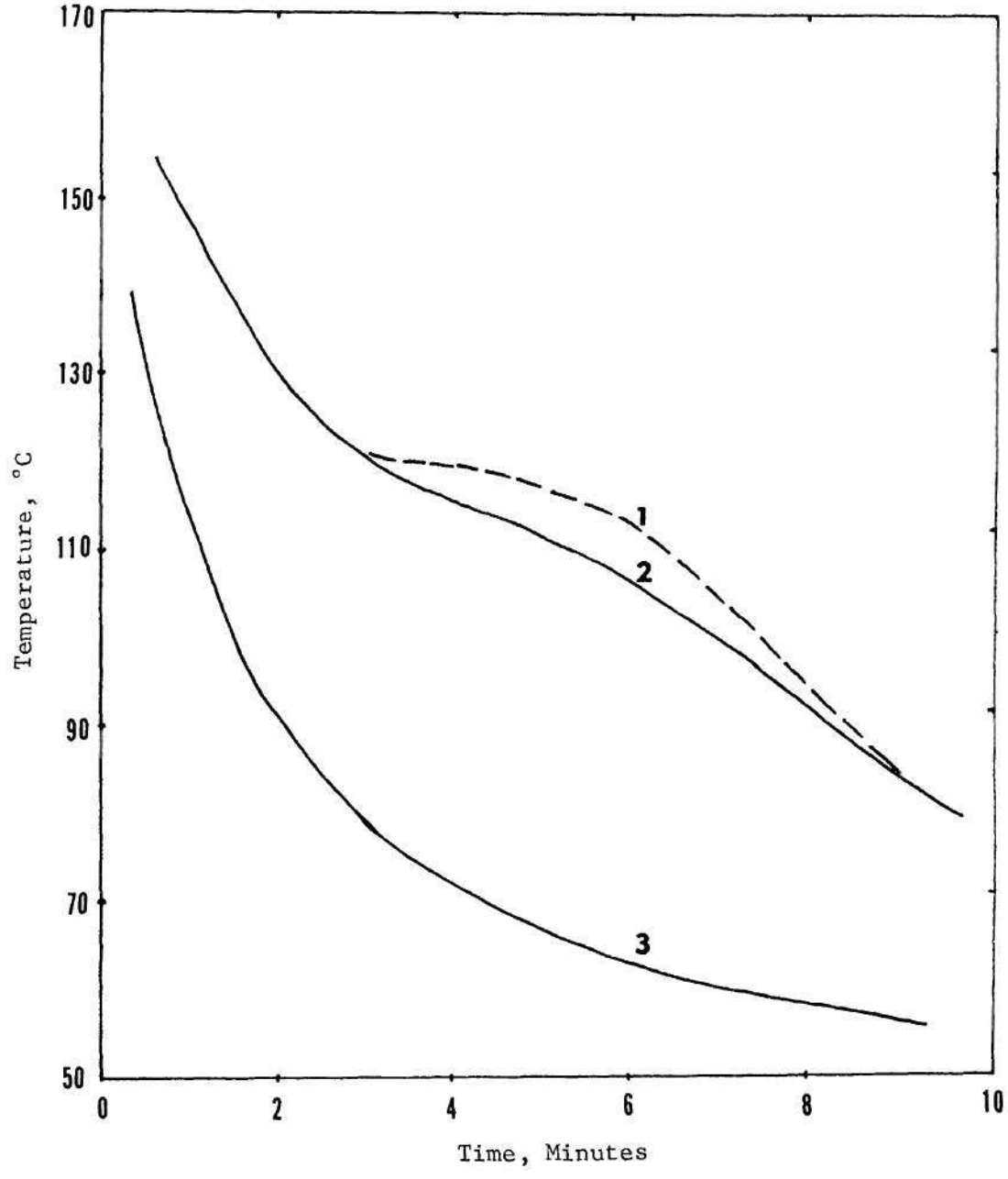

Figure 6. Time-Temperature Profiles of Quenched Crystallized Bulk Polyethylene [Curves: 1) Polyethylene 1600 microns from top surface, 2) Polyethylene 750 microns from top surface, 3) Polyethylene at the aluminum support surface]

the small amount of flash material on the sample's periphery was removed. All samples having noticeable defects were discarded.

Sample Deformation by Cold Drawing

All polyethylene tensile samples were deformed at 60°C by uniaxial extension, i.e., cold drawn. An Instron, model TT-C, having a 10,000 pound force capacity equipped with an environmental test chamber was used for this tack. The 60°C temperature of deformation was selected because it had been previously shown that MARLEX-HDPE rods could be cold drawn at this temperature.[75]

Because of the large sample size and the large shear forces forming during deformation, special heavy duty steel grips with serated surfaces were built and used to hold the test samples securely without slip during the cold drawing operation.

All test samples prior to deformation had gauge dimensions of $2.5" \times 2" \times 0.22 \pm 0.005"$. After being conditioned at 60°C for a minimum of eight hours in the Instron environmental chamber to insure isothermal conditions, the samples were deformed at an extension rate of one inch per minute (40%/minute). Depending upon the sample's crystallization history, the deformation response was either brittle or ductile.

Cryogenic Microtoming

Parts of the undeformed and deformed polyethylene bulk tensile samples were sectioned for microscopic observations by using a Porter-Blum ultramicrotome, model MT-2B. To minimize sample structural damage and the introduction of artifacts, low temperature microtoming conditions were required.[3]

Before microtoming, parts of the bulk samples were cut with a jig saw into 1/4 inch cubes to provide surfaces parallel and normal to the sample centerline. These blocks provided the geometry needed to view the polyethylene morphology from two directions, normal and parallel to the stress axis. Views from these directions are referred to as the end and the side or top views, respectively. See Figure 4. These small blocks were then embedded in a soft epoxy resin using empty gelatin capsules as molds. The epoxy resin was cured at room temperature.

The embedded blocks were mounted in the chuck of the microtome before being rough trimmed with a sharp steel knife or single edge razor blade. Rough trimming was done in accordance with standard thin sectioning procedures.[115]

Precision trimming of the embedded block was done by the glass knife of the ultramicrotome. Glass knives were prepared from 1/4 inch glass sheets by the "free break" method[115] and mounted at a 6^{o} knife angle. Precision trimming was done so that the final thin sectioning would be on a polyethylene surface of approximately 2×4 mm.

Before final thin sectioning, the microtome chuck containing the precision trimmed block was removed from the ultramicrotome and placed in a liquid nitrogen bath at 80^{o}K for ten minutes. After this time period, the cold chuck with block was quickly remounted in the ultramicrotome and six thin sections each of approximately five microns thickness were made from the head of the polyethylene block. The last thin section was collected and mounted with Permount between glass microslides for later observation by the light microscope. The polymer head was saved for etching and eventual observation by the scanning electron microscope.

By placing a chromel-constantan thermocouple in an epoxy block, the temperature increase occurring in the block in the average time interval between when the chuck was removed from the nitrogen bath and when the last thin section was microtomed from the head (~ 3 minutes) was measured. This measurement indicated that the polyethylene head temperature was about -80°C when the last thin section was microtomed. This temperature is below the linear polyethylene glass transition temperature, -30°C,[10] and therefore relatively undeformed sections and heads were obtained by using this cryogenic microtoming technique. These thin sections were only compressed to 87% of their original length. In contrast, microtoming at room remperature conditions was completely unacceptable because the thin sections made were compressed to approximately 30% of their original lengths.

Densitometry

The densities of all polyethylene samples, i.e., the microtomed thin sections, bulk crystallized sheet samples, and DSC crystallized films, were measured using a density gradient technique, ASTM test method D1505-68. This method is based on observing the level to which a test specimen sinks in a liquid column having a density gradient, in comparison with the levels of standard floats of known densities. This method has been used with excellent success in past studies on polyethylene.[33,82,103]

The gradient column and standard density floats were purchased from the Scientific Glass Apparatus Co., Bloomfield, N. J. The 1.3 meter long column contained one liter of usable volume and had one millimeter graduations in the length dimension. The liquids used to fill the column, 540 cc

of water (ρ = 1.0g/cc) and 720 cc of isopropanol (ρ = 0.79 g/cc), were added at a combined rate of 12 cc/min. by the continuous filling method described in ASTM test method D1505-68. By using this method, a linear fluid density gradient profile was obtained throughout the column. The standard floats placed in the column fluid had densities of 0.9000, 0.9300, 0.9499, 0.9700, and 0.9750 g/cm^3 at 23°C.

Using the above system operating at 24°C and after the polymer test samples had been placed in the column for a minimum of five hours to reach equilibrium, position measurements to the nearest millimeter were made and compared to the density gradient profile. In this manner, polyethylene sample densities could be measured to ± 0.0005 g/cc.

Calorimetry

Polyethylene dynamic crystallization kinetic studies and sample crystallinity measurements were made on a Perkin-Elmer differential scanning calorimeter (DSC), model 1B. Previous investigators have used this instrument to obtain polyethylene thermodynamic data[33,68] and crystallization kinetic information.[25,77]

Essentially, the DSC measures the energy flow rate into or out of a small sample, as the sample is heated or cooled at a specific rate (scan rate). The energy flow rate can be measured against time and sample temperature to provide a thermogram. From the size and shape of thermogram curves, thermodynamic properties can be determined.[116]

In this study, thermogram curves were obtained by placing the DSC output into the ordinate readout of a Hewlett-Packard, Model 7001AR, or Honeywell, Model 520, x-y recorder in the abscissa time mode. The DSC

calorimeter was calibrated at a sample scan rate of 10^{o}C/min and sensitivity of 16 mcal/sec by melting ~ 5 mg urea samples. Urea was selected as a standard because of its purity, stability, and close proximity of melt temperature, 406^{o}K, and heat of fusion, 57.8 cal/g, to that of perfect polyethylene single crystals, 413^{o}K and 68.4 cal/g.[112]

Two types of polyethylene samples were studied with the DSC, those taken from bulk samples, and those taken from films. All samples were weighed to ± 0.01 mg with a Cahn electrobalance, model RG. To obtain the best possible DSC response characteristic, all samples weighed between 4 and 9 mg. The DSC bulk samples were prepared from thin crosssections approximately 2 × 5.6 × 0.5 mm, taken from the drawn or undrawn center regions of the ductile or brittle bulk samples. These samples were heated at 10^{o}C/min to obtain melting endotherms.

Thin films (~ 270 microns thick) were prepared by melting HDPE fluff in a vacuum oven between glass plates held in compression. Quarter inch diameter disks were punched out of these films and used for DSC studies on bulk dynamic crystallization kinetics.

Surface Etching

Polyethylene samples have been treated at high temperatures with solvent vapors[95] and nitric acid.[12,72] These treatment techniques are unacceptable as surface etching processes because they drastically oxidize or swell the polymer structure.[63] These etching techniques do not reveal morphological features without introducing gross artifacts.

Armond and Atkinson[4] followed by others[6,27,47,97] have used a chromic acid surface etching technique to reveal the microstructures of polypropylene bulk samples. They found that the less ordered regions of the

polypropylene surface structure are attacked preferentially at a slower rate and that the oxidation reaction was confined by diffusion limitations to a thin surface layer. After etching, previously hidden features of the structure were observed by a scanning electron microscope.

A similar chromic acid etching technique was developed by the author to treat the microtomed surfaces located on the heads of the drawn and undrawn bulk crystallized high density polyethylene samples formed in this study.[76] After etching detailed structural features of the internal morphology could be observed by using a scanning electron microscope.

The acid etchant used was a 6 molar aqueous solution of chromium trioxide. The heated etching solution was constantly stirred and blanketed by an air purge in order to saturate the solution with atmospheric oxygen. A reflux condenser was used to eliminate water from the air purge leaving the etching bath. The bath temperature was controlled between 60° and $85^{\circ}C$ to tolerances of $\pm 2^{\circ}C$. Sample treatment ranged from 67 to 900 hours.

Polypropylene (MARLEX HGZ-050-02) and high density polyethylene (MARLEX 6050) film samples and the polyethylene heads obtained by cryogenic microtoming of bulk samples were submerged into the etchant bath with glass tubing. Various combinations of treatment times and etchant temperature conditions were used to determine etching rates and optimum etching conditions.

Observations

Light Microscopy

The five micron thin sections microtomed from the deformed high density polyethylene bulk samples were observed at 75 or 450X magnifications

by using a Bausch and Lomb, model LR-2, polarizing microscope with light polarizers crossed. Light microphotographs were taken by a Canon 35mm camera, model FT-QL, loaded with Kodak Plus-X film.

Scanning Electron Microscopy

The chromic acid etched polyethylene heads formed from the microtoming process were coated with 50 Å of carbon and 400 Å of gold-paladium before being examined by a Cambridge scanning electron microscope (SEM). The SEM was operated at 15,000 volts at a sample magnification of 50 to 10,000X. The electron beam was at 45^{o} to the sample surface. Sample structural alterations or damage from an electron beam has previously been reported,[13,32] but no sample changes were observed at the SEM conditions used in this study. Scanning electron microphotographs were taken with Polaroid PN-55 film.

Photomicrographs

All photomicrographs in this study show a low magnification side or end view of a bulk crystallized and cold drawn sample. In each photograph, the top of the sample, i.e., one of the two sample sides in contact with the aluminum support plates during crystallization, serves as a reference plane and distances into and toward the sample centerline from this reference are marked in 100 micron increments. For the drawn samples, this distance was normalized to have all structure points within the drawn sample relative to their position in an undrawn state, i.e., the distance increment is divided by the square root of the bulk sample draw ratio. Higher magnification photomicrographs taken from selected sample regions which are indicated by arrows in the low magnification photograph are shown to the right of the figure or on the following figure.

Two scale bars, vertical and horizontal, are shown on each photomicrograph. For the polarized light micrographs, these scale bars compensate for magnification differences due to the anisotropic microtoming distortion of the thin sample section. For the scanning electron micrographs, these scale bars compensate for magnification differences introduced due to the 45^{o} view angle of the sample head surface in the scanning electron microscope.

CHAPTER IV

EXPERIMENTAL RESULTS AND DISCUSSION

Surface Etching

Rates of HDPE surface etching with 6M chromic trioxide solution were low and comparable with the etching rates for polypropylene treated at the same conditions. Figure 7 indicates that normalized etching rates for HDPE are linear except after extended treatment at relatively high temperatures. At these extreme conditions (curve 4), the actual surface area reacting was greater than the initial surface area; therefore, area normalization was inaccurate and produced a false indication of an exponentially increasing etching rate. The calculated surface etching rate for HDPE treated at 65°C, curve 2, is 250 Å/hr; for PP at 65°C, curve 1, the rate is 65 Å/hr. The data given by Armond and Atkinson[4] on etching PP at 70°C (curve 3 of Figure 7) gives a calculated etching rate of 890 Å/hr.

Using a Perkin-Elmer model 700 spectrophotometer, the infrared spectra on 19 mil HDPE etched and unetched films were made, see Figure 8. The etched films have enhanced absorbance at a 5.8 micron wavelength. This indicates an increase in the concentration of carboxyl groups on the polyethylene surface with increasing etching treatment. Therefore the mechanism of the etching reaction must be an oxidation of the polyethylene by reduction of the chromic acid. Chromium ions are known to be catalysts for polyethylene oxidation.[35] The etching reaction appears to be limited

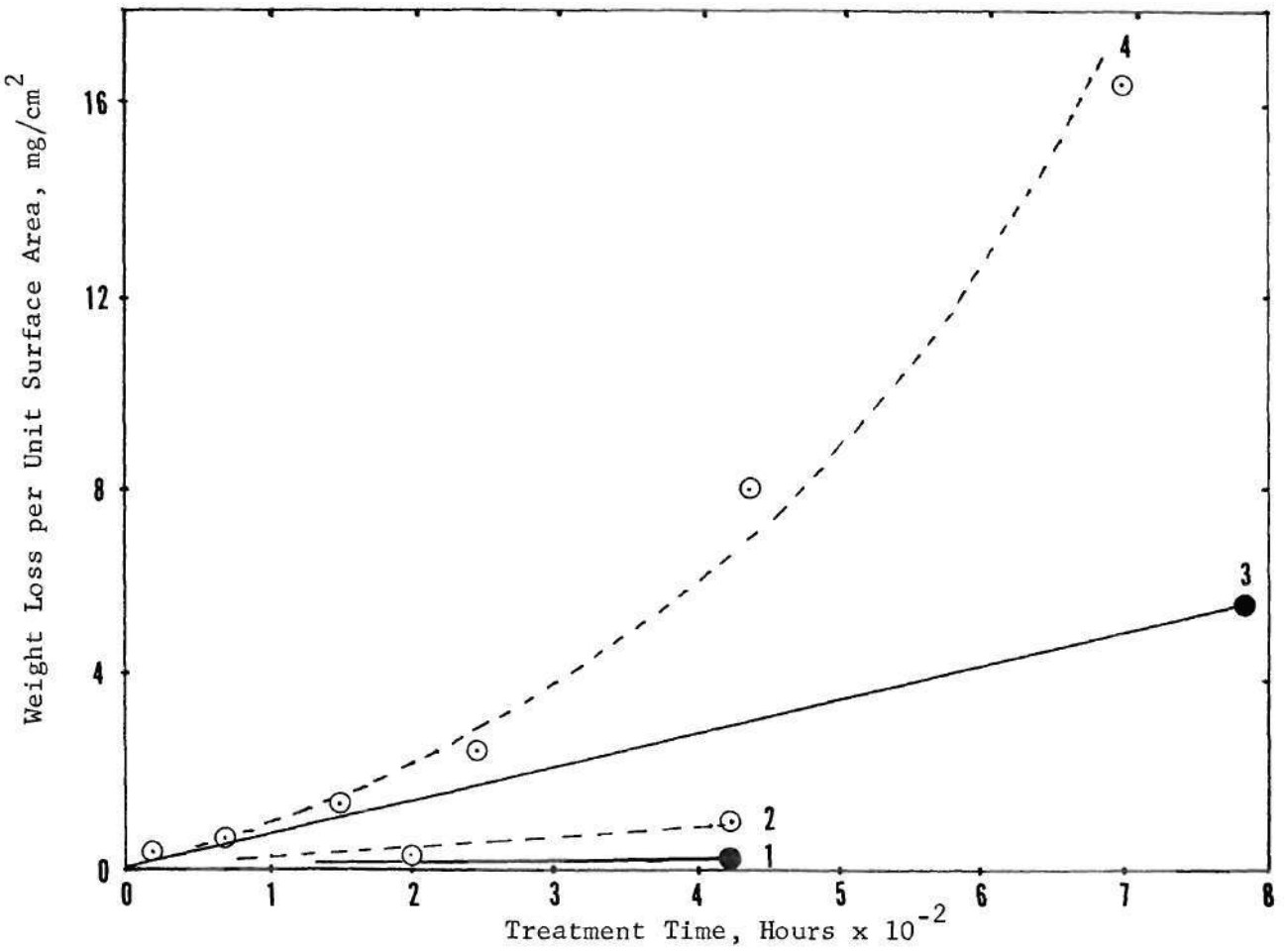

Figure 7. Chromic Acid Etching of Polyethylene and Polypropylene [Curves: 1) Polypropylene at 65°C; 2) Polyethylene at 65°C; 3) Polypropylene at 70°C; 4) Polyethylene at 85°C. Six molar chromic acid aqueous etching solution was used.]

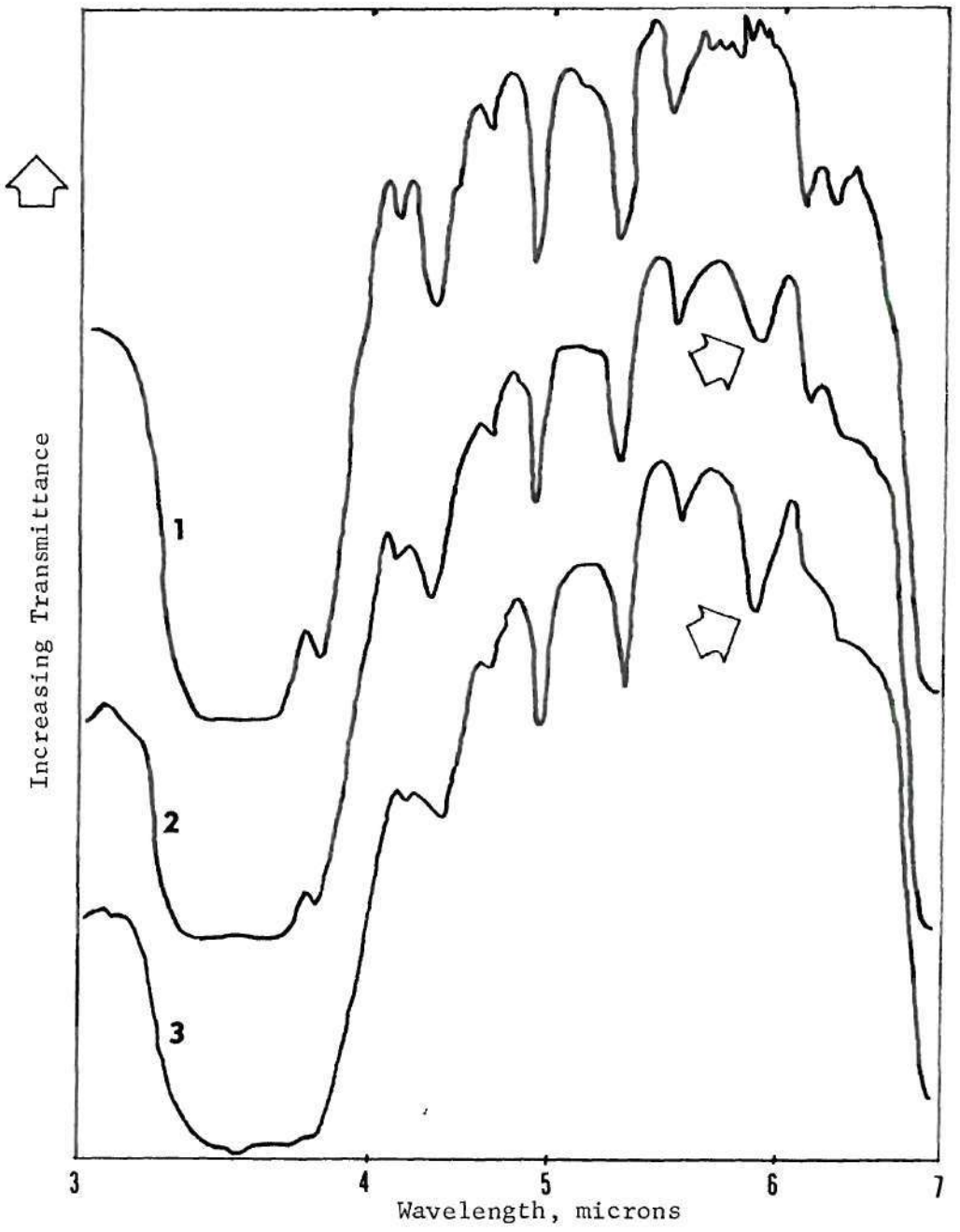

Figure 8. Infrared Spectra of Polyethylene Films [Curves: 1) Unetched film; 2) Film etched for 150 hr in 6M chromic acid at 85°C; 3) Film etched for 245 hr in 6M chromic acid at 85°C. Increased absorption occurs at 5.8 microns for longer etching times.]

to the polymer surface region, because only a slight increase in HDPE film density occurs after an extreme etching treatment for 700 hours at 85°C (0.96 to 0.99 g/cc). Also, the HDPE film mechanical properties and heats of melting were not noticeably altered by etching.

The etching reaction is limited to the polymer surface and the etching rates of polyethylene and polypropylene are approximately equivalent. This indicates that the rate controlling step may be chromic acid diffusion onto the polymer reaction site rather than the subsequent redox reactions. If this be the case, the less crystalline portions of the polymer structure and the regions containing excess surface area, e.g. crack or voids where diffusion is more rapid, were etched faster than crystalline regions. This produced structural contrast on the polyethylene surfaces. Such enhancement is particularly desirable for morphological studies of bulk HDPE when using the scanning electron microscope to observe the surfaces of microtomed bulk samples.

To determine the optimum etching conditions for HDPE surface structure enhancement, a series of bulk sample microtomed heads, sectioned for the side view, were treated at 60 or 65°C for different time periods up to 900 hours and observed using the scanning electron microscope. Higher treatment temperatures were not used because of the possible introduction of thermally induced polymer structural changes. Low magnification photomicrographs of some of these surfaces are shown in Figure 9. Higher magnifications are shown in Figure 10. Although the unetched sample of Figure 9A shows a large amount of surface distortion introduced by microtoming, a faint outline of the ringed spherulite structures appears on the unetched surface. This structure outline probably appears due to

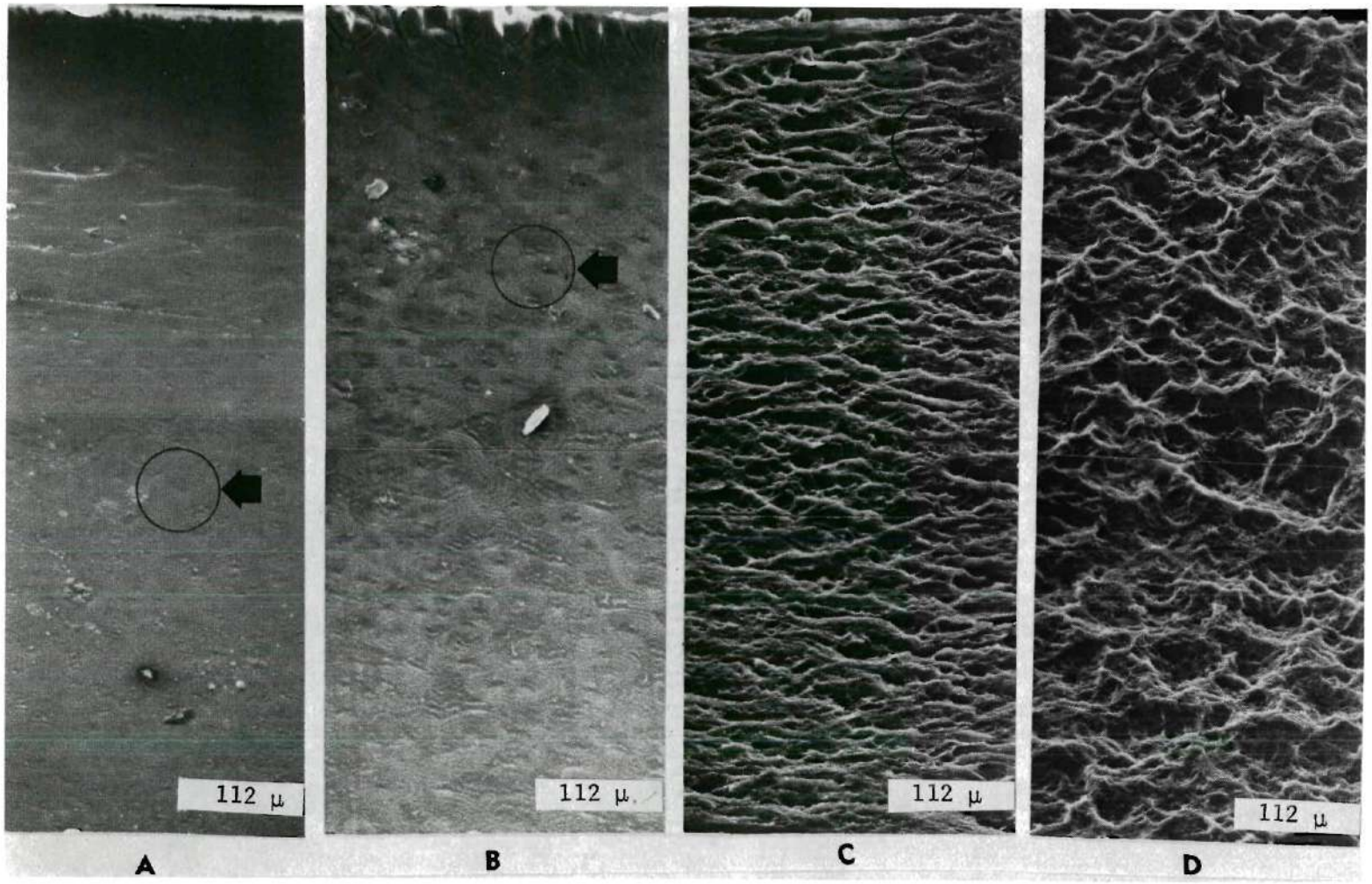

Figure 9. SEM of Sample Surfaces Etched with 6M Chromic Acid at 60°C [A. unetched Sample; B. 67 hr treatment; C. 310 hr treatment; D. 900 hr treatment]

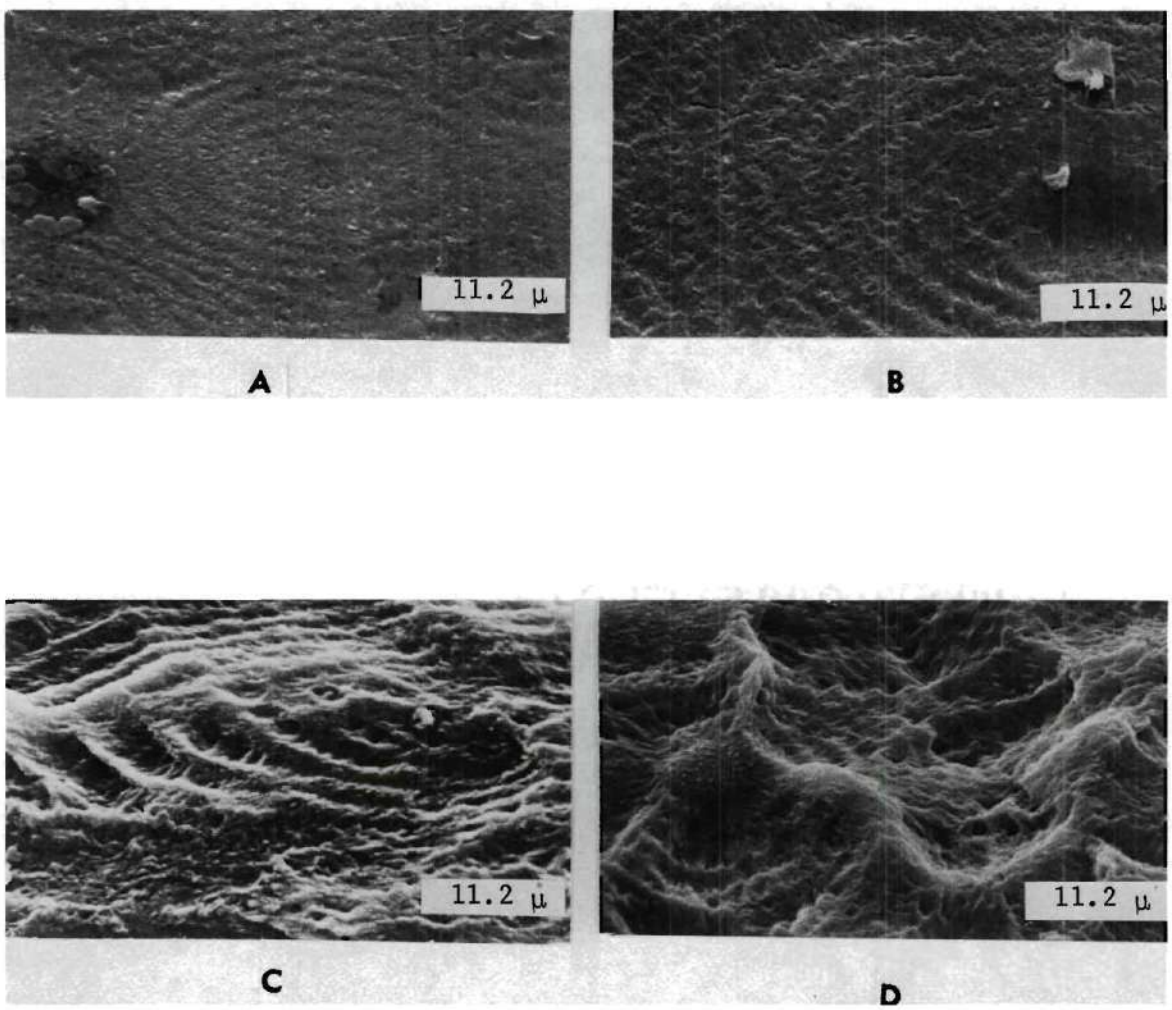

Figure 10. SEM High Magnifications of Etched Sample Surfaces Shown in Figure 9

a release of internal stresses after microtoming.[12] The etching treatment removes the polymer material distorted during microtoming and discloses the subsurface composed of spherulites having ring structures formed by lamellae radiating from the spherulite centers. Over-etching is revealed by the formation of pitted surfaces as shown by Figures 9C and 9D. Optimum etching results were accomplished after surface treatment for 60 to 120 hours with 6M chromic acid solution at 60 or 65°C.

Bulk Deformation

General Comments

MARLEX 6050 HDPE bulk samples were crystallized in the thermal gradient crystallizer (TGC) at temperatures of 115, 119, and 125°C. Most of these samples were mechanically weak and broke at about 40% elongation when extended at 60°C. In contrast, the quenched or dynamically crystallized bulk samples when drawn usually did not break but showed ductile deformation by tearing or uniform necking with subsequent elongation to a 8.0 draw ratio. The quenched bulk samples that did break contained macroscopic voids introduced during sheet forming operations and they are not indicative of the true sample deformation mode. Figure 11 shows typical force-elongation curves for the three modes of bulk deformation observed: brittle failure, ductile cold drawing and necking, and ductile tearing. Figure 12 shows photomacrographs of the drawn samples. Data on bulk sample deformation, undrawn sample heats of melting, and densities are summarized in Table 2.

Both bulk sample density and heat of melting data show that the ductile samples are less crystalline than the brittle break samples.

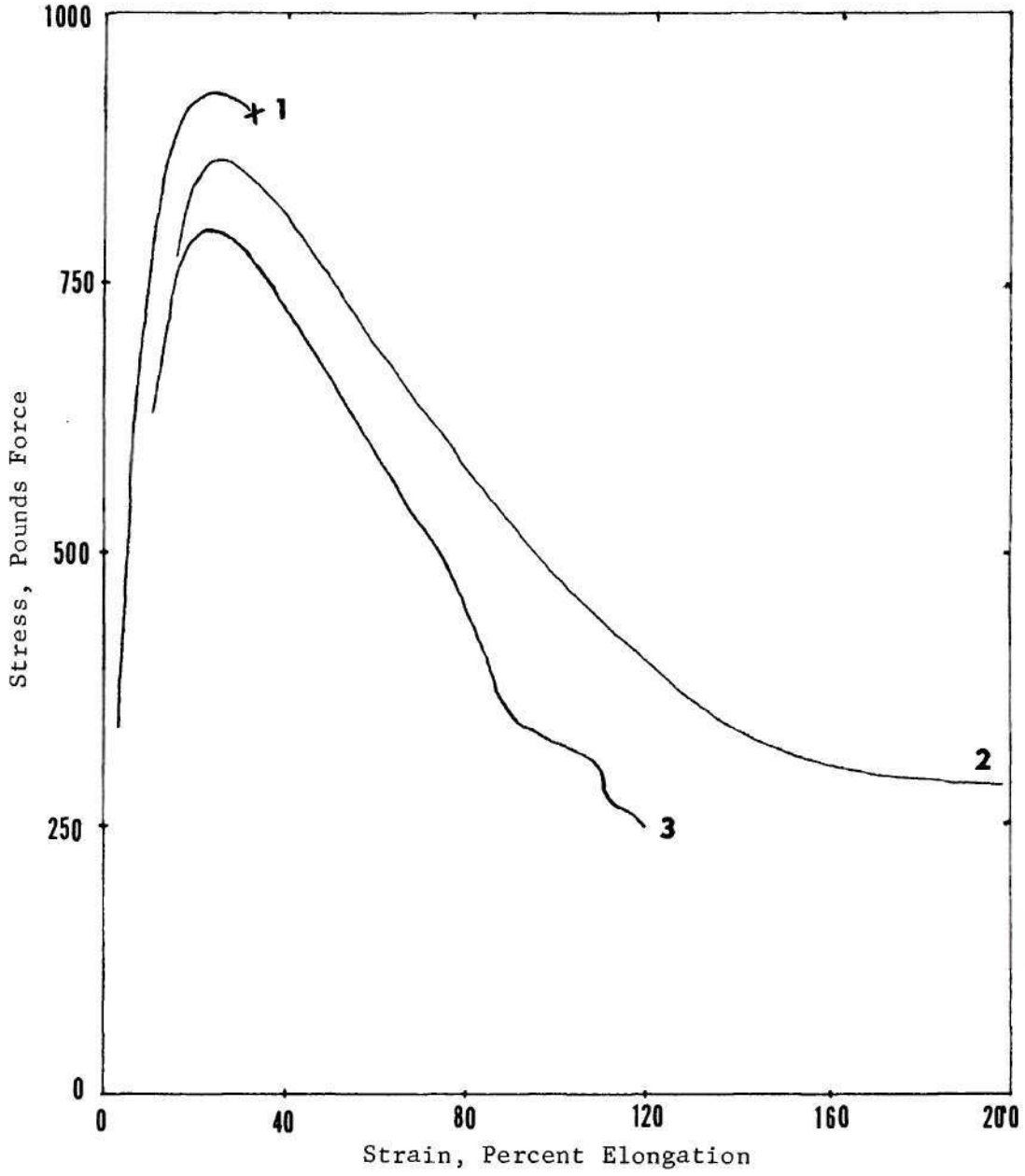

Figure 11. Engineering Stress-Strain Curves of Polyethylene Bulk Samples in Uniaxial Extension at 60°C [Curves: 1) Brittle Break Sample; 2) Ductile Neck Sample; 3) Ductile Tear Sample. Initial gauge dimensions were 0.56 x 5.1 x 6.4 centimeters. Initial draw rate was 40% per minute.]

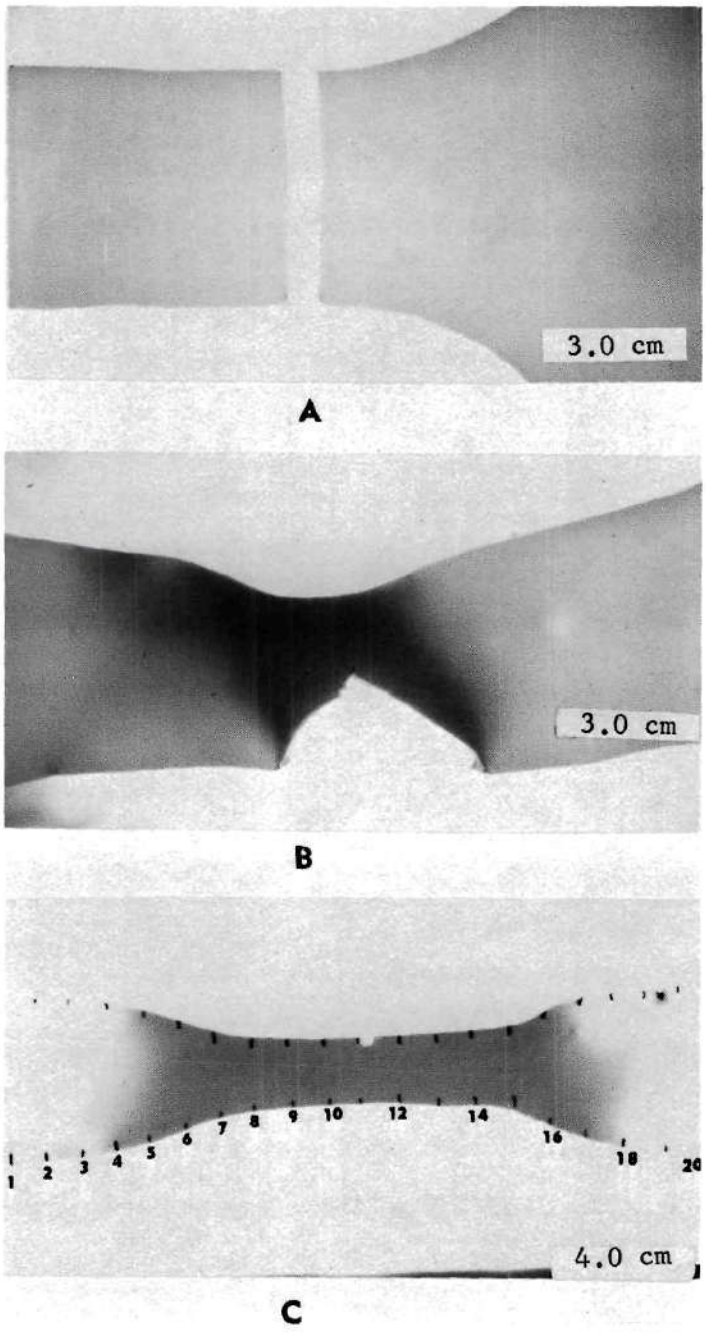

Figure 12. Macrographs of Drawn Bulk Samples [A. Brittle sample; B. Tear sample; C. Ductile draw sample. Dark regions show areas of stress whitening.]

Table 2. Bulk Sample Crystallization Conditioning and Uniaxial Deformation Performance

Sample No.	Isothermal Crystallization Temperature (°C)	Time at Isothermal Conditions (min).	Type of Deformation	Bulk Draw Ratio in Neck†	Average Heat of Crystallization of Undrawn sample‡ Region (cal/g)	Average Bulk Density** g/cm^3
55	125	480	Brittle Break		52.8	.977
56	119	68	Ductile Tear		47.0	
58	119	200	Brittle Break		49.6	.975
59	119	22	Brittle Break		47.0	.972
60	115	200	Brittle Break*		51.2	
61	115	22	Ductile Tear		49.0	
62	115	68	Brittle Break		47.2	.973
12	Air Quenched from Melt Temp to Room Temp		Ductile Neck	8.5	43.5	
45	"	"	Ductile Tear			.967
46	"	"	Brittle Break*			
47	"	"	Brittle Break			
48	"	"	Ductile Neck	7.9	38.2	.957
49	"	"	Brittle Break*			
50	"	"	Ductile Neck	7.7	42.2	.967

Table 2. Continued

51	Air Quenched from Melt Temp to Room Temp	Ductile Tear			.968
52	"	"	Ductile Tear	44.6	.966

†The Bulk Draw ratio is the ratio of initial to final drawn cross-sectional area in the fully developed neck.

‡Obtained from Differential Scanning Calorimeter. Average of four samples.

*Sample contained a macrovoid at break surface.

**0.1 g sample size taken from undrawn region. Average of three samples.

Ductile samples had crystallinities ranging between 71 and 78% when calculated from bulk densities and between 56 and 66% when calculated from bulk sample heats of melting. In comparison, the brittle samples had crystallinities between 84 and 93% and between 69 and 78% by density and heats of melting measurements, respectively.

In the crystallinity calculation, the density at 24°C and heat of melting for perfectly crystalline polyethylene, $\rho^{o}_{c(24^{o}C)}$ and ΔH^{o}_{c}, were taken as 1.001 g/cc[44] and 68 cal/g,[112] respectively. The density for peramorphous polyethylene, $\rho_{a}{}^{o}{}_{(27^{o}C)}$, was taken as 0.852 g/cc,[65] the equations for determining bulk sample degree of crystallinity, χ_{b}, are:

$$\chi_{b} = \frac{\rho_{b} - \rho_{a}{}^{o}}{\rho_{c}{}^{o} - \rho_{a}{}^{o}} \qquad (1)$$

$$\chi_{b} = \frac{\Delta H_{b}}{\Delta H_{c}{}^{o}} \qquad (2)$$

Observations on Brittle Sample Structures

Photomicrographs taken with a polarizing microscope of the side view thin sections microtomed from the brittle samples showed that the bulk superstructure is composed of coarse spherulites, see Figure 13. These spherulites have impinged upon one another and are approximately 60 μ in diameter. The boundaries between spherulites are not well defined. Lamellae radiate from the spherulite centers, but because of an absence of a uniform birefrigence effect which forms alternating dark and light rings, individual lamellar groups apparently are not twisting in large concert with their neighbors.

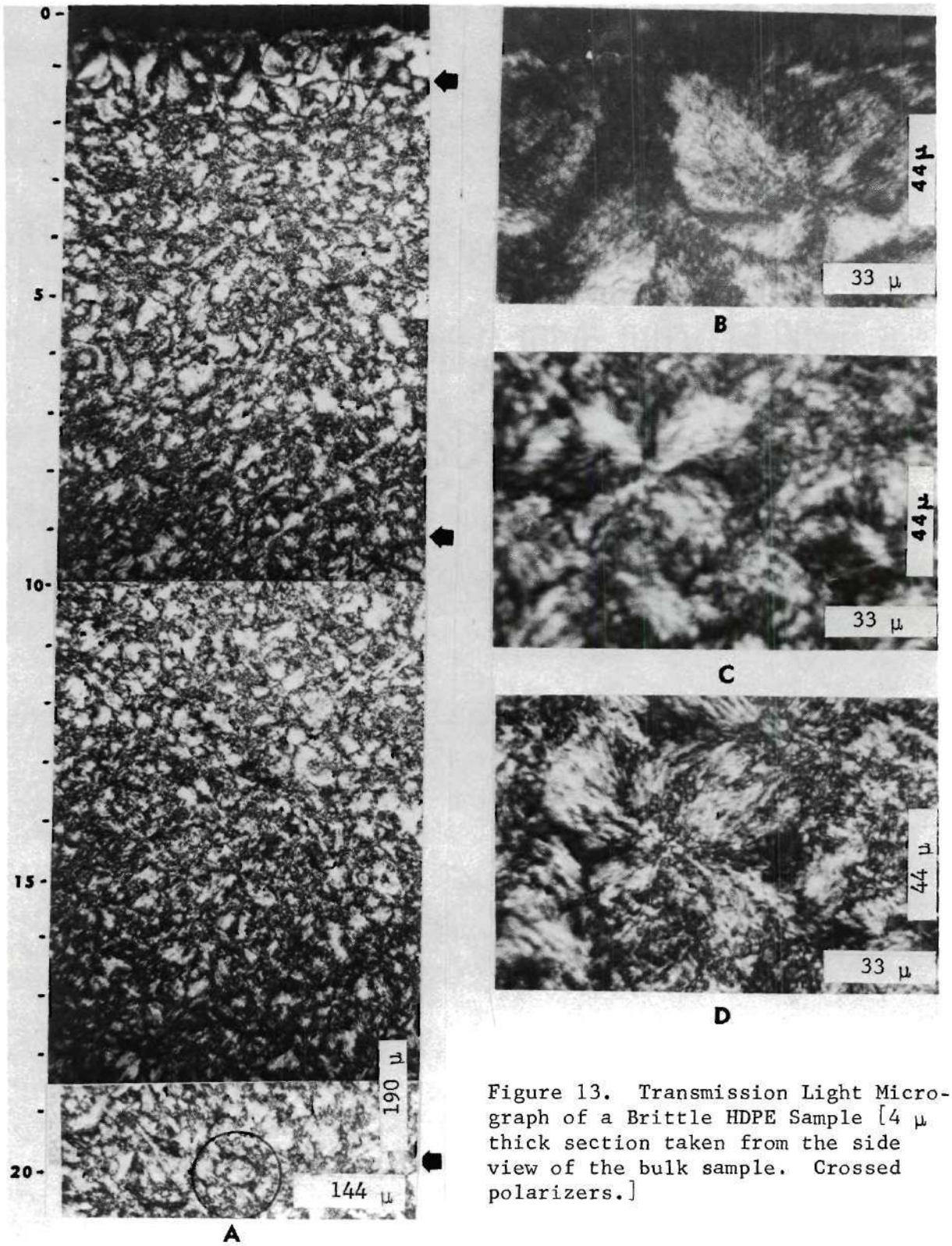

Figure 13. Transmission Light Micrograph of a Brittle HDPE Sample [4 μ thick section taken from the side view of the bulk sample. Crossed polarizers.]

Photomicrographs taken with the scanning electron microscope on the microtomed and etched head surfaces having side views of the structure also revealed that coarse spherulites form the brittle sample's bulk superstructure. Figure 14 shows a typical view of an undrawn brittle type sample. In each spherulite, groups of lamellae splay away from the spherulite center in an uncoordinated fashion. Also many deep cracks approximately 1/2 μ wide and over 50 μ long are present on the surfaces. These cracks and other smaller cracks have been enhanced by chromic acid etching. They are distributed randomly throughout the surface and appear to have no order with respect to the spherulite superstructure.

In summary, the brittle samples have superstructures composed of coarse spherulites and large cracks. Sample failure probably is due to the presence of these cracks and the inability of the superstructure to resist rapid growth of these cracks during uniaxial extension.

Observations on Ductile Sample Structures

Macro-observations. The quenched or dynamically crystallized samples necked and drew when uniaxially strained at 60^{o}C. During straining, if any large macrovoid formed from air entrapment was present in a quenched crystallized tensile sample, then these samples tore or experienced unsymmetric drawing at the macrovoid stress concentration point. Quenched tensile samples without macrovoids showed very uniform and symmetric macroscale necking during straining. Figure 15 shows the bulk draw ratio profile of the drawn sample shown in Figure 12C. The bulk draw ratio, BDR, is the ratio of undrawn sample cross-sectional area to the drawn sample cross-sectional area.

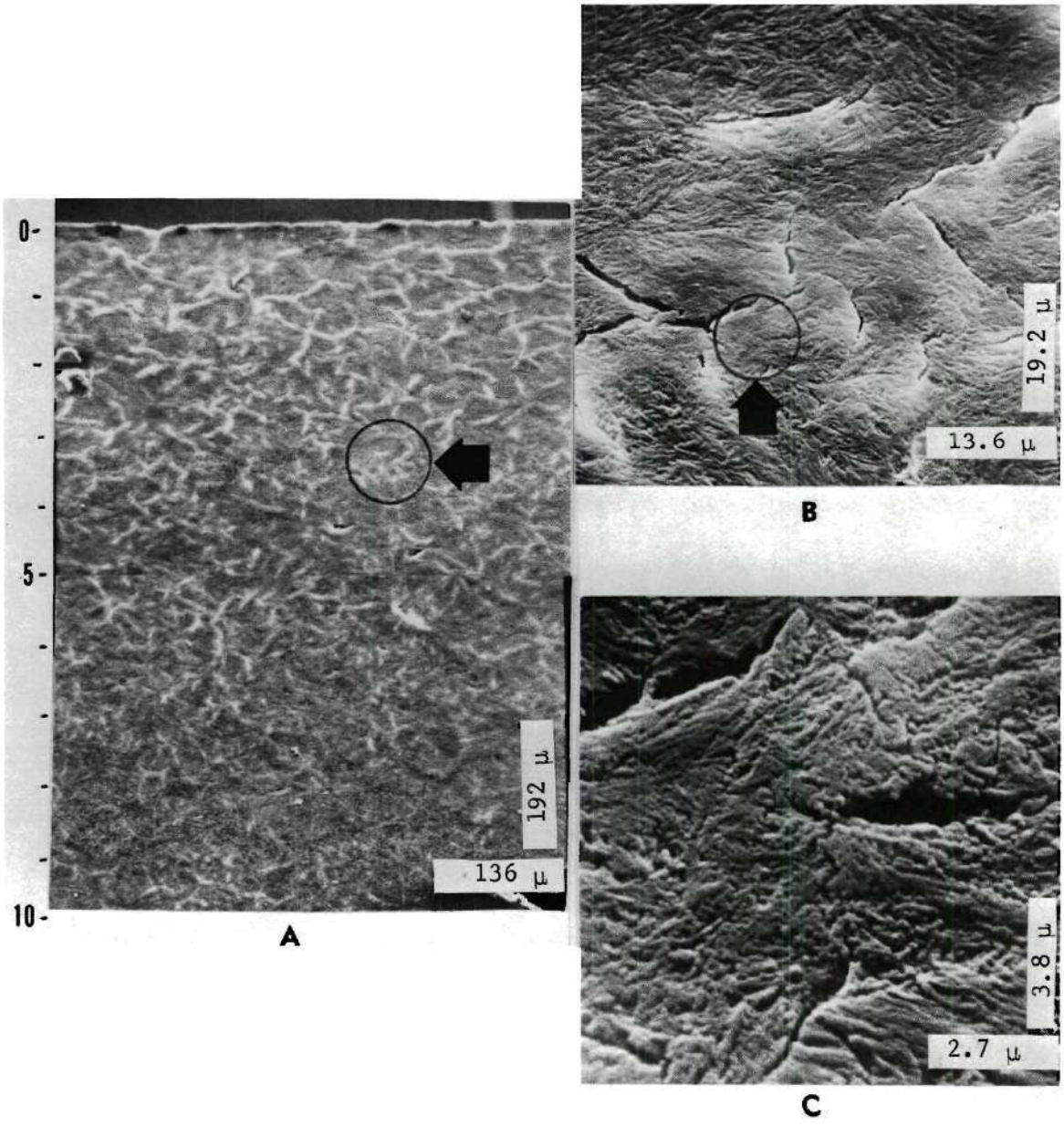

Figure 14. SEM of a Brittle HDPE Sample Surface [Surface was etched for 110 hr in 6M chromic acid at 65°C. Side view of bulk sample.]

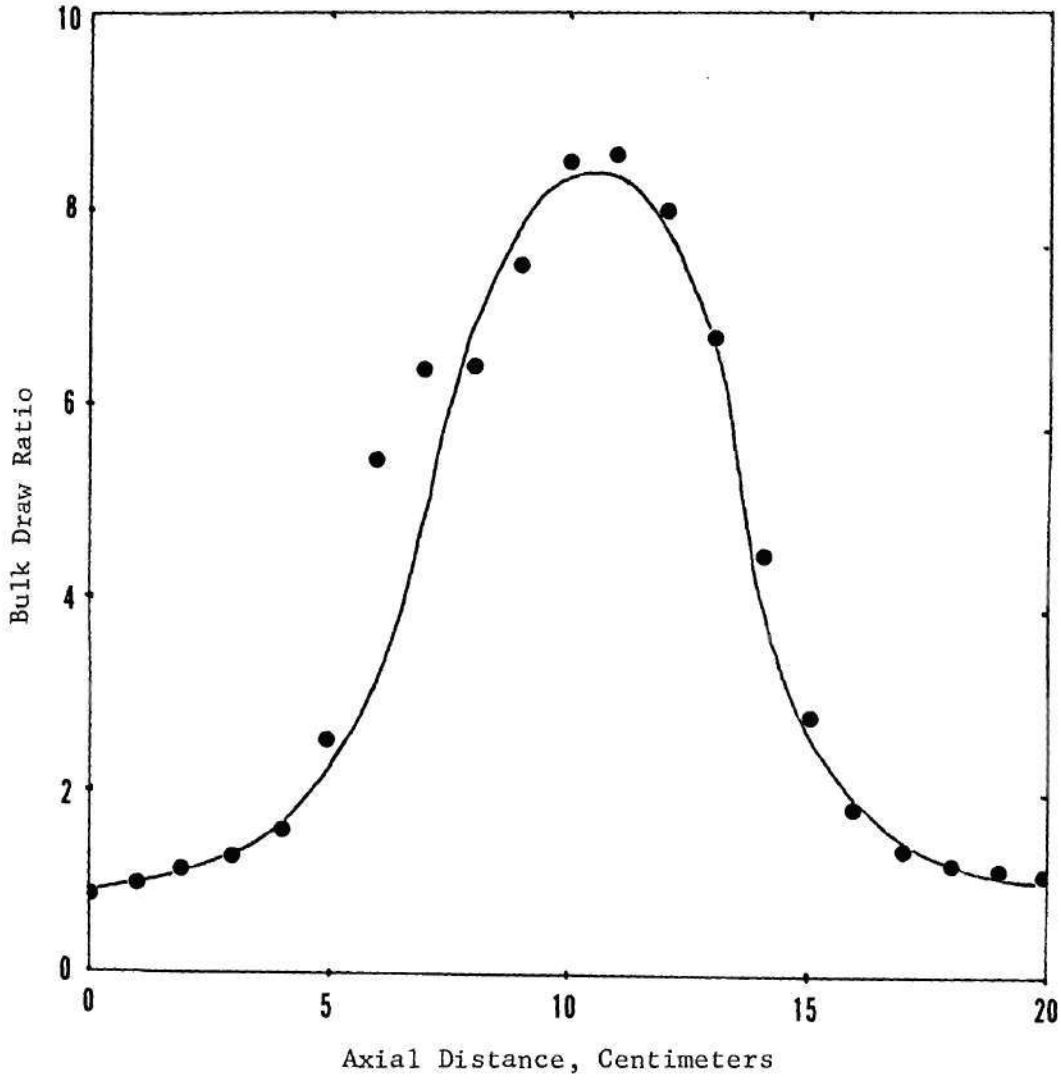

Figure 15. Draw Profile of Ductile Polyethylene Sample After Uniaxial Draw at 60°C [Initial draw rate was 40% per minute. Initial gauge dimensions were 0.56 x 5.1 x 6.4 centimeters.]

The sample section which shows a sudden increase in BDR is referred to as the neck zone. For the sample shown in Figure 12C, two neck zones existed at axial distances from 3 to 8 cm and 13 to 18 cm. The center section of the drawn sample, 8 to 13 cm, had a fibrillar structure, while the two outer pre-neck regions had spherulitic structures. Within the two-neck zones, a spherulitic to fibrillar structure transformation occurred. Note that stress whitening, which appears dark in the photographs, developed in the neck zones. Stress whitening or stress crazing is believed to be the result of small cracks forming in the sample superstructure during drawing.[75] This increases light scattering from the sample.

By defining bulk sample thickness and width compression ratios as the ratios of initial to drawn thickness dimensions and initial to drawn width dimensions, respectively, and plotting these values against equivalent BDR, it was observed that sample thickness compression exceeds width compression at BDR values of approximately 4.5, see Figure 16. This indicates that large non-affine deformation was occurring in the bulk sample at this point, i.e., the spherulites in the sample superstructure probably were not deforming uniformly with respect to their internal position within the bulk structure. This gross inhomogeneous deformation probably causes separation by macro-slipping of spherulites.

Micro-observations in the Pre-neck Region. In the sample pre-neck region which underwent almost no permanent deformation, the BDR was only slightly greater than one. This part of the drawn sample is referred to as the 1.0 BDR region. When side views of the quenched crystallized 1.0 BDR structure were examined with both the polarizing light and scanning

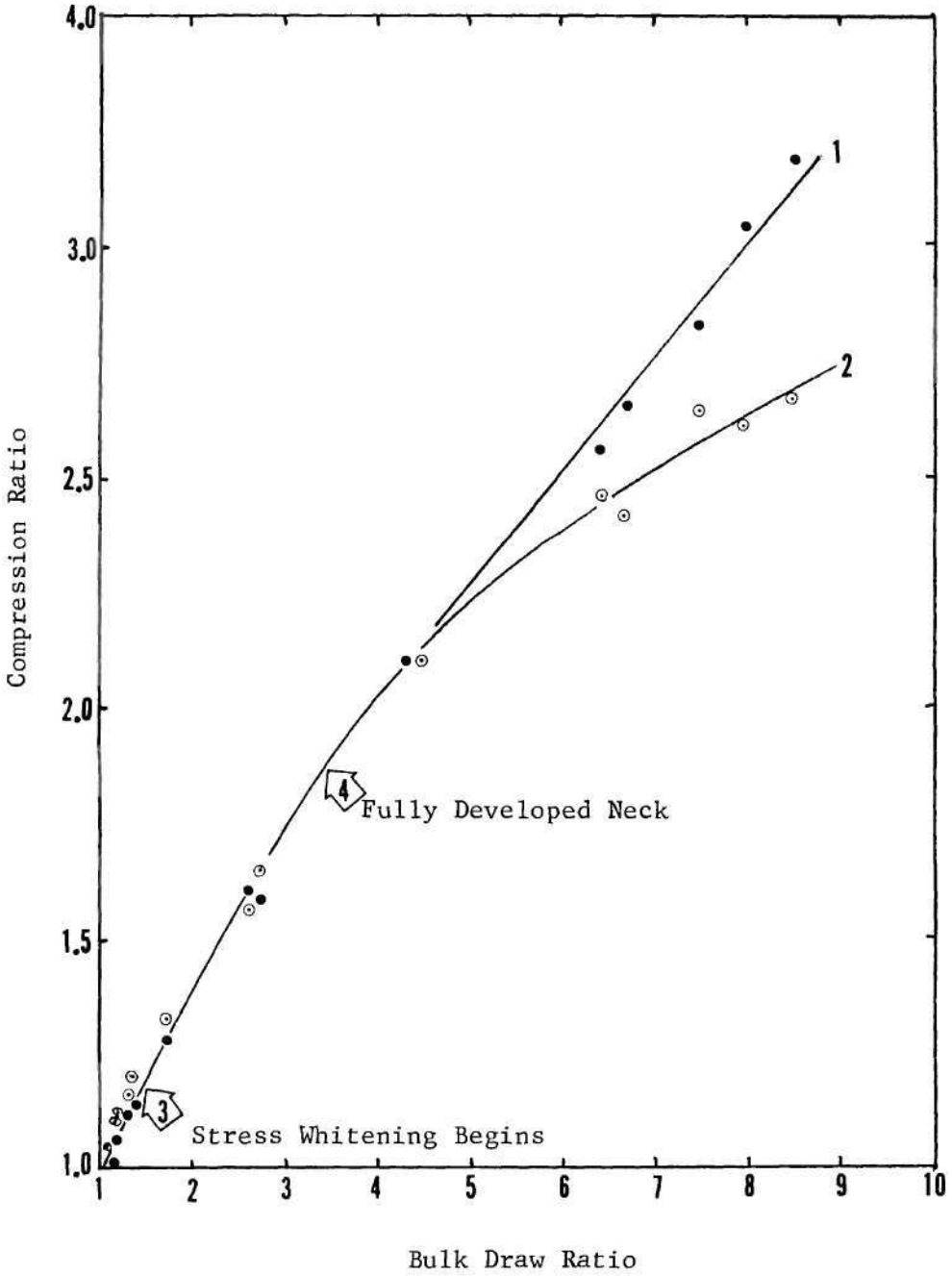

Figure 16. Dimensional Changes During Cold Drawing at 60°C [Curves: 1) Width Compression and 2) Thickness Compression]

electron microscopes, a structural gradient was observed. Figures 17 and 18, light and scanning electron photomicrographs, show a surface to centerline gradient of: 1) a transcrystalline surface structure, zero to 50 microns, 2) a ring spherulite structure zone where ring spacing increases with increasing sample depth, 50 to 900 microns, 3) a spherulite structure zone having incomplete rings, 900 to 1400 microns, and 4) a spherulite structure zone with no rings, 1400 microns to the sample centerline, 2850 microns. The quenched bulk sample structures were symmetric about their thickness centerline. This structural gradient was formed during the quenched crystallization process and was due to an increase in the overall heat transfer resistance as the melt crystallized from the surface toward the sample centerline. Polymer melt at the surface crystallized much faster and at a lower temperature than melt positioned within the sample.

At the sample surfaces, a high crystallization rate coupled with a large number of primary nucleation sites produced a transcrystalline structure. The larger number of primary nucleation sites was due to heterogeneities introduced at the surface by the tetrafluoroethylene release agent sprayed onto the crystallizer's aluminum support plates. Fitchman and Newman[27] have noted similar transcrystalline surface structures when isotactic polypropylene was melt crystallized against a Teflon surface. During transcrystallization, when so many nucleation sites are crowded together at one plane, lamellar growth from these sites in the lateral direction is inhibited and almost all growth is in the transverse direction into the bulk sample. Because of the rapid crystallization rate in this region, crystallinity is low and the lamellae formed are small

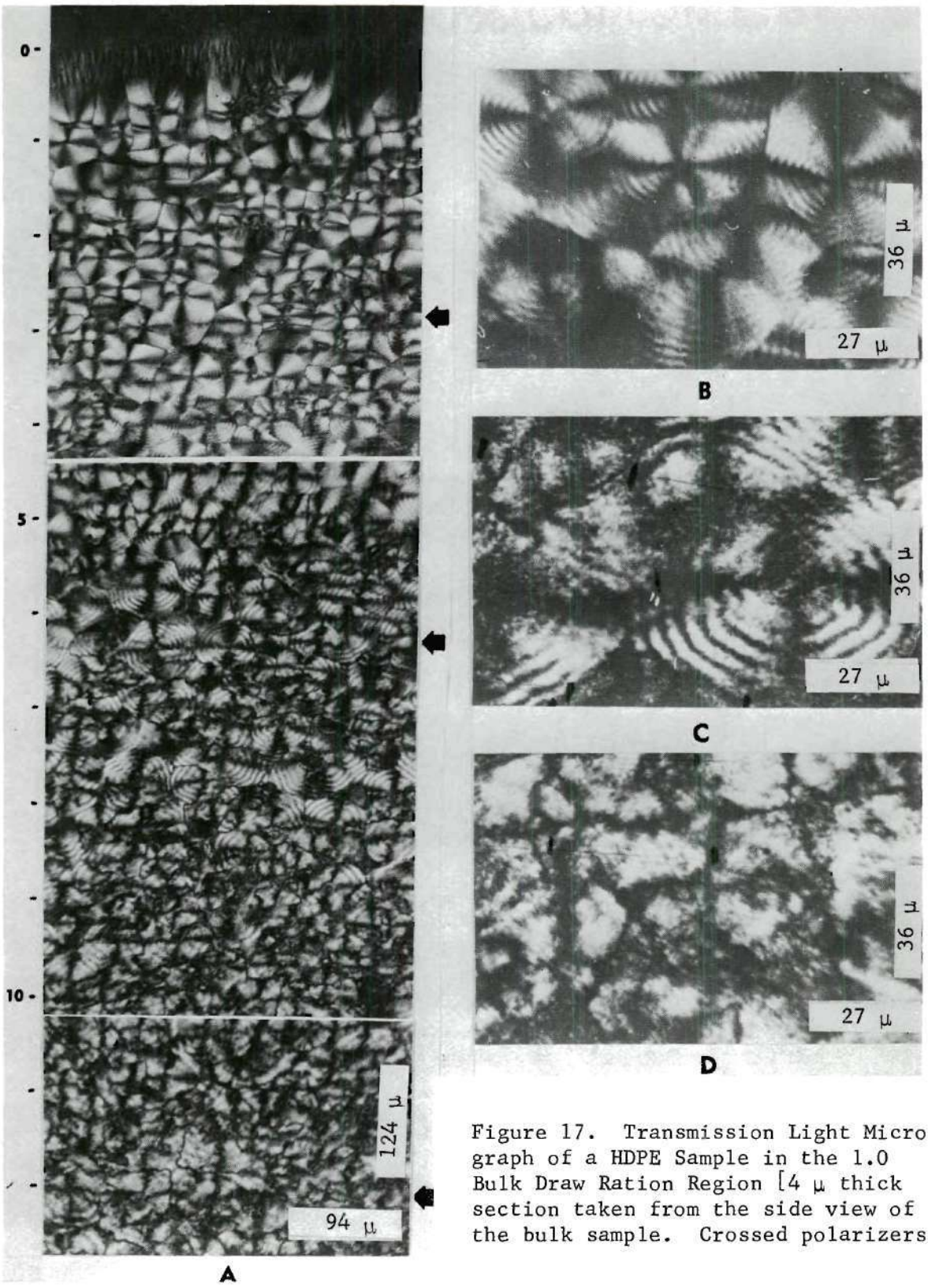

Figure 17. Transmission Light Micrograph of a HDPE Sample in the 1.0 Bulk Draw Ration Region [4 μ thick section taken from the side view of the bulk sample. Crossed polarizers.]

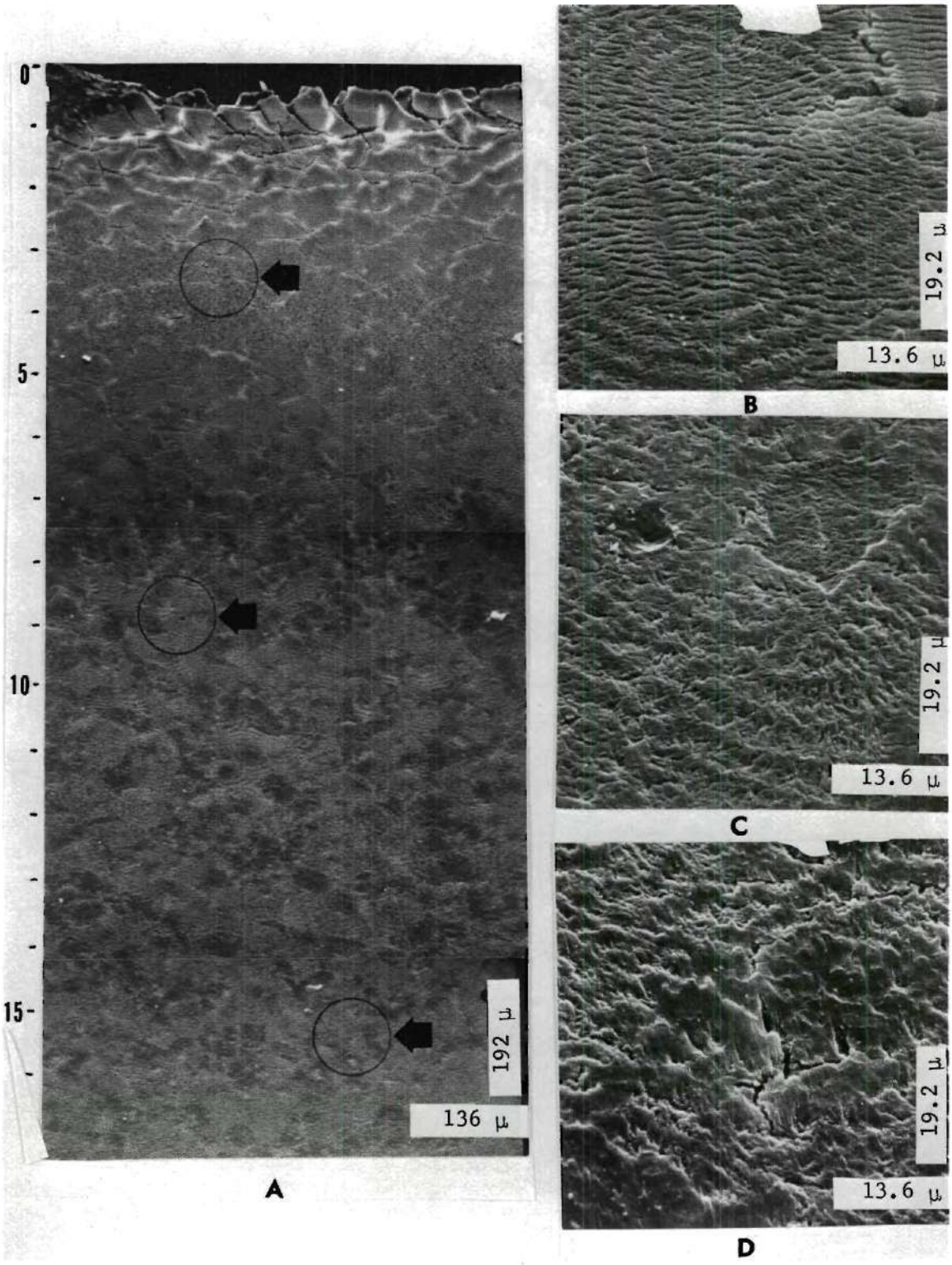

Figure 18. SEM of a HDPE Sample Surface in the 1.0 Bulk Draw Ratio Region [Surface was etched for 108 hr in 6M chromic acid at 65°C. Side view of bulk sample.]

in lateral width. As shown in the scanning electron photomicrographs, the transcrystalline region is cracked due to a high chromic acid etching rate in this low crystallinity region. Schonhorn[100] has also observed that polyethylene surfaces when melt crystallized against polytetrafluoroethylene had low crystallinities.

In the ringed spherulite structure zone, ring spacing increases with increasing penetration into the sample. This effect was observed in both the polarized light and scanning electron photomicrographs. In the light photomicrographs, rings are due to birefringence extinction as lamellae twist in concert.[30] However, the rings in the scanning electron photomicrographs are due to regular, circular surface relief features exposed by the surface etching process. Lindenmeyer and Holland[64] observed that, for thin MARLEX 6050 HDPE films, ring spacing increased with decreasing lamellar growth, i.e., a slower crystallization rate. Thus, the decrease in bulk crystallization rate with increasing penetration into the sample can be related to an increase in spherulite ring spacing.

Using the differential scanning calorimeter (DSC), 270 micron thick MARLEX 6050 HDPE films were crystallized from the melt at known cooling rates. These films were microtomed for thin cross sections. From observations of these thin sections with a polarizing microscope, spherulite ring spacings were measured and related to the DSC cooling or crystallization rate. Figure 19 compares ring spacing measurements made from the quenched crystallized bulk samples and ring spacing measurements made from the DSC crystallized film samples. Analysis of this comparison shows that the surface of the bulk crystallized samples experienced rapid cooling rates while the polymer crystallized below the surface was cooled slower.

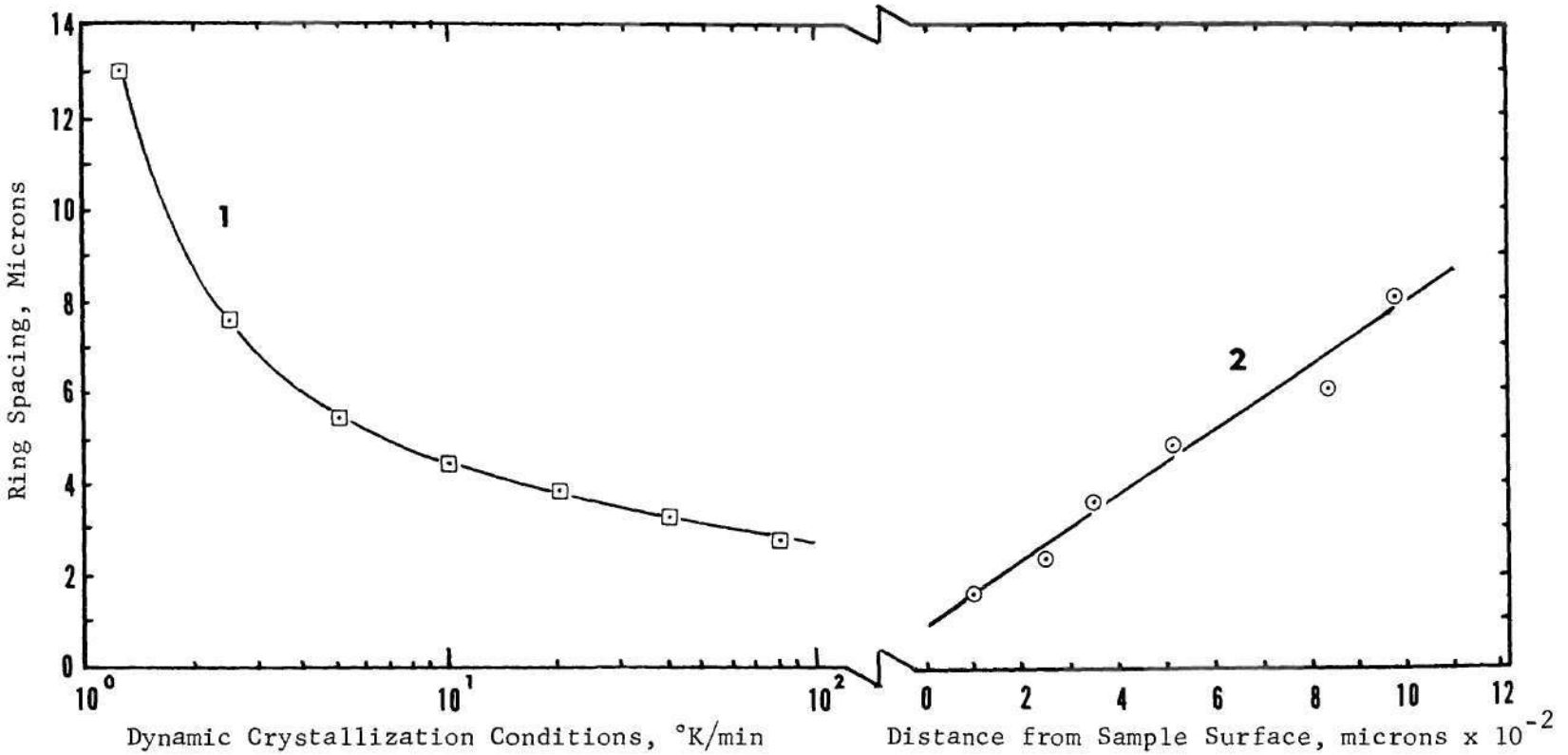

Figure 19. Spherulite Extinction Ring Spacing [Curves: 1) DSC Dynamically Crystallized Samples; 2) Air Quenched Crystallized Bulk Samples]

Apparently, a spherulite structure with complete rings cannot form at cooling rates less than $1^{o}C/min$. This cooling rate occurs at approximately one millimeter from the quenched sample surface.

In the sample region between 900 and 1400 microns from the top surface, spherulites with incomplete ring structures were formed. The ring spacing in this region was larger, and it appears that lamellae are unable to maintain a close concert of twist. At the lower portion of this region, spherulite structures having a splayed construction were formed. These spherulites have a similar structural appearance to those found in the brittle bulk samples formed by isothermal crystallization.

Close examination of both light and scanning electron photomicrographs of the structure of the 1.0 BDR samples revealed that the average diameter of spherulites found in any region, top to centerline, is approximately constant. This fact can be explained only by meeting all of the following conditions: 1) the number of primary nucleation sites for crystallization was the same throughout the bulk structure, i.e., the melt contained pre-existing nuclei, 2) lamellar growth from each primary nucleation site in any one region was started at approximately the same time, 3) the primary lamellar growth rate at each site in a region at any time was approximately constant, and 4) if lamellae growing from neighboring spherulites approach one another prematurely, then these spherulites separated in the melt in such a way as to maintain their growth. Thus, as a close approximation, a structure of perfectly packed uniform size spherulite exists when the growing spherulites first impinge with one another. Of course, after initial impingement some lamellae of the

spherulites continued to grow into the melt still existing between spherulites. This continuation of lamellar growth after initial impingement will be called post primary crystallization so it can be distinguished from secondary crystallization.

When a plane is passed through a body composed of uniform size spheres, the plane formed will contain circles having diameters equal to or less than the diameter of the spheres. If a line of given length is randomly placed on this plane and its mean intercept length with the circles on the surface is measured, $\bar{L}$, then the diameter of the spheres, d, in the three dimensional body can be calculated by the relation[107]:

$$d = \frac{6}{4} \bar{L} \tag{3}$$

In this work, a modified relation was used to compensate for the microtoming distortion introduced into the polyethylene thin sections. Thus the approximate diameter of the spherulites at impingement, d_i, was calculated by:

$$d_i = \frac{6}{4} \bar{L}_{//} f \tag{4}$$

where $\bar{L}_{//}$ is the mean intercept length of lines placed parallel to the sample top surface and f is the microtoming distortion factor, 0.87.

Also because of continued lamellar growth during the post primary crystallization period, some lamellae extend to lengths greater than that formed when the spherulites impinged. Therefore, the largest intercept lengths measured would correlate to spherulite boundaries formed from the

most extended lamellae. This maximum intercept length, $L_{//max}$, would be equal to the spherulite impingement diameter multiplied by a geometrical factor, cos 30^{o}. Figure 3 shows this geometrical relationship of perfectly packed spherulites. This relation was also used to calculate the spherulite impingement diameter, d_i, from the maximum intercept length:

$$d_i = f \frac{L_{//max}}{2} \sqrt{3} \tag{5}$$

These two independent relationships, equations (4) and (5), were used to estimate the spherulite diameter in several regions in a typical, quenched bulk sample (see Table 3). The spherulite impingement diameter in the bulk structure was found to be approximately constant at 60 microns.

From this result, the number of primary nucleation sites per unit volume of melt, ν, was calculated from the volume, V, occupied by perfectly packed spheres[110]:

$$\nu = \frac{1}{V} = \frac{1}{\frac{4}{3}\frac{\pi}{6} d_i^3} \tag{6}$$

$$\nu = \frac{9}{2\pi d_i^3} \tag{7}$$

For 60 micron diameter spherulites, the number of active heterogeneous nucleation sites for the quenched melt was calculated as $6.5 \times 10^6/cm^3$. This information was used to characterize the bulk structures observed in photomicrographs and the melt crystallization kinetics.

The polarized light photomicrographs of Figure 20 show a side view of the bulk sample in the pre-neck vicinity where only a small amount of

Table 3. Spherulite Diameter

Distance from Surface† (Microns)	Mean Intercept Length (Microns)	Largest Mean Intercept Length (Microns)	Calculated Spherulite Diameter† (Microns)	Spherulite Diameter Calculated from Largest Intercept Length† (Microns)
70- 230	43	88	56	68
230- 460	42	90	55	69
460- 690	45	83	59	64
690- 920	46	80	61	62
920-1150	53‡	91	69‡	70
1150-1400	56‡	77	73‡	59
		Average Diameter	62 μ	65 μ

†Corrected for Distortion produced by microtoming (see page 33).

‡Observation of small intercept lengths was difficult due to poorly defined spherulite shape, i.e. probably biased to larger than actual mean length values and therefore larger diameters.

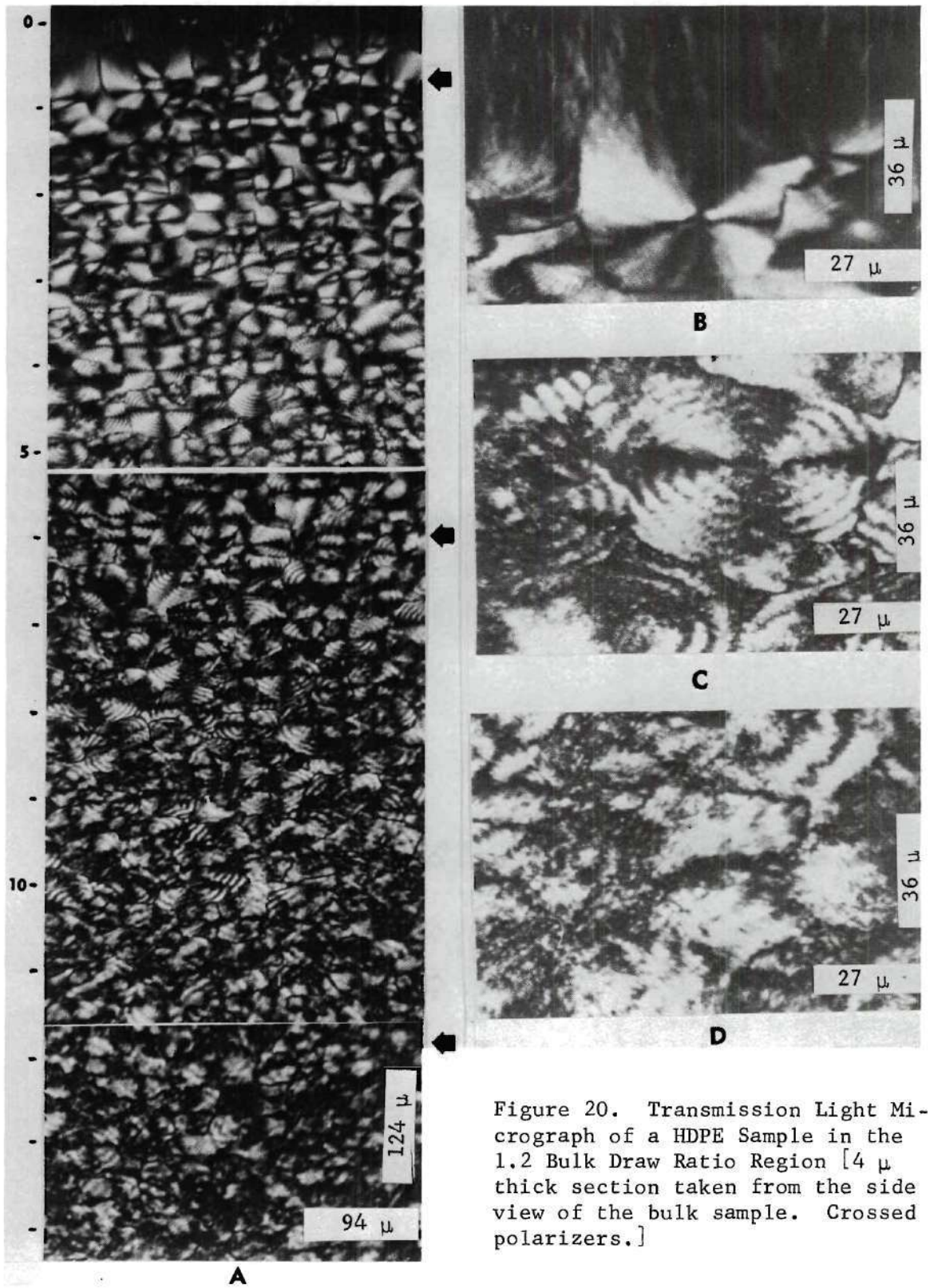

Figure 20. Transmission Light Micrograph of a HDPE Sample in the 1.2 Bulk Draw Ratio Region [4 μ thick section taken from the side view of the bulk sample. Crossed polarizers.]

permanent deformation has occurred. This sample region has a 1.2 BDR. Examination of these photomicrographs showed that, in this region, the spherulite ring structures were beginning to slide past one another and collapse laterally to become slightly ellipsoid in shape. The long axis was oriented parallel to the draw direction.

Micro-observations in the Neck Zone. In the ring spherulite structure region, 0 to 1300 microns from the sample surface, the local spherulite draw ratios were determined from ring spacing measurements taken from light photomicrographs. Ring spacing measurements parallel and normal to the draw axis were corrected for the microtoming distortion introduced during sectioning. The ratio of the parallel to normal ring spacing measurements for a single spherulite when taken to the two-thirds power represents the local draw ratio if affine deformation was occurring.[60] These deformation calculations for the spherulite ring structure region at sample points in the 1.0, 1.2, 1.5, 1.75, 3.0, and 4.0 BDR vicinities are listed in Table 4. These calculations show that the local draw deformation of single spherulites in the ring spherulite structure region was variable from spherulite to spherulite but always less than the overall bulk deformation. Therefore, deformation in the center portion of the bulk sample, i.e., the splayed spherulite structure region, was greater than the overall bulk deformation. Apparently sample deformation was not uniform with respect to the sample thickness direction. A local draw ratio gradient exists through the bulk sample due to the superstructure variation in the thickness direction. Relative to one another, spherulites also appear to be sliding in the draw direction, i.e., a strain profile exists in the sample thickness direction.

Table 4. Spherulite Ring Spacing vs Draw Ratio and Position, Ductile Draw Sample

Approximate Bulk Draw Ratio	Approximate Distance from Top Surface*, Microns	Distance from Top Surface Relative to Undrawn State, Microns	Measured Ring Spacing, Microns DD†	LD‡	Thin Section Distortion Factor f	Ring Spacing*, Microns (DD)f	LD/f	Draw Ratio** from Ring Space Measurements $(DD/LD)^{2/3}f^{4/3}$
1.0	92	92	2.00	1.27	.80	1.60	1.60	1.0
1.0	115	115	2.66	2.30	.93	2.48	2.48	1.0
1.0	352	352	3.21	2.62	.91	2.92	2.92	1.0
1.0	444	444	4.00	3.20	.90	3.60	3.60	1.0
1.0	675	675	5.30	4.00	.87	4.61	4.61	1.0
1.0	750	750	7.00	5.30	.87	6.10	6.10	1.0
1.0	910	910	8.0	6.0	.87	7.0	7.0	1.0
1.0	1360	1360	–	13.0	.87	-	14.80	-
1.2	92	100	1.84	1.14	.80	1.45	1.42	1.02
1.2	150	160	2.00	1.60	.94	1.88	1.70	1.07
1.2	270	285	3.00	2.68	.92	2.76	2.92	0.97
1.2	396	415	3.55	2.65	.90	3.20	2.95	1.05
1.2	605	635	8.0	6.0	.87	6.95	6.90	1.00
1.2	780	820	9.0	6.5	.87	7.85	7.45	1.03
1.2	1210	1270	14.0	-	.87	12.2	-	-
1.5	115	140	2.30	2.0	.94	2.17	2.13	1.01
1.5	195	240	2.68	1.23	.92	2.47	1.34	1.50
1.5	380	465	3.20	2.00	.87	2.78	2.30	1.13
1.5	655	800	6.42	4.0	.87	5.60	4.60	1.13
1.5	1080	1320	11.0	6.0	.87	9.6	6.9	1.25
1.75	115	150	2.00	1.20	.93	1.86	1.29	1.32
1.75	257	335	3.2	2.00	.87	2.79	2.30	1.13
1.75	518	680	5.35	4.00	.87	4.65	4.60	1.00

Table 4. Continued

1.75	620	810	6.00	5.00	.87	5.20	5.75	0.93
1.75	862	1080	8.00	5.00	.87	6.95	5.75	1.13
3.0	128	225	3.08	2.00	.90	2.8	2.2	1.15
3.0	253	450	4.00	2.00	.87	3.5	2.3	1.32
3.0	345	610	4.00	2.40	.87	3.5	2.75	1.17
3.0	520	920	7.00	4.00	.87	6.1	4.6	1.20
4.0	144	305	8.00	2.00	.87	6.95	2.3	2.1
4.0	230	490	7.00	2.00	.87	6.10	2.3	1.9

†DD - Draw Direction

‡LD - Normal to Draw Direction

*Corrected for thin section distortion during microtoming (see page 33).

**Draw Ratio calculated assuming affine deformation.[60]

In the neck zone, from a 1.5 to 8.0 BDR, a rapid decrease in the bulk sample's cross-sectional dimensions occurred and the structure was transformed from spherulitic to fibillar. The spherulites with ring structures were easily measured for local microdraw deformation. However, the local microdraw deformation in the splayed spherulite structures was not determined because these structures do not have discernible rings or definite boundaries that can be easily distinguished from either light or scanning electron microscopic observations.

Figures 21 and 22 show light photomicrographs taken from side views of the bulk structure at the 1.75 and 3.0 BDR regions, respectively. Again the bulk structure gradient in the thickness direction can be observed easily. Spherulites are continuing to elongate by shear deformation in the draw direction and are becoming ellipsoidally shaped. Ring spacing measurements indicate that local microdraw deformation was not uniform from spherulite to spherulite or even within a single spherulite and that the ring spherulite structures were on the average not deforming as rapidly as the overall bulk sample (see Table 4). Although microvoid formation has been observed in cold drawn samples of HDPE thin films[18,34,91] and high pressure crystallized rods,[75] no voids in the spherulite superstructures were observed by light microscopic examination of the bulk samples at the 1.75 and 3.0 BDR regions.

Scanning electron photomicrographs of etched, side-view bulk surfaces at the 3.0 and 4.0 BDR regions are shown in Figures 23 and 24, respectively. The bulk spherulite structure gradient is easily observed, but the microcracks between and through spherulites of the type previously detected from light microscopic observations of drawn thin films[18,34] are

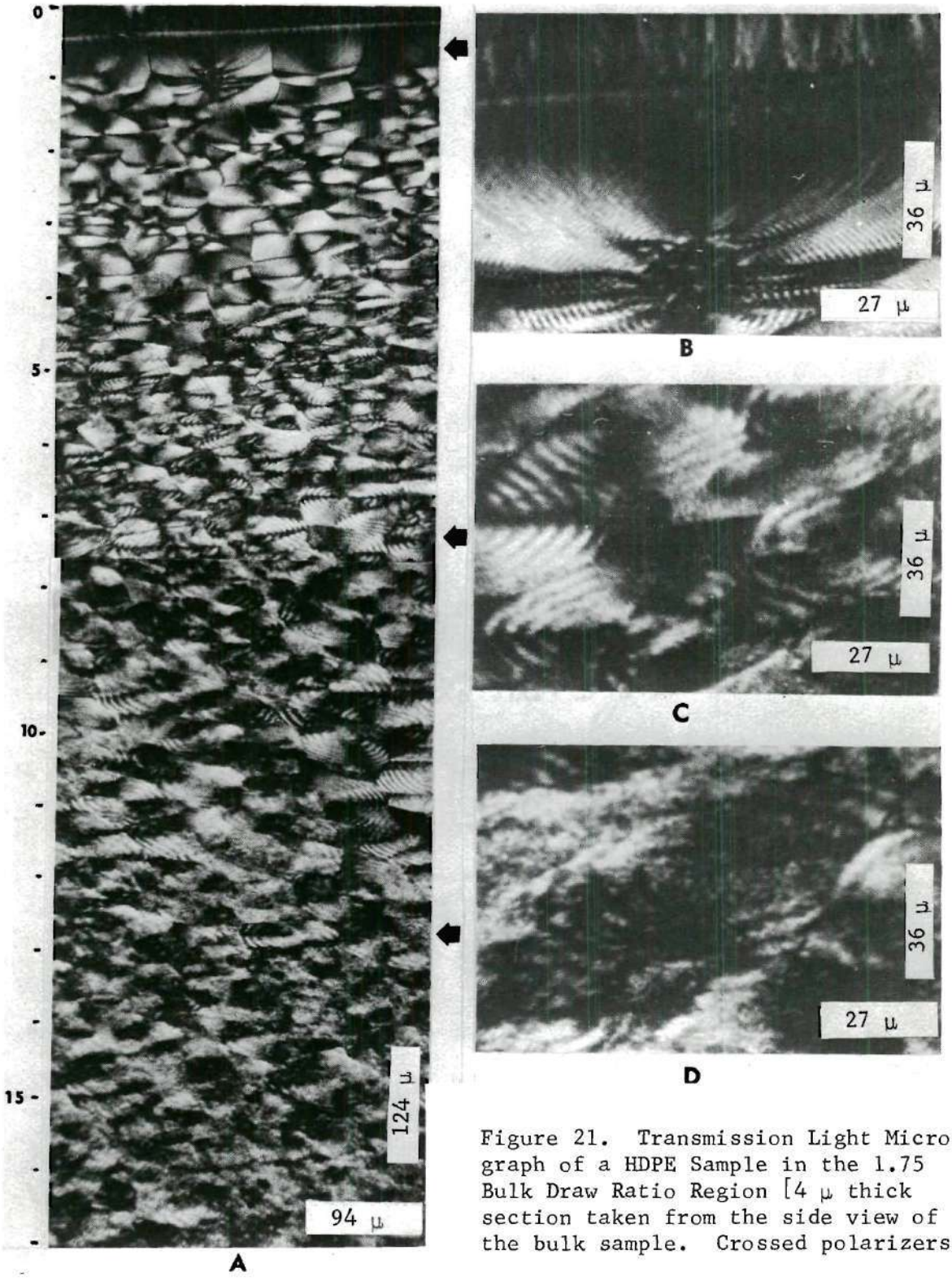

Figure 21. Transmission Light Micrograph of a HDPE Sample in the 1.75 Bulk Draw Ratio Region [4 μ thick section taken from the side view of the bulk sample. Crossed polarizers.]

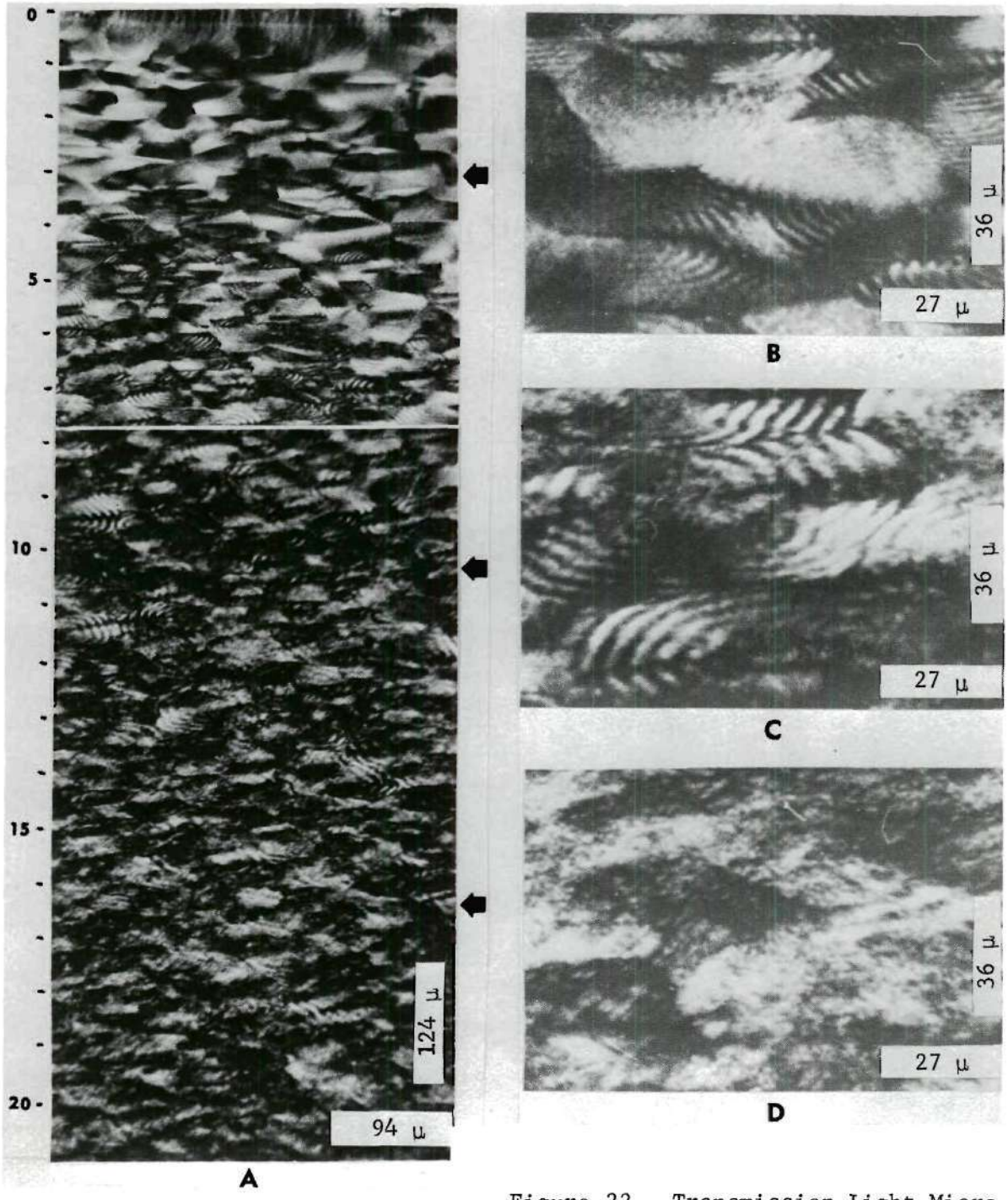

Figure 22. Transmission Light Micrograph of a HDPE Sample in the 3.0 Bulk Draw Ratio Region [4 μ thick section taken from the side view of the bulk sample. Crossed polarizers.]

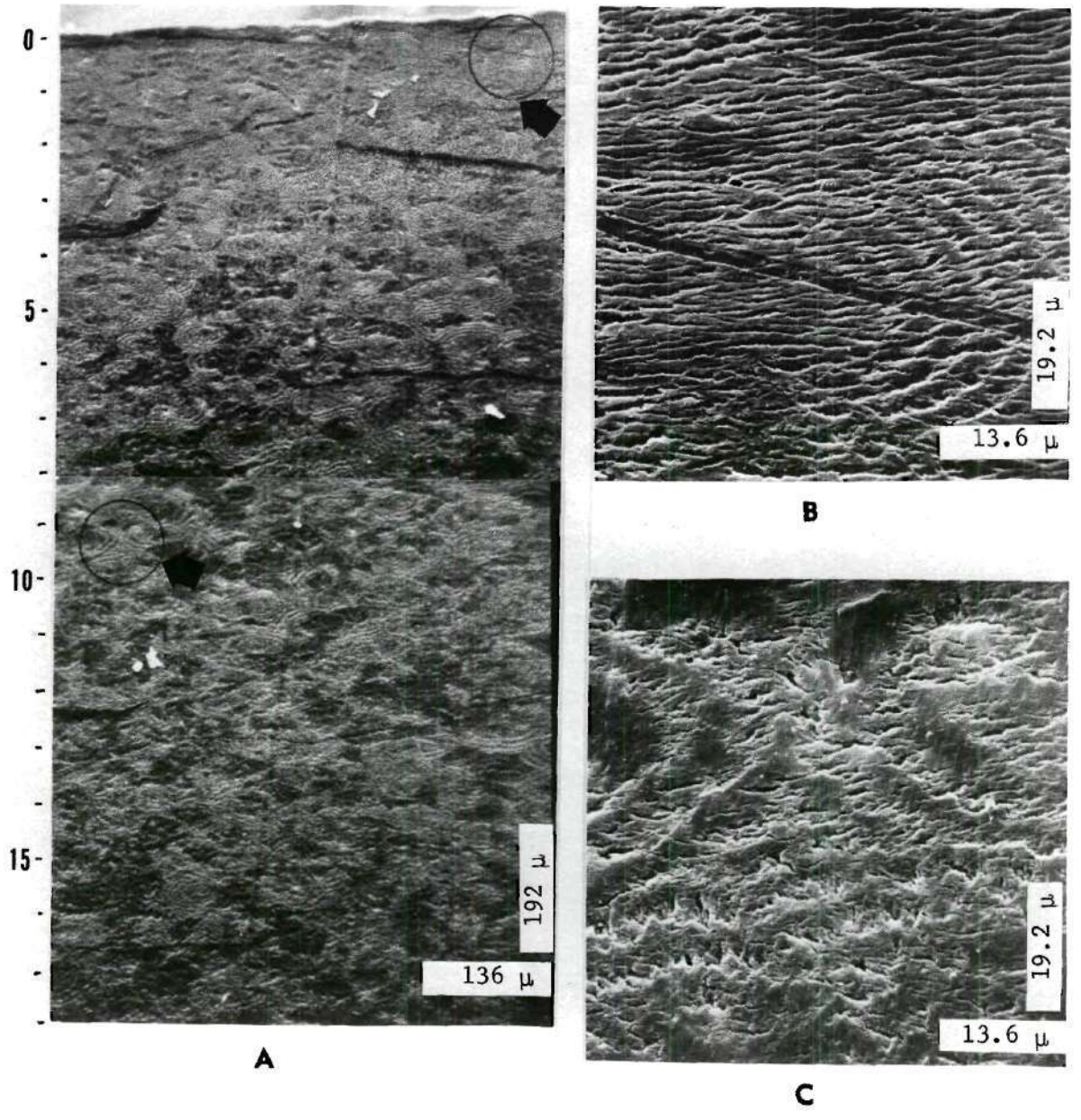

Figure 23. SEM of a HDPE Sample Surface in the 3.0 Bulk Draw Ratio Region [Surface was etched for 108 hr in 6M chromic acid at 65°C. Side view of bulk sample.]

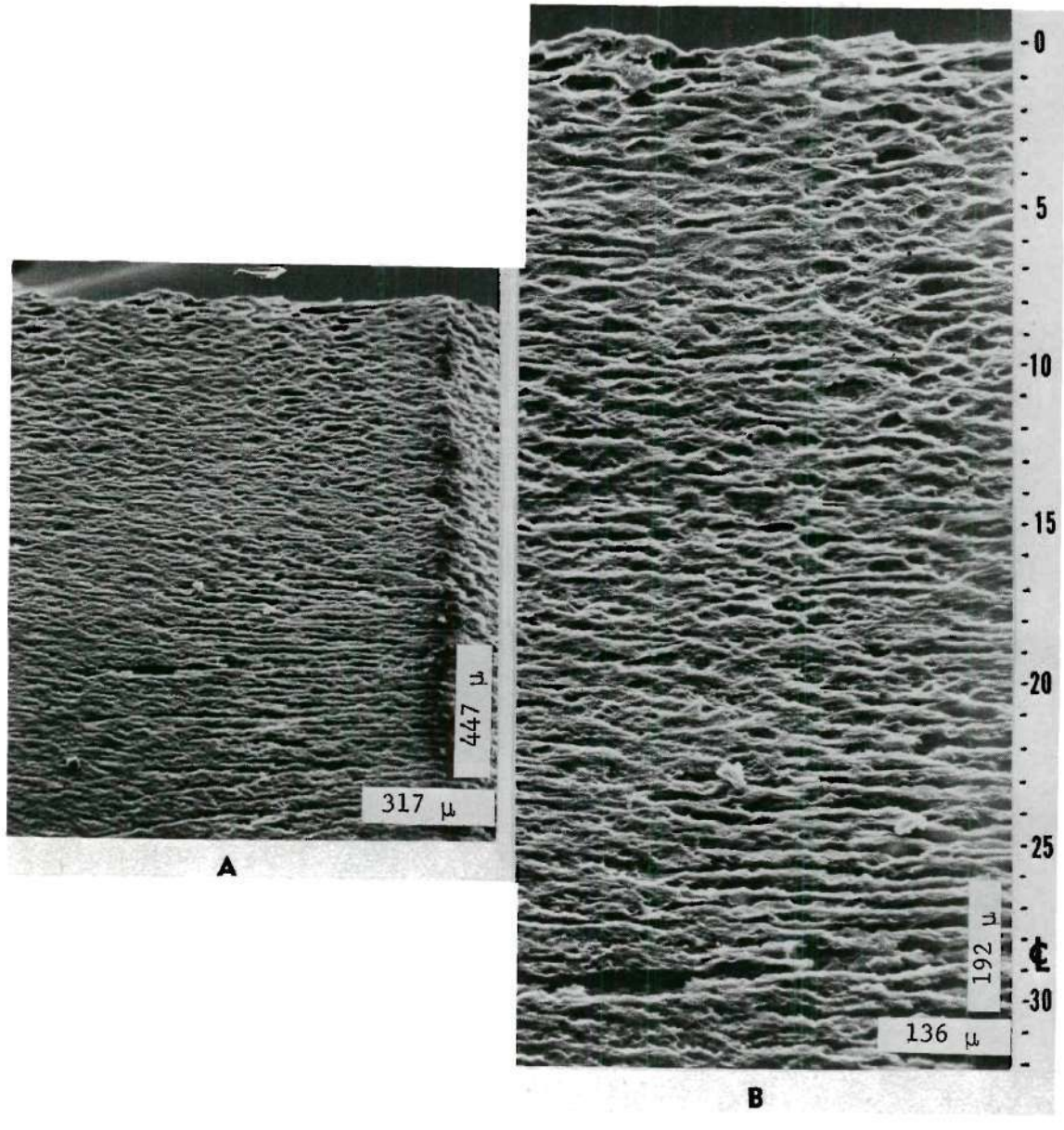

Figure 24. SEM of a HDPE Sample Surface in the 4.0 Bulk Draw Ratio Region [Surface was etched for 310 hr in 6M chromic acid at 60°C. Side view of bulk sample.]

apparently not present. However, a multitude of small openings are present which separate pockets of lamellar bundles radiating from the spherulite centers. These openings are probably formed during the etching process from the removal of the less crystalline material that collects between lamellar bundles during crystallization.

Figure 24 shows a sample surface at the 4.0 BDR region after extensive chromic acid etching. This sample was etched for 310 hours, three times the normal treatment. Voids are present in the sample center section, i.e., in the splayed spherulite region. These voids are greatly elongated in the draw direction. Structure transformation is more pronounced near the centerline than near the surface. At the centerline, drawn spherulites appear to split into individual sections separated by elongated voids. Thus, cold draw deformation with formation of a striated structure starts at the centerline region with deformation decreasing toward the bulk sample surfaces. Apparently the splayed spherulites formed by slow crystallization in the interior region are more easily deformed during cold drawing than are the ringed spherulite structures formed by more rapid crystallization in the bulk sample exterior regions.

Because of the geometry of the neck region in the drawn tensile samples, a greater proportion of the stress during elongation was probably transmitted through the sample's interior regions. Because of this stress distribution, the internal splayed spherulite superstructures underwent a strain rate which was larger than the ringed spherulite superstructures found in the sample's exterior regions. Also, these splayed spherulites probably contained fewer molecular tie groups, which give structural strength, than the ringed spherulites. This combination of

high strain and weak superstructure probably produced the larger deformation of the quenched crystallized sample's interior regions. Also during elongation, the stronger and less strained ringed spherulite structures found externally probably acted as a supporting jacket to prevent brittle fracture of the internal superstructure.

Densitometry

Bulk Sample Macrostructure

Densities of the isothermally and quenched bulk crystallized samples before cold draw deformation are given in Table 2. The isothermally crystallized samples, which showed brittle fracture when strained, have higher densities than the dynamically or quenched crystallized samples which showed ductile deformation when extended. The higher densities of the isothermal samples reflect a higher degree of molecular order in the superstructure. Along with an increase in molecular order, apparently the number of tie molecules in the sample superstructure has decreased and thereby lowered the isothermally crystallized bulk sample's resistance to brittle fracture. In contrast, the quench crystallized samples have less molecular order than the isothermal samples as measured by densities. Apparently the quenched HDPE has a larger number of tie links than the isothermal HDPE. Secondary crystallization has been restricted in the quenched bulk samples; this may be the cause of lower order and increased tie links. During quench crystallization, the polyethylene samples are not exposed for extended time periods to high temperatures after primary crystallization. Because of this, secondary crystallization is not as complete in the quenched bulk samples as in the isothermally crystallized

samples.

Densities of isothermal and quenched polyethylene are plotted versus heat of melting data measured by DSC in Figure 25 together with similar data for DSC dynamically crystallized film samples. To a first approximation densities and heat of melting are directly related to the degree of sample crystallinity and therefore the linear best fit of data in Figure 25 was expected. Kavesh and Schultz[44] have calculated from unit cell measurements by x-ray diffraction that the density of a perfectly crystalline polyethylene structure would be 1.001 g/cm^3 at 24°C. By extrapolation to this density, the data of Figure 25 suggest that the heat of melting of perfectly crystalline linear polyethylene would be 67.5 cal/g. This value is very similar to the values estimated by Mandelkern[67,68] and Wunderlich,[112] 70 and 68 cal/g, respectively.

Ductile Sample Bulk Superstructure

By cold sectioning the ductile polyethylene samples in thin sections from the sample top surface toward the sample thickness centerline, 15 micron thick specimens representing the various bulk superstructures at different draw ratios and sample depths were obtained and measured for densities by using a density gradient column. Densities for a typical quenched and drawn bulk sample at the pre-neck and necked regions are shown in Figure 26.

As expected, the density of the superstructures increased with increasing depth into the bulk sample. This occurred because during quenching the rates of crystallization decreased as freezing front penetrated from the sample surface toward the sample centerline. As shown by the density data in Figure 27, the more slowly crystallized structures are

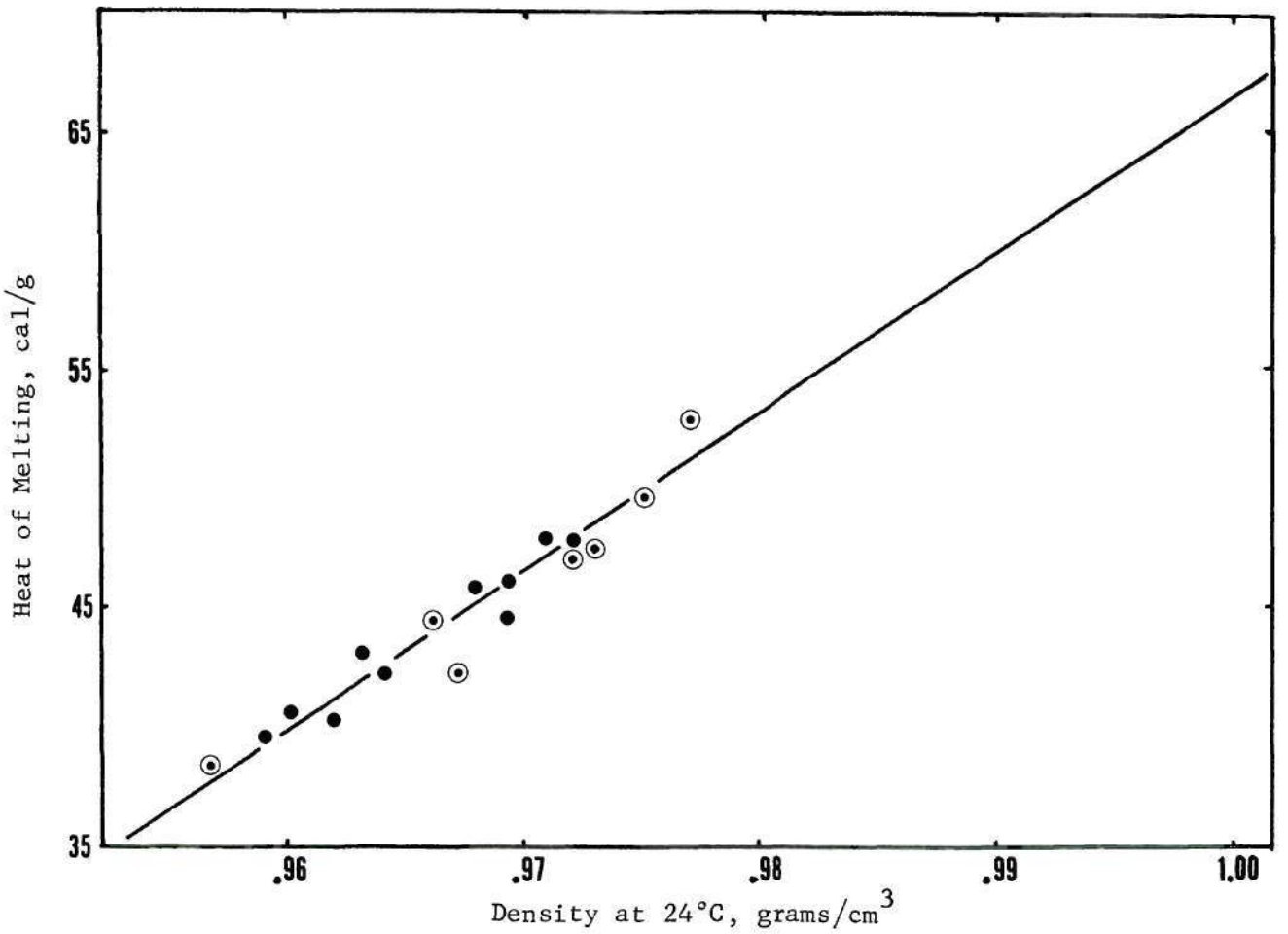

Figure 25. Heat of Melting vs Polyethylene Density [DSC Films, Black Data Points; Bulk Samples, Unblackened Data Points]

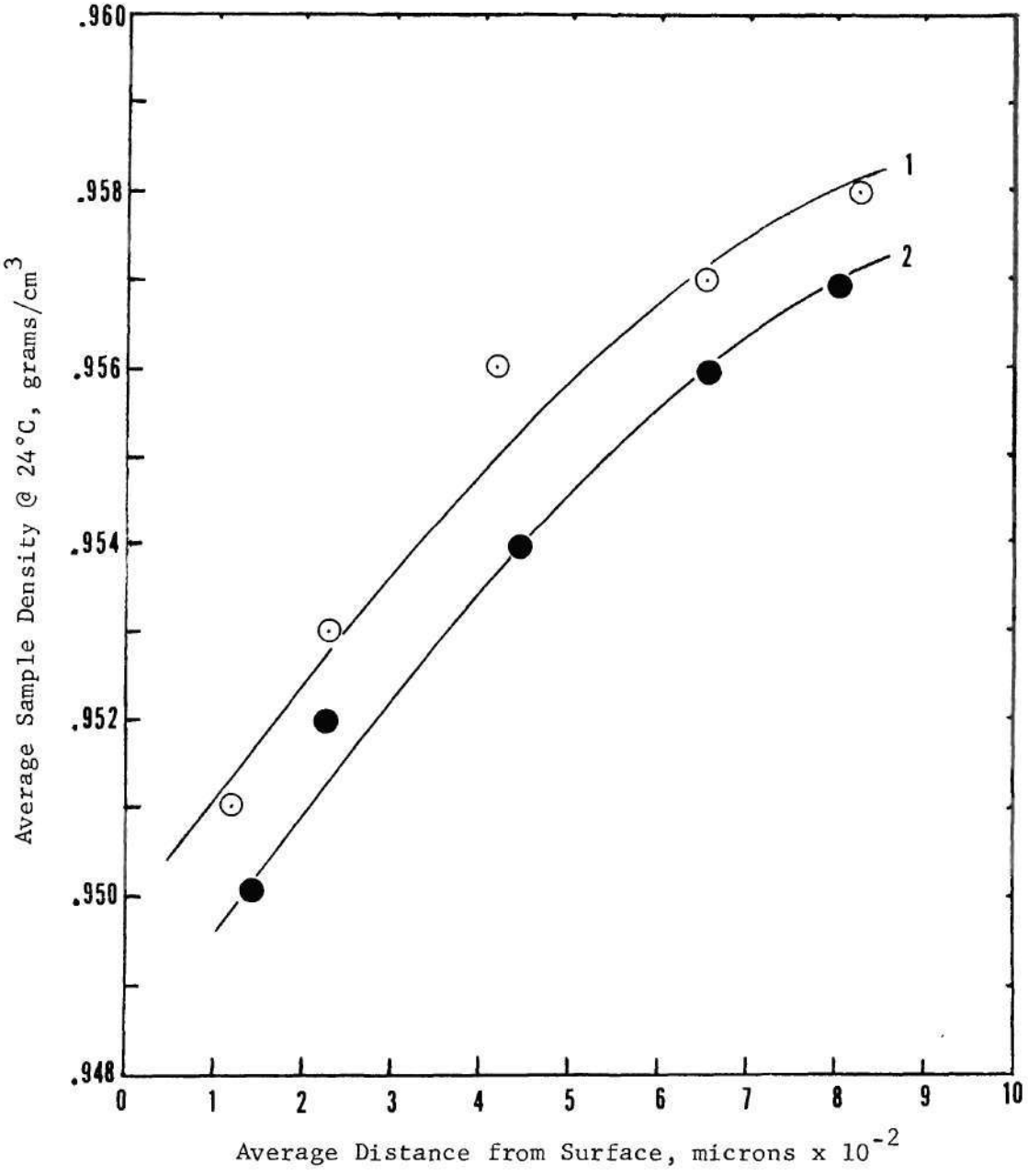

Figure 26. Density of Cold Drawn Ductile Sample [Curves: 1) 1.0 BDR, 2) 1.75 BDR. Distances are normalized to an undrawn condition.]

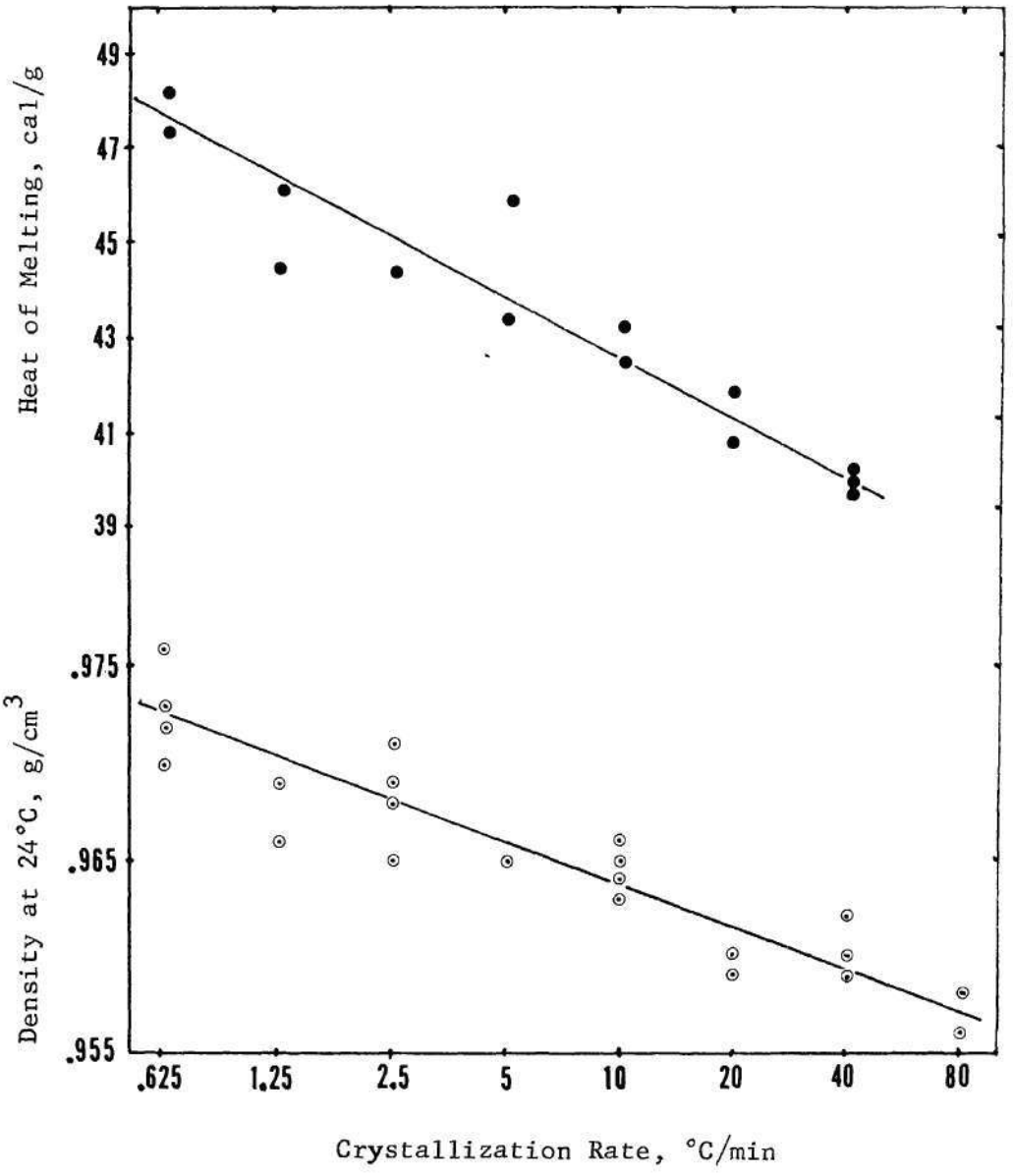

Figure 27. Properties of Polyethylene Film Crystallized Using the Differential Scanning Calorimeter

more dense. Figure 26 shows that the densities of the drawn, ring spherulite superstructures at any depth position are approximately 0.0015 g/cm^3 less dense than the corresponding superstructure in the undrawn state. This indicates that microvoids, in a volume concentration of one part per 700 parts, have formed within the ring spherulite superstructures at the onset of spherulite deformation. This crazing at small draw ratios has been noted previously for polyethylene[9,75] and polypropylene.[98] These microvoids presumably are responsible for the whitening of drawn samples in the pre-neck regions (darkening in Figure 12C) and represent the start of spherulite superstructure alignment in the draw direction.

Calorimetry

General Remarks

In past crystallization studies,[5,36,64,78,79,92] films, usually less than 25 microns in thickness, were crystallized isothermally on a hot stage microscope so that spherulite growth rates could be determined by direct visual observation. Of course this technique does not simulate the dynamic crystallization conditions usually experienced by thicker bulk polyethylene. Also, because thin samples were used, surface crystallization effects were introduced. Therefore, results from these past studies probably poorly represent the usual crystallization process.[5]

The differential scanning calorimeter (DSC) is well suited for dynamic crystallization studies and was used in this work to simulate bulk crystallization conditions. Although the polyethylene samples used in the DSC were small, 1/4 inch diameter film disks, the disk thickness, 270 microns, was much larger than the 60 micron diameter spherulite

structures which formed in the bulk samples. By using this thickness DSC sample disk, excessive surface crystallization effects were largely eliminated and the structures crystallized in the DSC sample disk were similar to the structures observed in the dynamically crystallized bulk samples.

Figure 19 shows a comparison of DSC and bulk sample superstructure ring spacings. When the DSC sample disk thickness was reduced to smaller values, 120 or 60 microns, microscopic examination of thin sections of these disks revealed surface effects not characteristic of bulk structures, i.e., incomplete ringed spherulites and large amounts of transcrystalline structures. Therefore, by using the 270 micron thick DSC sample disks, primary crystallization in bulk was simulated and studied at fixed dynamic crystallization rates. The densities and heats of melting of the dynamically crystallized DSC sample disks are shown in Figure 27. The values of these properties are comparable to those values of the bulk crystallized samples listed in Table 2 or shown in Figure 25.

Lamellar Growth Rate During Bulk Crystallization

The DSC was programmed to reduce sample temperature from the melt at a fixed rate, the scan rate, and the rate of energy absorbed by the sample during solidification was measured along with time and sample temperature. The energy thermograms obtained from dynamic crystallization in the DSC were related to the lamellar growth rate through the following analysis.

From quantitative examinations of bulk sample photomicrographs it was shown previously that dynamic crystallization of MARLEX 6050 HDPE melt occurred by a process in which almost all primary nucleation sites

form instantaneously and that three dimensional growth from each site in a local area is uniform. This approximates a bulk spherulite superstructure as being one of perfectly packed, equal diameter spheres. Using this model, the energy of crystallization was taken to be the energy absorbed by one spherulite multiplied by the total number of identical spherulites which simultaneously are forming and growing in the DSC sample.

Figure 28 shows a typical DSC thermogram of a HDPE sample disk dynamically crystallized from the melt at $10^{o}C/min$. Point A indicates the start of measurable crystallization by spherulite growth. From the model standpoint, point B, the maximum rate of energy release, represents the start of all spherulites colliding or impinging upon one another. After this impingement, additional energy is absorbed by post primary crystallization of the melt located between the impinged spherulites. This energy, calculated from a packed sphere volume relationship, is approximately one third of the energy absorbed during primary crystallization up to the time of spherulitic impingement, i.e., area ABEA is approximately three times as large as area EBCDE. Line AEDF, the DSC thermogram baseline, represents zero release of crystallization energy, i.e., no sample crystallization. Area DCFD represents the energy absorbed during secondary crystallization of the melt which remained between the crystallized lamellae formed during primary crystallization.

For three dimensional free growth of a single spherulite from a point nucleus, the differential energy balance for primary crystallization is:

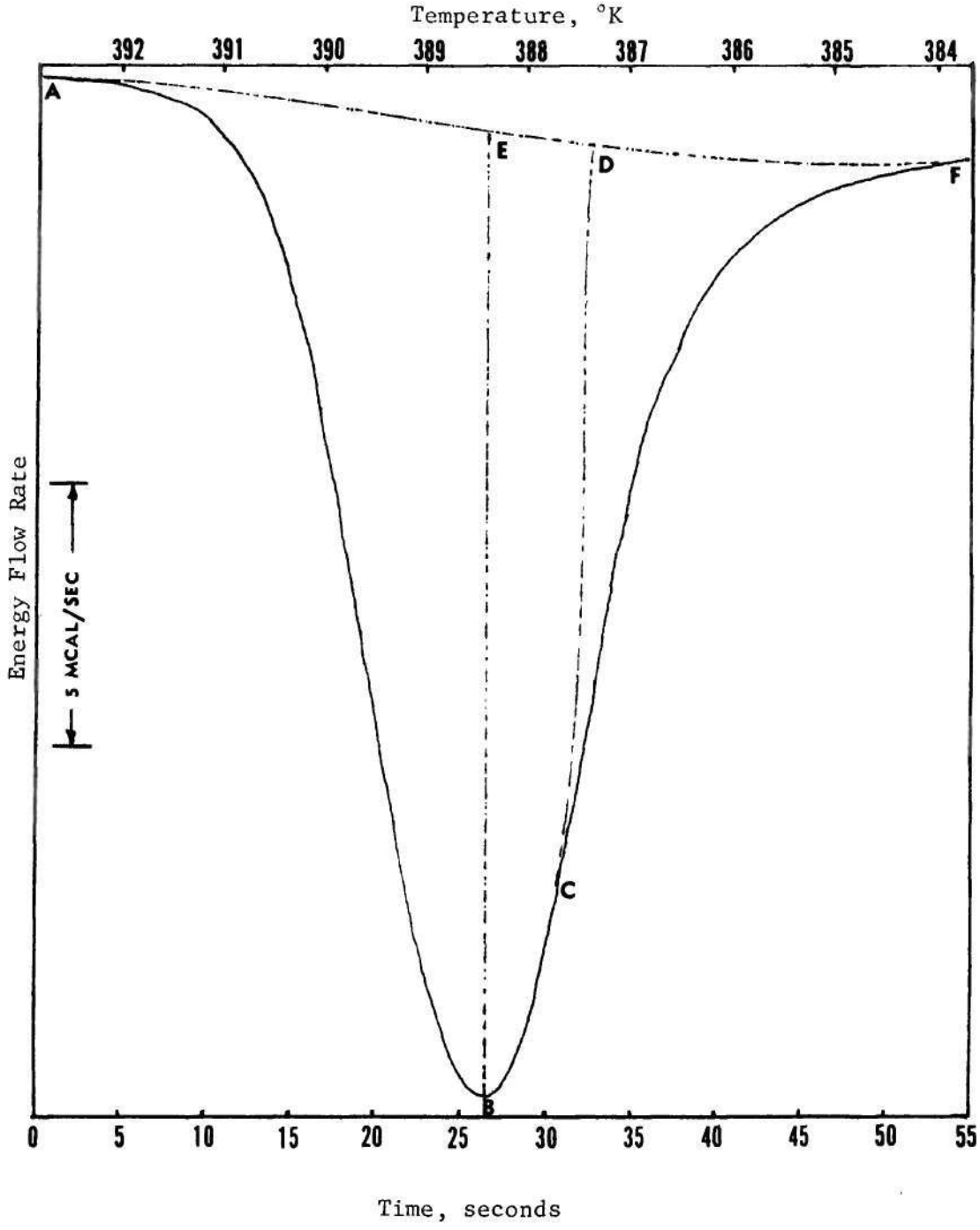

Figure 28. Dynamic Crystallization DSC Thermogram

$$\partial H = \rho_c \lambda \beta \frac{\pi}{2} d^2 \partial d \tag{8}$$

where H, ρ_c, λ, d, and β are, respectively, the enthalpy, crystal density, heat of crystallization, spherulite diameter, and volume fraction of the growing spherulite that is occupied by crystallized material. The change in a spherulite's diameter can be expressed as a function of the time of crystallization, θ, and the spherulite's radial growth rate, G. At the start of measurable crystallization, time is set equal to zero.

$$\partial d = 2G \partial\theta + 2\theta \partial G \tag{9}$$

At the beginning of crystallization, the radial growth rate is approximately constant. Therefore at the start of crystallization, the second term of equation (9) is the product of two small values and, consequently, is small compared to the first term and can be neglected. Thus, equation (9) can be approximated by:

$$\partial d \simeq 2G \partial\theta \tag{10}$$

and

$$d \simeq 2G\theta \tag{11}$$

Substitution of equations (10) and (11) into equation (8) gives an energy balance equation for the formation of a single spherulite:

$$\frac{\partial H}{\partial \theta} \simeq 4\pi\rho_c\lambda\beta G^3\theta^2 \tag{12}$$

The total number of spherulites in a DSC sample, N, is equal to the number of primary nucleation sites per unit volume, ν, and the DSC sample weight, W, by the relation:

$$N = \frac{W}{\rho_c} \nu \tag{13}$$

The number of nucleation sites was inversely proportional to the cube of the diameter of the growing spherulites at the moment of impingement, d_i (see equation (7), page 64), Thus combining equation (7) with equation (13), the rate of energy absorption at the onset of primary crystallization would be N times the energy absorbed by one spherulite or:

$$\frac{dH}{d\theta} = 18W\lambda\beta G^3\theta^2 d_i^{-3} \tag{14}$$

When spheres of equal diameter are perfectly packed, approximately 75% of the total volume is occupied by the spheres. The remaining volume is space between spheres. Therefore, approximately 75% of the total DSC sample volume is occupied by the spherulites at the moment of impingement, or when the spherulites have a diameter of approximately 60 microns. Using the sphere packing relationship, the structural factor, β, was defined from an energy-volume consideration:

$$\beta = \left(\int_{\theta=0}^{\theta_i} \frac{dH}{d\theta} \, d\theta \right) / \frac{3W\lambda}{4} \tag{15}$$

The numerator of equation (15) is the cumulative energy absorbed from the start of crystallization to the time of spherulite impingement, e.g., area

ABEA of Figure 28. The denominator is the energy that would be absorbed if all the material within the spherulites at the time of impingement was perfectly crystalline. By this mathematical definition, the structural factor, β, represents the fraction of polyethylene molecules actually involved in formation of the spherulite superstructures during primary crystallization. In past HDPE isothermal crystallization studies,[38] this factor was usually calculated as about one half. In this study, β ranges between 0.3 and 0.4.

Combination of equations (14) and (15) gives:

$$\frac{dH}{d\theta} \cong 24G^3\theta^2 d_i^{-3} \int_{\theta=0}^{\theta_i} \frac{dH}{d\theta}\, d\theta \qquad (16)$$

Solving equation (16) for the radial growth rate gives the working equation:

$$G \cong \frac{1}{2} \frac{d_i}{\sqrt[3]{3}}\, \theta^{-2/3} \left(\frac{dH}{d\theta}\right)^{1/3} \left(\int_{\theta=0}^{\theta_i} \frac{dH}{d\theta}\, d\theta\right)^{-1/3} \qquad (17)$$

If the impingement diameter is known, equation (17) can be used to determine the instantaneous lamellar growth rate at the start of primary crystallization directly from DSC data. However, equation (17) is accurate only if spherulites do form simultaneously and grow at the same rate; therefore, impinging on one another at the same time. HDPE appears to behave this way.

Hoffman and co-workers[38,39,40] have shown that primary crystallization of polyethylene is by lamellar growth from coherent secondary nucleation. Their analysis provides a mathematical model for the lamellar

growth rate dependence on the melt temperature, T, and the degree of melt supercooling, ΔT:

$$G = G_o e^{-\frac{\epsilon}{RT}} e^{\frac{E}{T\Delta T}} \tag{18}$$

In equation (18), the growth rate constant, G_o, is defined by Hoffman[38] as:

$$G_o = \frac{b_o kT}{h} e^2 e^{-\frac{b_o \Delta H_f \Delta T}{\sigma_s T_m^o}} \tag{19}$$

Although G_o is a function of the melt temperature, it can be considered as a molecular jump rate constant in the narrow temperature range in which polyethylene crystallizes. Using equation (19) and a melt temperature of 394^oK, G_o was calculated to have a value of 1.44×10^{10} microns/sec. The first exponential term in equation (18) represents the probability that a polymer molecule will overcome a viscous flow resistance or energy barrier in approaching the lamellar growth surface. Therefore, ϵ may be taken as the Eyring activation energy for viscous flow. The second exponential term in equation (18) represents the probability that a polymer molecule in the vicinity of the growth surface will fold onto the crystal surface. In this term E is defined by Hoffman[38] as:

$$E = -\frac{4 b_o \sigma_s \sigma_e T_m^o}{\Delta H_f k} \tag{20}$$

In equations (18) through (20) the terms, R, b_o, k, h, ΔH_f, σ_e, σ_s, T_m^o, are, respectively, the gas constant, molecular thickness on the crystal growth face, Boltzmann constant, Planck constant, perfect energy of crystallization, the lamellar fold surface energy, the lamellar lateral surface energy, and the ideal crystal melting point. For HDPE the values for b_o, ΔH_f, σ_s, and T_m^o are 4.11×10^{-8} cm, 2.8×10^9 erg/cm^3, 9.6 erg/cm^2, and 413^{o}K, respectively.

For HDPE, most of the temperature dependence of G resides mainly in the second exponential term of equation (18). The first exponential term can be collected with the G_o term and written as a constant. Equation (18) can be expressed as:

$$G = Ae^{\frac{E}{T\Delta T}} \tag{21}$$

or in logarithmic form:

$$\text{Ln}G = \text{Ln}A + \frac{E}{T\Delta T} \tag{22}$$

In equations (21) and (22), the kinetic rate constant A is defined by:

$$A = G_o e^{-\frac{\varepsilon}{RT}} \tag{23}$$

Nardin and Price[78] developed a similar growth rate expression of this form for crystallization studies on polyethylene oxide. They found that this relationship could apply to crystallization from the bulk melt state and from solvent solutions.

Using equation (17), DSC data were used to calculate the lamellar growth rates during dynamic crystallization at fixed cooling rates of 40, 10, 2.5, and 0.625 $^{o}C/min$. Results appear in Table 5. As suggested by equation (22), the logarithmic growth rates when plotted against the temperature term $(T\Delta T)^{-1}$ should be linear. This data plot is shown in Figure 29. Each data set on Figure 29 is for a fixed rate of cooling. As expected, data extrapolated to the start of crystallization fit the linear relationship of equation (22) better than data at later times. Growth rates are measured after the onset of crystallization and, therefore, the assumption used to obtain equations (10) and (11) is not correct; this results in negative departure from the linear relationship based on extrapolation of initial growth rates.

The radial growth rates calculated from the DSC data of this study are not comparable to the isothermal crystallization growth rates observed by Price[92] and Lindenmeyer[64] for MARLEX 6050. Figure 30 shows that the dynamic crystallization growth rates found by this study, curve 1, are lower than rates measured in the isothermal studies of Price, curve 4, and Lindenmeyer, curves 2 and 3. In Figure 30, all curves were calculated by using an ideal HDPE melt temperature of $413^{o}K$. The difference between the curve of this study and the curves of Price and Lindenmeyer could be explained from differences in HDPE material. Their material may have contained nucleation sites which were active at higher temperatures than the material used in this work. But most probably this difference exists because Price and Lindenmeyer in their use of a hot stage microscope technique, had to use very thin melt films which were

Table 5. DSC Dynamic Crystallization Growth Rate Data

$\frac{dT}{d\theta}$, β Crystallization Rate, °K/min & (Structure Factor)	θ Elasped Time,* Sec	$\frac{dH}{d\theta}$ Energy flow Rate mcal/sec	T Sample Temp °K	G Calculated Radial Growth Rate Microns/sec	r Calculated Spherulite Radius** Microns	ℓn G	$T_m^{\dagger}-T$ °K	$\frac{1}{T\Delta T}$ °K^{-2}x10^4
.625	0	0	396.5	0	0	-∞	16.5	1.528
(.33)	100	.06	395.5	.0726	7.3	-2.62	17.5	1.448
	150	.20	394.9	.0830	11.4	-2.49	18.1	1.399
	200	.74	394.4	.1059	16.7	-2.25	18.6	1.363
	250	2.14	393.9	.1299	23.2	-2.04	19.1	1.329
	265	2.36	393.8	.1307	25.2	-2.03	19.2	1.322
2.5	0	0	395.1	0	0	-∞	17.9	1.414
(.34)	25	.11	394.1	.220	5.5	-1.51	18.9	1.343
	50	1.00	393.1	.289	12.7	-1.24	19.9	1.278
	75	6.40	392.1	.410	23.0	-0.89	20.9	1.220
	90	7.41	391.8	.380	28.7	-0.97	21.2	1.204
10	0	0	392.9	0	0	-∞	20.1	1.266
(.37)	10	.864	391.2	.793	7.9	- .23	21.8	1.173
	15	3.84	390.4	.995	12.9	- .01	22.6	1.133
	20	12.2	389.5	1.203	18.9	+ .19	23.5	1.093
	25	18.6	388.7	1.196	24.9	+ .18	24.3	1.059
	26.5	19.0	388.4	1.161	26.6	+ .15	24.6	1.047
40	0	0	391.3	0	0	-∞	21.7	1.178
(.38)	2.5	.420	389.6	1.549	3.8	+ .44	23.4	1.097
	5.0	5.28	387.9	2.271	9.6	+ .82	25.1	1.027
	7.5	21.6	386.2	2.766	16.5	+1.02	26.8	0.966
	12.25	26.9	383.0	2.115	26.5	+0.75	30.0	0.870

Table 5. Continued

*Zero Time is defined as the start of the Crystallization Exotherm.

**Impingement radius was measured as 30 microns.

†413°K was assigned as the melting point.

8.59 mg of MARLEX 6050 high density polyethylene was used for each DSC thermogram.

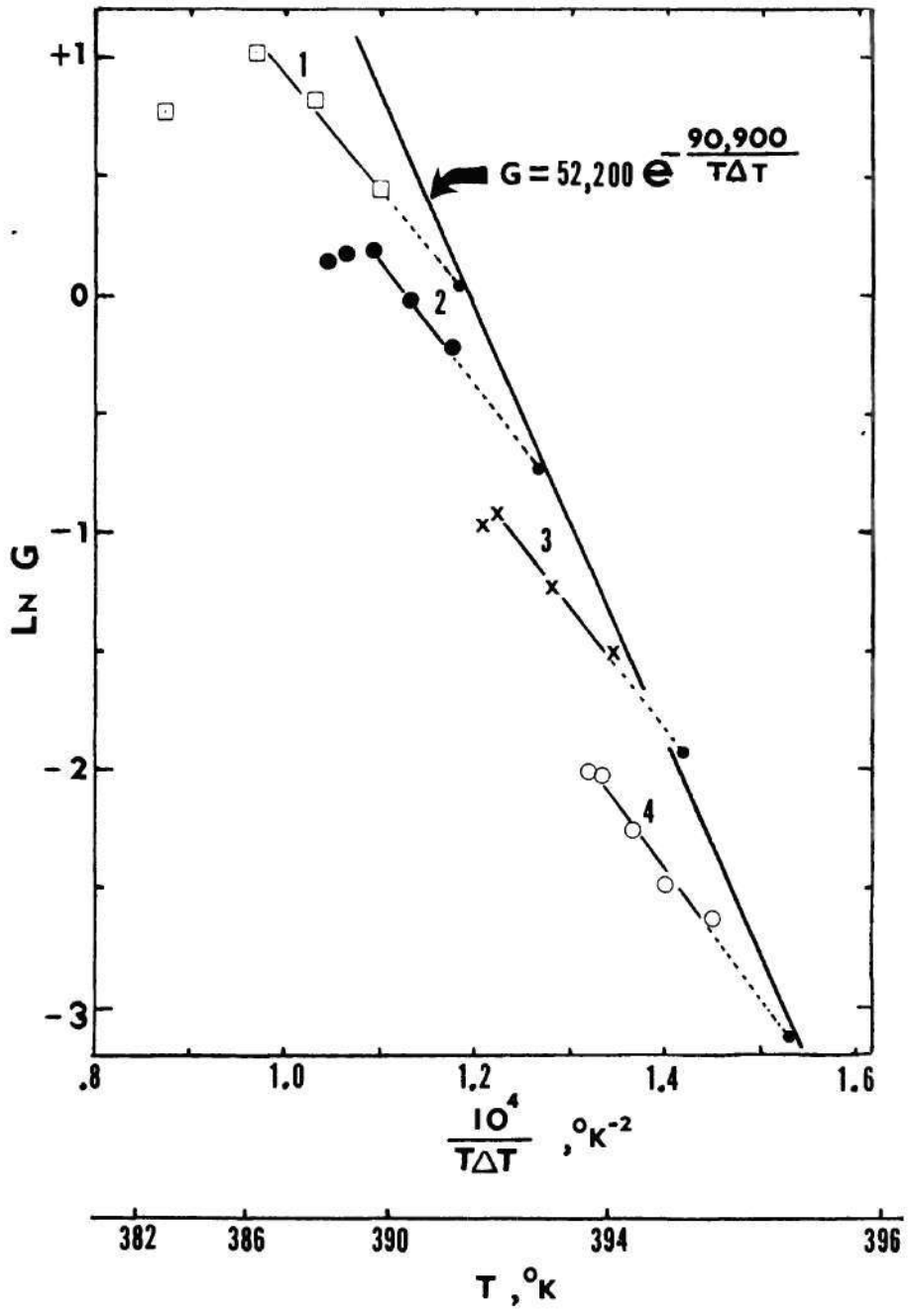

Figure 29. Spherulite Radial Growth Rate During Dynamic Crystallization [Temperature Scans: 1) 40°K/min; 2) 10°K/min; 3) 2.5°K/min; 4) .625°K/min]

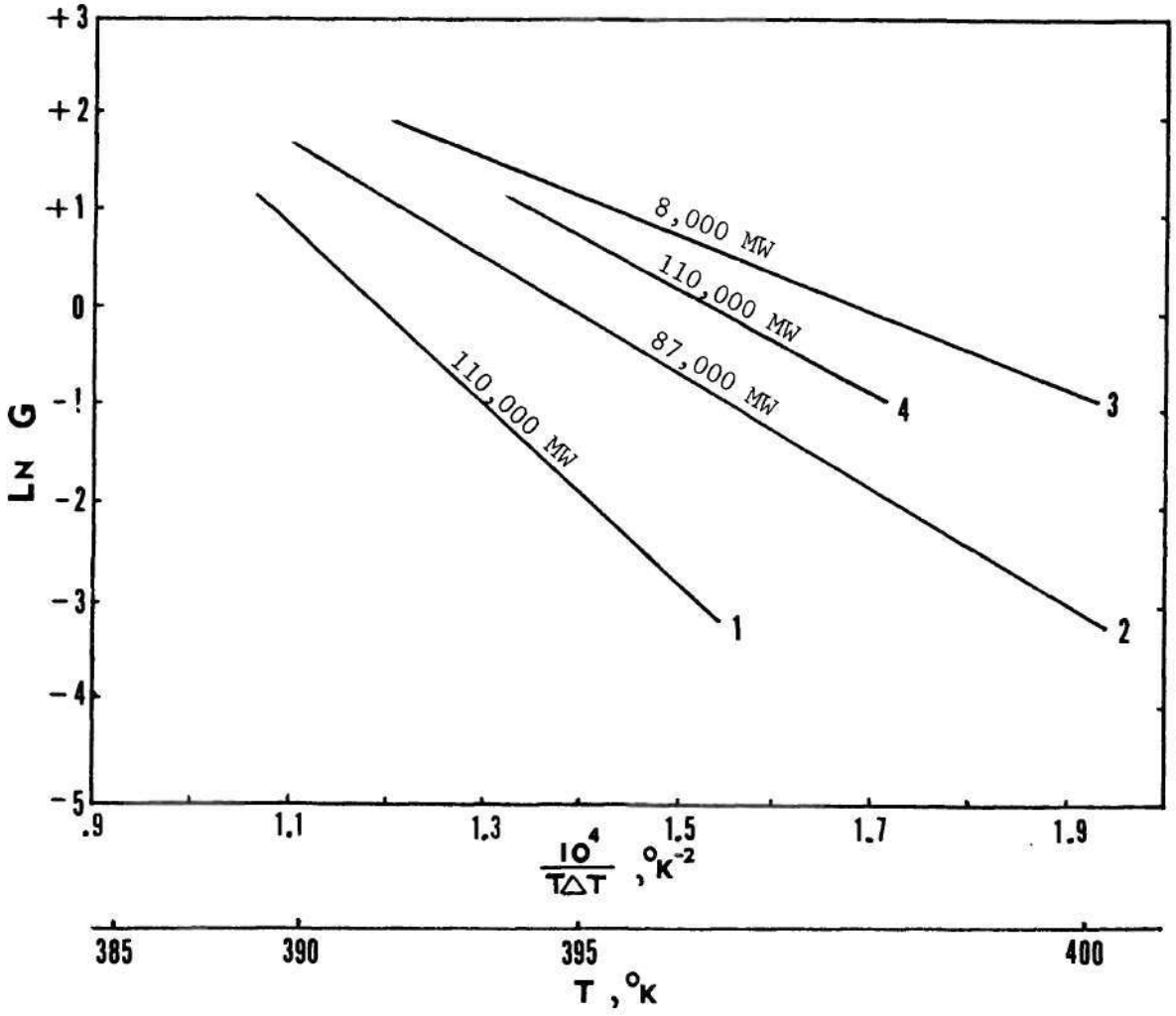

Figure 30. Comparison of MARLEX 6050 HDPE Radial Growth Rate Data [Curves: 1) This work; 2) and 3) Lindenmeyer; 4) Price]

less than 25 microns. Therefore the crystallization phenomenon they observed was probably influenced by surface effects which were not present in crystallizing the thicker DSC samples.

The best straight line fit of the data in Figure 29 gives values for A and E in equation (21) of 52,200 microns/sec and $-90{,}900\,^{\circ}K^2$, respectively. Using these values for A and E and equations (19), (20), and (23), the lamellar fold surface energy, σ_e, and the Eyring activation energy for viscous flow, ϵ, were calculated as 54 ergs/cm^2 and 9,800 cal/mole, respectively. This fold surface energy value is slightly lower than previous estimates[19,36,38] which gave values ranging from 57 to 168 ergs/cm^2. These past estimates were made by melting crystallized material and therefore are not necessarily indicative of the surfaces formed exclusively during primary crystallization. Thus the past estimates could reflect the effects of secondary crystallization.

The low surface energy value calculated in this study for the crystallizing lamellae, 54 ergs/cm^2, implies that molecular folding at the lamellar surface during primary crystallization should be uniform and is probably accomplished by four or five gauche configurations of the polyethylene molecule at each fold. Therefore because of the low surface energy, the highly irregular molecular switchboard type fold surface as described by the Flory model[28] does not appear to form during primary crystallization of HDPE.

In this study, the calculated viscous flow activation energy value, 9,800 cal/mole, indicates that polyethylene molecules are probably experiencing a low shear rate as they move to attach themselves to the lamellar

growth surfaces. According to McKelvey,[73] this particular activation energy would closely correspond to melt flow at a shear rate of 1.5 sec^{-1}. Therefore during primary HDPE crystallization, polyethylene molecules or molecular segments apparently are not moving at high velocities or over large distances in traveling in the melt to the lamellar growth surfaces.

In summary, the lamellar growth rates of HDPE during primary melt crystallization, as calculated from DSC data, have been shown to fit the model of Hoffman and Weeks for crystallization by coherent secondary nucleation. The growth rate in microns per second occurring during primary crystallization can be expressed by the equation:

$$G = 52{,}200\ e^{\frac{-90{,}900}{T\Delta T}} \tag{24}$$

Lamellar Separation and Dimensions

By working with concentrated polyethylene solutions, Keith and Padden[48,49] have qualitatively shown that bundles of discrete crystalline lamellae are formed during spherulitic crystallization whose width, δ, is approximately proportional to the ratio of molecular self diffusion in the melt, D, to the spherulitic radial growth rate, G.

$$\delta \cong \frac{D}{G} \tag{25}$$

Also they have argued that these crystalline bundles fill space during primary crystallization by noncrystallographic branching with a frequency inversely proportional to the magnitude of the bundle width, δ, and that these bundles are separated from one another by melt containing impurities

and high molecular weight polymer. The melt between crystalline bundles has a thickness approximately equal to the bundle width. Therefore, during primary crystallization of polyethylene melts, approximately one half of the melt solidifies; the remaining melt between lamella bundles partially crystallizes during the secondary stage of crystallization. Also, Keith, Padden, and Vadimsky[52] have suggested that the number of molecular tie links between lamellar bundles formed from the melt during primary crystallization increases as the distance between bundles decreases. In this work, they estimated that the maximum distance in Angstroms that a polymer molecule can span to tie together lamellar bundles, d, is related to the weight average molecular weight, MW, by:

$$d \cong 20(MW)^{1/2} \tag{26}$$

The HDPE polymer used in this study, MARLEX 6050, had a weight average molecular weight of 10^5. Therefore equation (26) indicates that very few tie molecules would connect lamellar bundles that are separated by distances greater than 0.6 micron.

To determine the bundle width dependence upon bulk crystallization conditions, an expression for molecular self diffusion in the melt, D, must be established. Few experimental self-diffusion data on high molecular weight polymers in the melt were available and therefore estimates were made from theoretical considerations and the limited experimental self-diffusion data available on low molecular weight polymers and hydrocarbons.

McCall and co-workers have measured the self-diffusion coefficients for linear hydrocarbons[23] and low molecular weight linear polyethylene fractions.[71] From these studies, they showed that, for number average molecular weights up to 5800, the coefficient of self diffusion, D, measured in cm^2/sec at 150^oC was proportional to the number of carbon atoms in the polymer chain, n, by the relationship:

$$D = 2.5\ n^{-5/3} \times 10^{-3} \tag{27}$$

For a saturated hydrocarbon or linear polyethylene, n is related to the number average molecular weight by:

$$n = \frac{MN}{14} \tag{28}$$

Therefore, for the 10^4 molecular weight MARLEX 6050 HDPE melt at 150^oC, the self-diffusion coefficient as calculated by equation (27) would be $4.38 \times 10^{-8}\ cm^2/sec$.

McCall and Huggins[70] also found that a similar empirical relationship of the form of equation (27) applied for molecular self diffusion of siloxane liquids with molecular weights up to 32,000. Therefore, the extrapolation of equation (27) into the domain of higher molecular weight linear polyethylene melts does not appear unreasonable.

Many investigators[7,15,109,111,116] have shown experimentally and theoretically that molecular self diffusion within a material is inversely proportional to the material's viscosity, η, and directly proportional to the absolute temperature, T.

$$D \propto \frac{T}{\eta} \tag{29}$$

By introducing a proportionality factor which incorporates the intrinsic properties of the polymer molecule, C, equation (29) can be expressed as:

$$D = \frac{CT}{\eta} \tag{30}$$

The factor C can be determined for linear polyethylene melts from a knowledge of molecular self diffusion and melt viscosity at a single temperature. The self diffusion of 10^4 molecular weight MARLEX 6050 HDPE melt at 150°C was determined from equation (27). An estimate of melt viscosity is still required before the factor C can be calculated.

From the lamellar growth rate data obtained by DSC experiments, it was previously shown that during primary crystallization from the melt state the viscous flow activation energy, 9,800 cal/mole, suggested that molecular movement was at a 1.5 sec^{-1} shear rate. Cross[20] found that for HDPE melt flow at 190°C in this shear field, the viscosity was 8.0×10^4 poise. Using this viscosity value and the general jump rate viscosity relationship, the effect of molecular weight on viscosity, F(z), was determined from:

$$\eta = F(z) \frac{h}{kT} e^{\frac{\epsilon}{RT}} \tag{31}$$

F(z) for HDPE had a calculated value of 1.81×10^{13} dynes/cm^2. Using this value of F(z), equation (31) was used to determine the viscosity of

a HDPE melt flowing at a 1.5 sec^{-1} shear rate. The polyethylene melt viscosity at a 1.5 sec^{-1} shear rate and 150°C was calculated by equation (31) to be 2.39×10^5 poise. This viscosity value together with the self-diffusion value at 150°C was used in equation (30) to calculate the molecular proportionality factor, C. This factor C, which was assumed to be constant over the narrow temperature range of interest, has a value of 2.47×10^{-5} dynes/°K.

Combining equations (30) and (31) and inserting the values for the proportionality factor, C, and the viscous flow activation energy, ϵ, a working equation which estimates the self diffusion of a crystallizing HDPE melt as a function of melt temperature was formulated:

$$D = 2.84 \times 10^{-8} \, T^2 \, e^{\frac{-4930}{T}} \qquad (32)$$

The self-diffusion and temperature units are cm^2/sec and °K, respectively.

Equations (24) and (32) which represent the lamellar growth rate and molecular self-diffusion relationships, respectively, were used together with Keith and Padden's equation (25) to provide estimates of the lamellar bundle size formed during primary crystallization. Table 6 lists the calculated properties of a MARLEX 6050 HDPE crystallizing melt and the lamellar dimension forming as a function of crystallization or melt temperature. In Table 6, the lamellar thickness, ℓ^*, in Angstroms, was calculated using the kinetic relationship of Hoffman.[38]

$$\ell^* = \frac{1387}{413-T} + 0.035 \, T \qquad (33)$$

Table 6. Calculation of Lamellar Dimensions Forming During Primary Crystallization from the Melt

T Melt Temp. °K	η Melt Viscosity @1.5 sec^{-1} Shear dyne-sec $cm^{-2} x10^{-6}$	D Self Diffusion $cm^2\ sec^{-1}$ $x10^{10}$	G Lamellar Growth Rate cm $sec^{-1} x10^4$	δ Lamellar Width microns	ℓ^* Lamellar Thickness Å
400	.49	200	.0013	1500	121
398	.52	189	.013	145	106
396	.56	175	.071	25	95
394	.60	162	.28	5.8	87
392	.64	151	.84	1.8	80
390	.69	140	1.9	.74	74
388	.74	130	4.4	.29	70
386	.79	120	8.5	.14	65

$$\eta = \frac{868}{T} e^{\frac{4930}{T}} \qquad D = 2.47 \frac{T}{\eta} \times 10^{-5} \qquad G = 5.22\, e^{\frac{-90,900}{T\Delta T}}$$

$$\delta = \frac{D}{G} \qquad \ell^* = \frac{1387}{413-T} + .035\ T$$

Formation of Tie Molecules During Primary Bulk Crystallization

Figure 31 gives the calculated exponential dependence of lamellar width with melt crystallization temperature (see Table 6). For HDPE, only small changes in melt crystallization temperature can produce extreme changes in lamellar widths. Lower crystallization temperatures, which are promoted by rapid dynamic crystallization, produce lamellar dimensions and separations which are small and can be easily connected by groups of tie molecules. Higher crystallization temperatures produce large lamellae which are widely separated and probably connected by fewer molecular tie links. Indeed, if equation (26) is correct, the maximum distance that can be spanned by a tie molecule having a 10^5 weight average molecular weight would be 0.6 micron. Therefore, by referring to Figure 31, the isothermally or dynamically crystallized MARLEX 6050 HDPE whose structures are formed at temperatures greater than $390^{o}K$ ($117^{o}C$) should have almost no tie links connecting lamellar superstructures. These structures can be expected and were found to be brittle when unaxially strained (see Table 2, page 48). Figure 31 is based on approximate relationships and rough estimates of parameters; hence it is only approximate, but it does indicate the correct relationship that a finer and stronger superstructure should form at lower HDPE melt crystallization temperatures.

It was observed from spherulite ring spacings that the fine to coarse structural gradient in the dynamically crystallized bulk samples was related to a corresponding low to high melt crystallization temperature gradient. This gradient of structure can be clearly seen in the end view scanning electron photomicrograph of the etched bulk dynamically

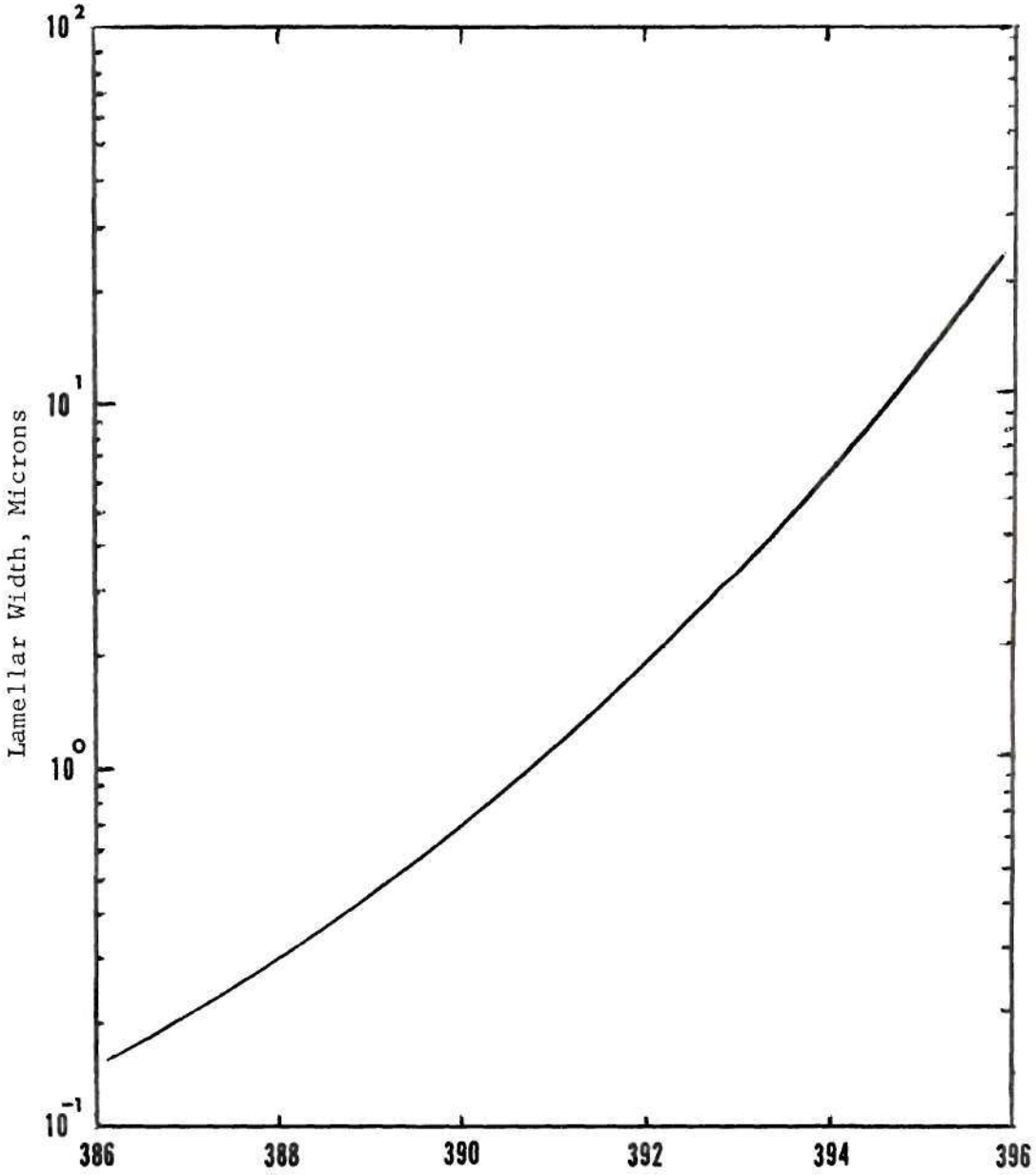

Figure 31. Width of Lamellar Bundles Forming During Primary Crystallization

crystallized structure at the 1.5 BDR region shown in Figure 32. Magnified views are shown in Figures 33 and 34. The spherulite superstructure close to the bulk sample top surface (see Figure 33) which was formed at temperatures between 388 to 390^{o}K shows a fine radiating substructure with lamellar groups having dimensions in the submicron range. The superstructures formed within the bulk sample (see Figure 34), which crystallized at temperatures between 391 to 396^{o}K, have coarser substructures. These lamellar groups have dimensions in the micron range and closely correspond to the value shown in Figure 31. Therefore, the general ideas on molecular tie groups and structure formations presented by Keith and Padden in their work with thin polyethylene films appear to hold for the thick bulk melt crystallized HDPE samples formed and stressed in this study.

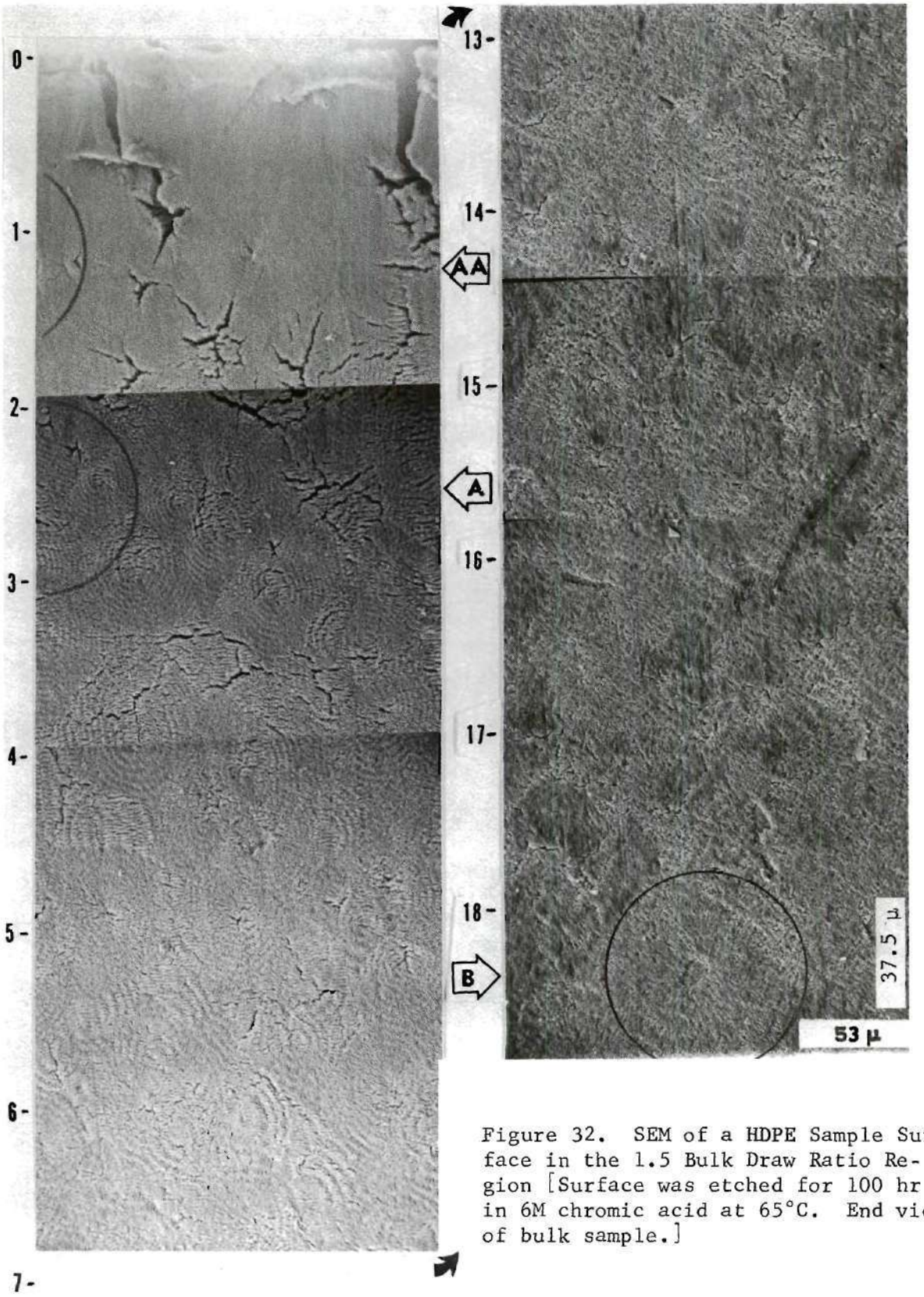

Figure 32. SEM of a HDPE Sample Surface in the 1.5 Bulk Draw Ratio Region [Surface was etched for 100 hr in 6M chromic acid at 65°C. End view of bulk sample.]

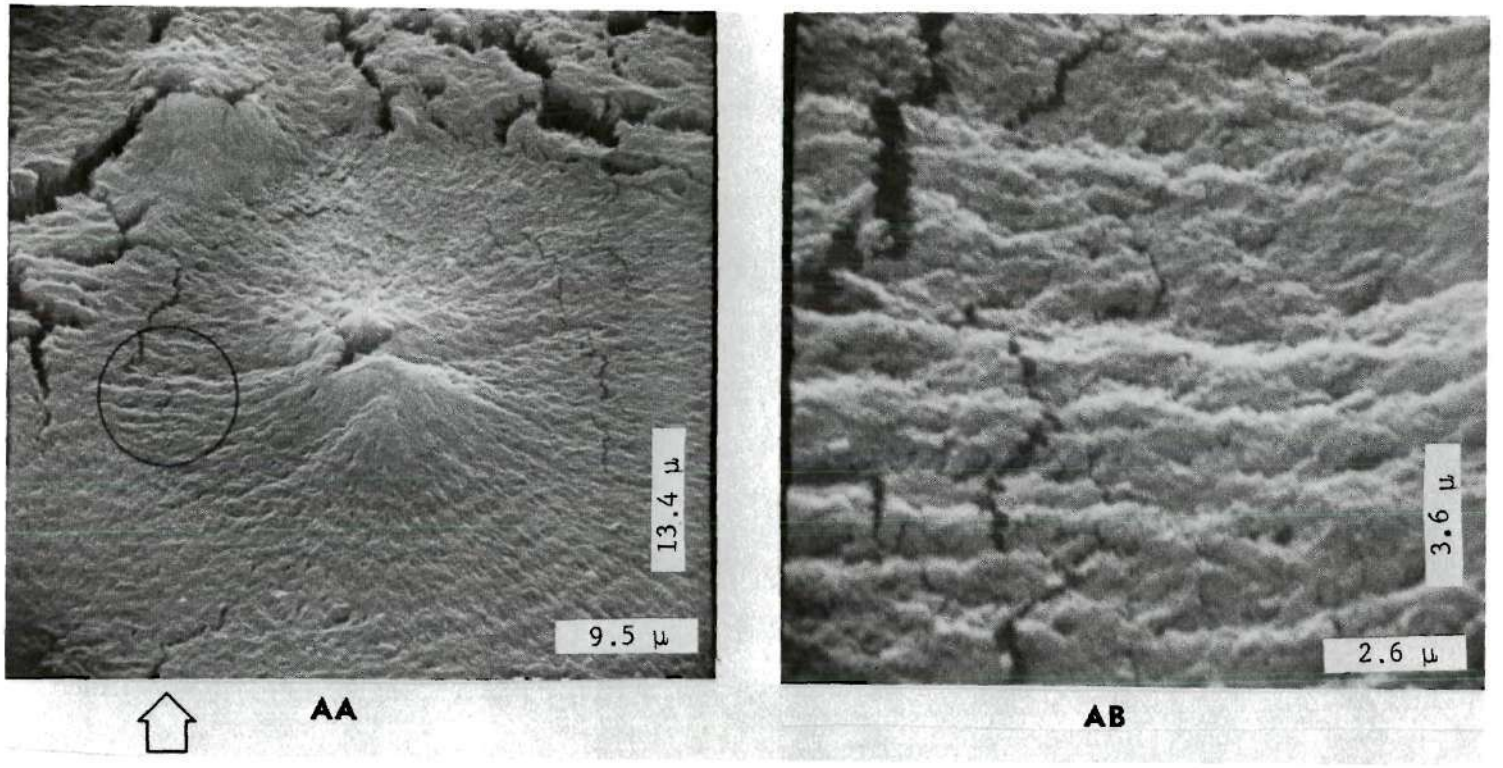

Figure 33. SEM High Magnifications of Surface AA in Figure 32

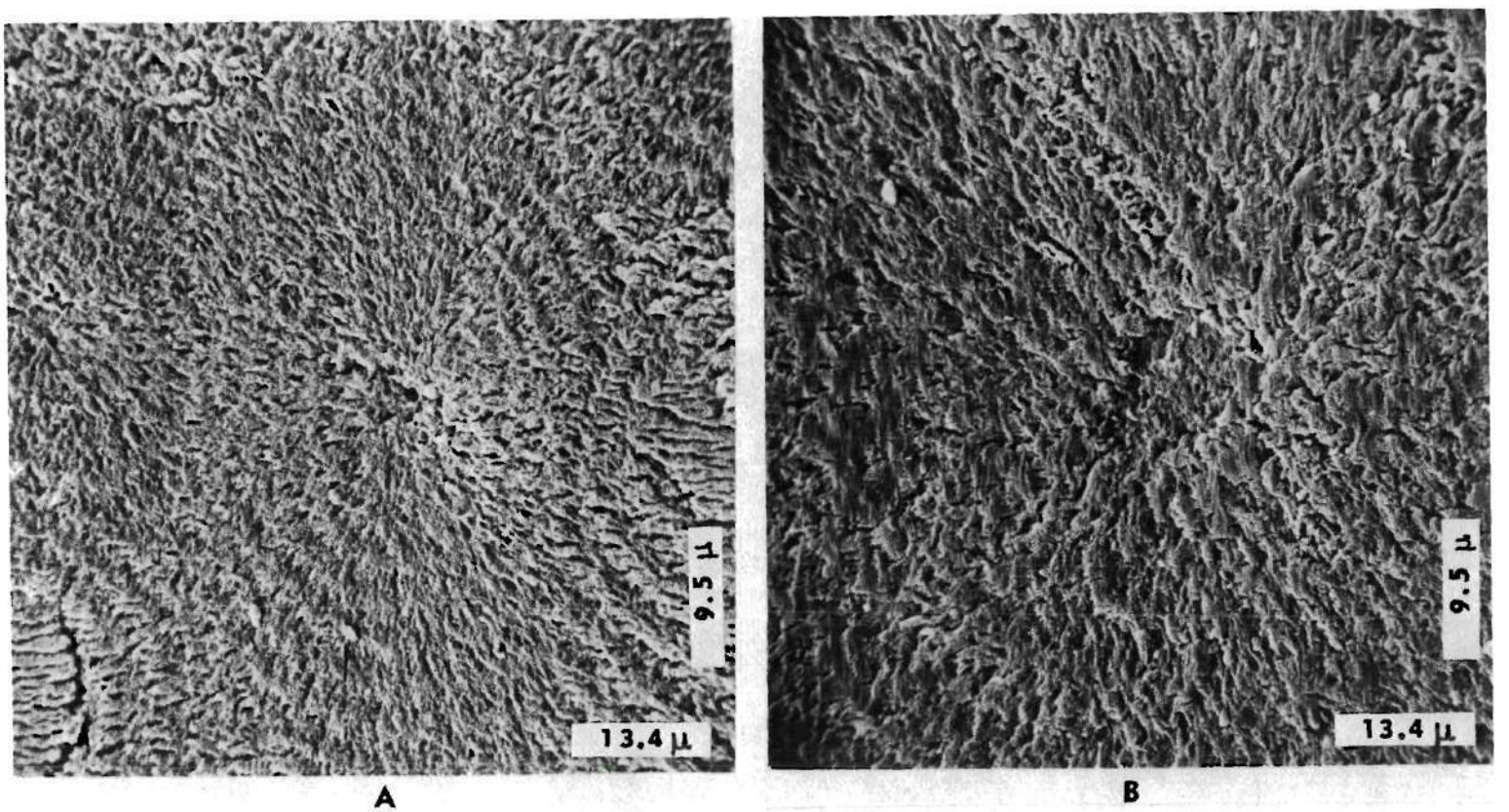

Figure 34. SEM High Magnifications of Surfaces A and B in Figure 32

CHAPTER V

CONCLUSIONS

A chromic acid etching treatment technique was developed; it reveals the superstructure of high density polyethylene in surfaces formed by cryogenic sectioning from bulk polymers. The chromic acid chemical attack on the polymer appears to be limited by the rate of acid diffusion to the polyethylene surface rather than by the rates of subsequent oxidation reactions. This confines the reaction to the polyethylene surface. Diffusion is more rapid in the less ordered polyethylene structure regions. Thus, surface etching is accelerated at the less ordered portions near the polymer surface or at structural discontinuities where acid could penetrate such as cracks and regions of steep contours. Etching disclosed the undisturbed polyethylene structural features found below the sectioned surfaces. These morphological features were observed using a scanning electron microscope.

Large isothermal and quenched melt crystallized, high density polyethylene samples were deformed by uniaxial extension at 60^{o}C. Morphological examination of the pre-drawn bulk sample structures by light and scanning electron microscopy showed that the isothermally crystallized samples had a uniform splayed spherulitic superstructure; the quenched crystallized samples had a superstructure gradient. Ringed spherulites were found at the quenched sample surface regions. However, with increasing sample depth, a gradual transition to splayed spherulite superstructures

occurred. This structural transition was due to the non-isothermal microcrystallization of the quenched samples in the thickness direction. Ringed spherulites were formed at the lower melt crystallization temperatures which occurred at the bulk sample surfaces. Due to an increase in thermal insulation with sample depth, splayed spherulites found in the bulk sample's interior regions were formed at higher melt crystallization temperatures.

As determined from heats of melting and density measurements, the splayed spherulite superstructures found in the isothermally crystallized samples and in the internal region of the quenched crystallized samples were more crystalline than the ringed spherulite superstructures.

This high crystallinity was probably responsible for the brittle behavior of isothermally crystallized bulk samples. The splayed spherulite superstructures of these bulk samples when observed by the scanning electron microscope were found to contain many randomly positioned cracks having dimensions in the micron range. These cracks were arranged without order between and through the splayed superstructures and were probably formed because of internal stresses introduced by a sample volume reduction occurring with high degrees of crystallinity. Because of the size of these cracks, they were free to be enlarged with an application of a uniaxial load and thereby by crack propagation these isothermally crystallized bulk samples experienced brittle failure.

No cracks of large magnitude were observed before or after initial deformation in the quenched crystallized bulk sample superstructures, but density data showed that an apparent volume increase occurred in the ringed

spherulite structures after limited drawing. This density decrease could be due to the formation of voids within and/or between the spherulite superstructures.

No cracks were observed by light microscopy in the quenched crystallized and drawn samples; nevertheless deformation of the ringed spherulites was inhomogeneous. Although the deformation response of neighboring spherulites varied, generally, all ringed superstructures deformed less than that measured for the overall bulk sample. This infers that the center portions of the quenched crystallized bulk samples where the splayed spherulites were found deformed more than that measured for the overall bulk sample. Also this implies that spherulites slipped past one another during deformation. These inferences were confirmed from scanning electron microscopic observations made on highly drawn quenched samples where more severe superstructure deformation was seen clearly near the sample centerline regions. Here, drawn splayed spherulite structures were highly elongated and were split into individual fibrous structures. Thus, during extension, ringed spherulite superstructures formed at low crystallization temperatures experience less deformation than splayed spherulite superstructures formed at higher crystallization temperatures.

The stability of deformation for the quenched samples was due to the supporting jacket of ringed spherulites found in the external region of the bulk samples. This outer structure probably prevented catastrophic fracture of the weak splayed structure found internally. This action of constrained fracturing of the internal structure probably produced fibrilation of the bulk sample.

The variation of sample deformation will be explained from the abundance of molecular tie groups found in the various types of spherulite superstructures.

All spherulites regardless of crystallization conditions had approximately the same 60 micron diameter. This situation can exist only if in cooling at any rate all spherulite nuclei formed simultaneously at some specific melt temperature and, thereafter, all spherulites grew in concert without interference with one another until all spherulites collided or impinged at the same time. Therefore, melt crystallized bulk polyethylene was considered to be constructed from many small perfectly packed spherical superstructures. From this model, spherulitic radial growth rates during primary crystallization at fixed cooling rates were calculated from energy thermograms obtained by a differential scanning calorimeter. From these thermograms, it was found that crystallization temperature decreased with increasing cooling rates. Spherulitic radial growth rates were calculated to increase with faster coolings. This growth rate dependence was compatible with the Hoffman[38] model of primary crystallization by a mechanism of coherent, secondary nucleation.

Analysis of the polyethylene, primary crystallization, spherulitic growth rate data using the Hoffman model indicated that molecular movement during bulk crystallization was at a low shear rate and that molecular folding at the lamellar growth surfaces was uniform with each molecular fold probably accomplished by five gauche configurations. This result was surprising because previous studies of spherulitic growth rates measured on isothermally crystallized thin films when analyzed using the

Hoffman model, showed that a higher molecular shear rate was occurring and that molecular folding at the lamellar surfaces was less uniform. These inconsistencies were probably the result of large surface effects occurring in their thin film samples. These surface effects were not present in the much thicker polyethylene samples used in the differential scanning calorimeter.

From thin film crystallization studies, Keith and Padden have proposed that the number of molecular tie groups forming during primary melt crystallization, which connect the lamellae of spherulite superstructures and provide mechanical strength, is proportional to the ratio of molecular mobility in the melt to the rate of primary crystallization. If molecular mobility or self diffusion is large with respect to the rate of lamellar growth, then polymer molecules would not be expected to simultaneously crystallize onto two widely separated lamellar growth surfaces. However, single polymer molecules would more likely crystallize at two different lamellar growth surfaces if the small lamellae formed close together at rapid rates.

By estimating molecular self diffusion and lamellar growth rates for high density polyethylene systems as functions of melt crystallization temperatures, Keith and Padden's molecular tie group formation model was tested against the mechanical response and morphologies of the large bulk crystallized samples formed in this study. As expected, the isothermally crystallized bulk samples which were frozen at elevated melt temperatures were observed to have a coarse, splayed, spherulitic superstructure. This indicates that large lamellar bundles did indeed form its

substructure. Also, as expected, these samples were brittle when cold drawn and therefore suggest that only a few tie molecules provided sample strength. Also, as predicted, the quenched crystallized bulk samples which were frozen at lower melt temperatures were found to have fine structured, ringed spherulites which were probably made up of small closely packed lamellar bundles. Because of the large number of tie molecules bridging these small lamellae, stresses introduced into the spherulitic superstructures were easily dissipated without catastropic sample fracture. This enabled these spherulitic superstructures to align in the stress direction during the initial stages of sample extension and thereby position lamellar substructures for micronecking during further ductile drawing. Additional support for Keith and Padden's ideas was shown from the strain distribution found in the highly drawn, quenched, crystallized bulk samples. Here, as expected, ringed spherulites because of a larger number of molecular tie groups deformed less readily than the splayed spherulites found in the same bulk sample.

In summary, it was determined that the ductile draw behavior of high density polyethylene is critically dependent upon the melt crystallization condition used to form the solid polymer. Slow cooling or use of high isothermal temperature conditions to crystallize polyethylene melts were found to form highly crystalline solids. These solids contained large cracks probably introduced by unrelieved volume contractions. These crystallization conditions produced superstructures which contained few molecular tie groups to blunt the growth of these cracks when these samples were extended at $60^{o}C$. Therefore, sample fracture occurred. In

contrast, rapid cooling of polyethylene melts was found to form solids of spherulite superstructures composed of closely packed lamellar bundles which are probably connected by many tie molecules. These tie molecules redistributed stress concentrations imposed by the initial stages of drawing and thereby blunted any submicroscopic crack propagation. This allowed these spherulite structures to rearrange themselves without fracture and begin the ductile draw transformation into a fibrous material.

CHAPTER VI

RECOMMENDATIONS

For future studies on the morphologies and mechanical responses of semicrystalline polymer systems, I recommend:

1. Other crystallization studies similar to this one using polymer systems which have slower crystallization rates should be carried out to verify the applicability of kinetic crystallization theory over wide temperature and rate ranges. Polyethylene oxide, polymethylene oxide, polypropylene, nylon, and polyethylene terephthalate systems would be excellent candidates.

2. Although a polyethylene etching technique was established in this study, it required long treatment times. Therefore, a faster polymer surface etching agent should be found which could be used at low temperatures. Such an agent could also be used in the surface treatment step required in polymer metalizing processes.

3. From this study, it was found that almost no experimental data are available on molecular diffusion in the melt state. Work in this area is needed to confirm present molecular mobility theories. I suggest that experiments using an autoradiographic technique[96] be attempted to collect this self-diffusion data.

4. A micro-tensile testing machine should be built which could determine the physical properties of the small film samples crystallized

by the differential scanning calorimeter. With this machine, physical properties could be directly correlated with controlled dynamic crystallization conditions. Possibly, a micro-biaxial, stress-rupture apparatus similar to that constructed by Cooney[18] would be acceptable for this work.

5. Primary crystallization data obtained from the differential scanning calorimeter should be thoroughly analyzed for possible error introduction due to polymer secondary crystallization and the thermal response limitation of the DSC instrument. If this data correction can be accomplished, secondary crystallization effects can be separated from primary effects and the influence of secondary crystallization on the final physical properties of semicrystalline polymers can be studied.

6. The experimental techniques developed in this work to study the structure of bulk samples should be used to examine surface effects of various materials on the morphologies and properties of thin polymer films and fibers. Use of surface nucleation agents to alter crystallization kinetics and thereby possibly form desired polymer structures should also be explored for commercial importance.

BIBLIOGRAPHY

1. Anderson, F. R., "Morphology of Bulk Crystallized Linear Polyethylene," J. Applied Physics 35, 64 (1964).

2. Anderson, F. R., "Fracture Studies of Isothermal Bulk Crystallized Linear Polyethylene," J. Polymer Sci. C-3, 123 (1963).

3. Andrews, E. H., Bennett, N. W., and Markham, A., "Microstructure of Bulk Polymers as Revealed in Ultra-thin Sections," J. Polymer Sci. A-2, 5,1235 (1967).

4. Armond, V. J. and Atkinson, J. R., "Chromic Acid as an Etchant for Bulk Polypropylene and Its Use to Study (i) Nitric Acid Attack on Polypropylene (ii) Cracks in Polypropylene Induced by Tensile Stress," J. Materials Sci. 4, 509 (1969).

5. Banks, W., Hay, J. N., Sharples, A., and Thompson, G., "The Crystallization of Polyethylene II," Polymer 5, 163 (1964).

6. Barber, P. and Atkinson, J. R., "Some Microstructural Features of the Welds in Butt-Welded Polyethylene and Polybutene-1 Pipes," J. Materials Sci. 7, 1131 (1972).

7. Barrer, R. M., "Permeability in Relation to Viscosity and Structure of Rubber," Trans. Faraday Soc. 38, 322 (1942).

8. Bassett, D. C., Keller, A., and Mitsuhashi, H. H., "New Features of Polymer Crystal Growth from Concentrated Solutions," J. Poly. Sci. A-1, 763 (1963).

9. Bettelheim, F. A. and Stein, R. S., "The Changes in Density of Low Pressure Polyethylene on Stretching," J. Polymer Sci. 31, 523 (1958).

10. Billmeyer, F. W., Textbook of Polymer Science, 2nd Edition, John Wiley & Sons: New York, 1971, p. 230.

11. Binsbergen, F. L., "Heterogeneous Nucleation in the Crystallization of Polyolefins: Part 1. Chemical and Physical Nature of Nucleating Agents," Polymer 11, 253 (1970).

12. Breedon, J. E., Jackson, J. F., Marcinkowski, M. J., and Taylor Jun, M. E., "Scanning Electron Microscopy of Polyethylene Spherulites," J. Matl. Sci. 8, 143 (1973).

BIBLIOGRAPHY (Continued)

13. Breedon, J. E., Jackson, J. F., Marcinkowski, M. J., and Taylor Jun, M. E., "Studies of Polyethylene Spherulites Using the Scanning Electron Microscope," J. Matl. Sci. 8, 1071 (1973).

14. Buchdahl, R., Miller, R. L., and Newman, S., "Crystallization Kinetics and Mechanical Properties of Polyethylene," J. Polymer Sci. 36, 215 (1959).

15. Bueche, F., "Viscosity, Self Diffusion, and Allied Effects in Solid Polymers," J. Chem. Physics 20, 1959 (1952).

16. Bueche, F., Cashin, W. M., and Debye, P., "The Measurement of Self Diffusion in Solid Polymers," J. Chem. Physics 20, 1956 (1952).

17. Cherry, B. W. and McGinley, P. L., "Deformation of Polymers at the Molecular Level," Applied Polymer Symposium No. 17, 59 (1971).

18. Cooney, J. L., "Effect of Morphology on Biaxial Stress Rupture of Polyethylene," J. Applied Poly. Sci. 8, 1889 (1969).

19. Cormia, R. L., Price, F. P., and Turnbull, D., "Kinetics of Crystal Nucleation in PE," J. Chemical Physics 37, 1333 (1962).

20. Cross, M. M., "Analysis of Flow Data on Molten Polymers," Europe Polymer J. 2, 299 (1966).

21. Crystal, R. G. and Hansen, D., "Morphology of Cold-Drawn Nylon 66," J. Polymer Sci. A-2, 6, 981 (1968).

22. Davidson, T. and Wunderlich, B., "Extended Chain Crystals. II. Crystallization under Elevated Pressure," J. Polymer Sci. A-2, 7, 2051 (1969).

23. Douglass, D. C. and McCall, D. W., "Diffusion in Paraffin Hydrocarbons," J. Physical Chem. 62, 1102 (1958).

24. Eirich, F. R. and Smith, T. L., "Molecular Mechanical Aspects of the Isothermal Rupture of Elastomers," in Fracture, Vol. 7, Chapter 7, Edited by H. Liebowitz; Academic Press: New York, 1972.

25. Fatou, J. M. G. and Barrales-Rienda, J. M., "Rates of Crystallization of Polyethylene Fractions by Calorimetry," J. Polymer Sci. A-2, 7, 1755 (1969).

26. Fitchmun, D. R. and Mencik, Z., "Morphology of Injection-Molded Polypropylene," J. Polymer Sci. A-2, 11, 951 (1973).

BIBLIOGRAPHY (Continued)

27. Fitchmun, D. R. and Newman, S., "Surface Crystallization of Polypropylene," J. Polymer Sci. A-2, 8, 1545 (1970).

28. Flory, P. J., "On the Morphology of the Crystalline State in Polymers," J. Am. Chem. Soc. 84, 2857 (1962).

29. Fujiyama, M. and Kagiyama, Y., "Melt Reology of HDPE," J. Applied Poly. Sci. 16, 3361 (1972).

30. Fujiwara, Y., "The Superstructure of Melt Crystallized Polyethylene. I. Screwlike Orientation of Unit Cell in Polyethylene Spherulites with Periodic Extinction Rings," J. Applied Poly. Sci. 10, 10 (1959).

31. Griffith, A. A., "The Phenomena of Rupture and Flow in Solids," Philosophical Trans. Royal Soc. A-22, 163 (1921).

32. Grubb, D. T. and Keller, A., "Origin of Contrast Effects in the Electron Microscopy of Polymers, Part 2: Polyethylene Spherulites," J. Materials Sci. 7, 822 (1972).

33. Hamada, F. and Wunderlich, B., "Density and Heat of Fusion of Folder Chain Polyethylene Crystals," J. Physical Chem. 72, 178 (1968).

34. Hass, T. W. and McRae, P. H., "Microscopic Observation of Fracture in Spherulitic Films of Linear Polyethylene," SPE Journal 24, 27 (1968).

35. Heaps, J. M. and Austin, A., "Degradation of Polyolefins," in Weathering and Degradation of Plastics, Edited by S. H. Pinner; Addison-Wesley Publishing Co.: Reading, Mass., 1966, p. 104.

36. Heber, I., "Die Sekundare Keimbildung bei Polyathylen-Spharolithen," J. Polymer Sci. A-2, 1291 (1964).

37. Hester, R. D. and Muzzy, J. D., "The Effect of Crystalline Morphology on Stress Crazing in Polyethylene," 165th ACS National Meeting, Dallas, Texas, April 1973.

38. Hoffman, J. D., "Theoretical Aspects of Polymer Crystallization with Chain Folds: Bulk Polymers," S.P.E. Trans. Oct. 1964, p. 319.

39. Hoffman, J. D. and Lauritze, J. I., "Crystallization of Bulk Polymers with Chain Folding Theory of Growth of Lamellar Spherulites," J. Research 65A, 297 (1961).

BIBLIOGRAPHY (Continued)

40. Hoffman, J. D. and Weeks, J. J., "Rate of Spherulite Crystallization with Chain Folds in Polychlorotrifluoroethylene," J. Chem. Physics 37, 1723 (1962).

41. Karasev, S. N., et al., "Relationship Between Mechanical Behavior of High Density Polyethylene and Molecular Weight Distribution," Vysokomole Kuliarnye Soedineniia 12, 27 (1970).

42. Kasatkin, B. S., Grinyuk, V. D., and Gaidarenko, H. L., "Spherulite Boundaries and Certain Aspects of Interspherulite Fracture," Polymer Mechanics 5, 327 (1969).

43. Kaufman, W. E. and Schultz, J. M., "Lamellar and Interlamellar Structure in Melt Crystallized Polyethylene. III. Effects of Small Deformation," J. Materials Sci. 8, 41 (1973).

44. Kavesh, S. and Schultz, J. M., "Lamellar and Interlamellar Structure of Melt Crystallized Polyethylene," J. Poly. Sci. A-2, 8, 243 (1970) and J. Poly. Sci. A-2, 9, 85 (1971).

45. Kavesh, S. and Schultz, J. M., "Meaning and Measurement of Crystallinity in Polymers," SPE 27th Annual Tech. Conf. 15, 3 (1969).

46. Keith, H. D. and Padden, F. J., "Deformation Mechanisms in Crystalline Polymers," J. Poly. Sci. 41, 525 (1959).

47. Keith, H. D. and Padden, F. J., "The Optical Behavior of Spherulites in Crystalline Polymers. II the Growth and Structure of Spherulites," J. Polymer Sci. 34, 128 (1959).

48. Keith, H. D. and Padden, F. J., "A Phenomenological Theory of Spherulitic Crystallization," J. Applied Physics 34, 2409 (1963).

49. Keith, H. D. and Padden, F. J., "Spherulitic Crystallization from the Melt. I Fractionation and Impurity Segregation and their Influence on Crystalline Morphology," J. Applied Physics 35,, 1270, 1286 (1964).

50. Keith, H. D. and Padden, F. J., "Spherulite Crystallization from the Melt," J. Applied Physics 35, 1270, 1286 (1964).

51. Keith, H. D., Padden, F. J., and Vadimsky, R. G., "Further Studies of Intercrystalline Links in Polyethylene," J. Applied Physics 37, 4027 (1966).

52. Keith, H. D., Padden, F. J., and Vadimsky, R. G., "Intercrystalline Links in Polyethylene Crystallized from the Melt," J. Polymer Sci. A-2, 4, 276 (1966).

BIBLIOGRAPHY (Continued)

53. Keith, H. D., "Crystallization of Polymers from the Melt and the Structure of Bulk Semicrystalline Polymers," Kolloid Z. 231, 421 (1969).

54. Keith, H. D., Padden, F. J., and Vadimsky, R. G., "Intercrystalline Links: Critical Evaluation," J. Applied Physics 42, 4584 (1971).

55. Keith, H. D., "Phase Transformations in High Polymers," Metallurgical Trans. 4, 2747 (1973).

56. Keller, A., "Investigations on Banded Spherulites," J. Poly. Sci. 39, 151 (1959).

57. Keller, A. and Sawada, S., "On the Interior Morphology of Bulk Polyethylene," Macromol. Chemi. 74, 190 (1964).

58. Keller, A., "Polymer Crystals," Report on Progress in Physics 31, 623 (1968).

59. Keller, A. and Pope, D. P., "Identification of Structural Processes in Deformation of Oriented Polyethylene," J. Materials Sci. 8, 453 (1971).

60. Kobayashi, K. and Nagasawa, T., "Mechanical Properties of Polyethylene Crystals. II. Deformation Process of Spherulite," J. Polymer Sci. C-15, 163 (1966).

61. Krigbaum, W. R., "Structure and Physical Properties of Crystalline Polymers," J. Polymer Sci. C-15, 251 (1966).

62. Krueger, D. and Yeh, G. S. Y., "Morphology of High Strength Transparent Polyethylene Under Controlled Condition," J. Applied Phys. 43, 4339 (1972).

63. Kubota, K., "Formation of a New Crystalline Structure on a Polyolefine Surface as a Result of Vapor Etching," J. Polymer Sci. C-3, 545 (1965).

64. Lindenmeyer, P. H. and Holland, V. F., "Relationship between Molecular Weight, Radial Growth Rate and the Width of the Extinction Bands in Polyethylene Spherulites," J. Applied Phys. 35, 55 (1964).

65. Mandelkern, L., Posner, A. S., Diorio, A. F., and Roberts, D., "Low Angle X-Ray Diffraction of Crystalline Nonoriented Polyethylene and Its Relation to Crystallization Mechanisms," J. Applied Physics 32, 1509 (1961).

BIBLIOGRAPHY (Continued)

66. Mandelkern, L., Crystallization of Polymers, McGraw Hill Book Company: New York, 1964.

67. Mandelkern, L., Fatou, J. G., Denison, R., and Justin, J., "A Calorimetric Study of the Fusion of Molecular Weight Fractions of Linear Polyethylene," Polymer Letter 3, 803 (1965).

68. Mandelkern, L., Allou, A. L., and Goplan, M., "The Enthalpy of Fusion of Linear Polyethylene," J. Physical Chem. 72, 309 (1968).

69. Matsuoka, A., "Hypothesis of Voids in Semicrystalline Polymers," J. Applied Physics 32, 2334 (1961).

70. McCall, D. W. and Huggins, C. M., "Self Diffusion in Linear Polydimethyl Siloxane Liquids," Applied Physics Letters 7, 153 (1965).

71. McCall, D. W., Douglass, D. C., and Anderson, E. W., "Diffusion in Ethylene Polymers IV," J. Chem. Physics 30, 771 (1959).

72. McHugh, A. J. and Schultz, J. M., "Morphological Effects of Annealing in Linear Polyethylene," Philosophical Mag. 24, 155 (1971).

73. McKelvey, J. M., Polymer Processing, John Wiley & Sons: New York, 1962, p. 45.

74. Muzzy, J. D. and Hansen, D., "Fibrous Structure Formation in Cold Drawing of Polyethylene," Text. Res. J. 41, 436 (1971).

75. Muzzy, J. D., "Fibrous Structure Formation in Drawing Crystalline High Polymers," Ph.D. Thesis, Rensselaer Polytechnic Institute, Troy, New York, 1970.

76. Muzzy, J. D., Hester, R. D., and Hubbard, J. L., "Chromic Acid Etching of Polyethylene," The Electron Microscopy Society of America, 21st EMSA National Meeting, New Orleans, Louisiana, Aug. 1973.

77. Muzzy, J. D., Hester, R. D., and Bright, D. G., "Dynamic Crystallization Kinetics of Polyolefins Analyzed by Differential Scanning Calorimetry," Society Plastic Engineers 32nd ANTEC, San Francisco, Cal., May 1974, p. 591.

78. Nardini, M. J. and Price, F. P., "The Measurement of Polymer Single-Crystal Growth in Situ: Poly(ethylene-oxide)," Crystal Growth, Proc. Int. Conf. on Crystal Growth, Boston, Mass., 1966, p. 395.

BIBLIOGRAPHY (Continued)

79. Ohlberg, S. M., Roth, J., and Raff, R. V. A., "Relationship Between Impact Strength and Spherulite Growth in Linear Polyethylene," J. Applied Polymer Sci. 1, 114 (1959).

80. Oppenlander, G. C., "Structure and Properties of Crystalline Polymers," Science 159, 1311 (1968).

81. Pennings, A. J., Van der Mark, J. M., and Kiel, A. M., "Hydrodynamically Induced Crystallization of Polymers from Solutions," Kolloid Z. 237, 336 (1970).

82. Peterlin, A. and Meinel, G., "Plastic Deformation of Polyethylene. II. Change of Mechanical Properties during Drawing," J. Polymer Sci. A-2, 9, 67 (1971).

83. Peterlin, A., "Bond Rupture in Highly Oriented Crystalline Polymers," J. Polymer Sci. A-2, 7, 1151 (1969).

84. Peterlin, A., "Chain Scission and Plastic Deformation in the Strained Crystalline Polymer," J. Polymer Sci. C-3, 297 (1971).

85. Peterlin, A., "Molecular Model of Drawing Polyethylene and Polypropylene," J. Materials Sci. 6, 490 (1971).

86. Peterlin, A., "Chain Scission and Plastic Deformation in Strained Crystalline Polymers," J. Poly. Sci. C-32, 297 (1971).

87. Peterlin, A., "Morphology and Properties of Crystalline Polymers with Fiber Structure," Textile Research J. 42, 20 (1972).

88. Peterlin, A. and Sakaoku, K., "Plastic Deformation of Nylon 6 Single Crystals and Thin Membranes," Die Makromol. Chem. 157, 131 (1972).

89. Petermann, J. and Gleiter, H., "Structure of Fibers Drawn from Polyethylene Single Crystals," J. Polymer Sci. A-2, 10, 2333 (1972).

90. Predecki, P. and Statton, W. O., "Dislocations Causes by Chain Ends in Crystalline Polymers," J. Applied Physics 37, 4053 (1966).

91. Predecki, P. and Thornton, A. W., "Observation of Deformation in Spherulitic Polyethylene," J. Applied Physics 41, 4342 (1970).

92. Price, F. P., "Spherulite Growth Rates in Polyethylene Crosslinked with High Energy Electrons," J. Physical Chem. 64, 169 (1960).

93. Price, F. P., "Kinetics of Crystallization," Encyclopedia of Polymer Sci. 8, 63 (1968).

BIBLIOGRAPHY (Continued)

94. Prime, B. R. and Wunderlick, B., "Extended Chain Crystals. III. Size Distribution of Polyethylene Crystals Grown under Elevated Pressures," J. Polymer Sci. A-2, 7, 2061 (1969).

95. Reding, F. P. and Walter, E. R., "An Electron Microscope Study of the Growth and Structure of Spherulites in Polyethylene," J. Polymer Sci. 38, 141 (1959).

96. Rogers, A. W., Techniques of Autoradiography, Elsevier Publishing Co.: New York, 1967.

97. Sakaoku, K. and Peterlin, A., "Electron Microscopy of Drawn Polypropylene," J. Polymer Sci. A-2, 9, 895 (1971).

98. Samuels, R. J., "Spherulite Structure Deformation Morphology and Mechanical Properties of Isotactic Polypropylene Fibers," J. Polymer Sci. C-20, 253 (1967).

99. Samuels, R. J., "Quantitative Structural Characterization of the Mechanical Properties of Isotactic Polypropylene," J. Macromol. Sci. B-4, 701 (1970).

100. Schonhorn, H., "Heterogeneous Nucleation of Polymer Melts on High Energy Surfaces. II. Effect of Substrate on Morphology and Wettability," Macromolecules 1, 145 (1968).

101. Schultz, J. M. and Kinlock, D. R., "Transverse Screw Dislocations: A Source of Twist in Crystalline Polymer Ribbons," Polymer 10, 271 (1969).

102. Schuur, G., "The Auto-orientation Mechanism of Crystallization," J. Poly. Sci. 50, 191 (1961).

103. Sharma, R. K. and Mandelkern, L., "The Density of Polyethylene Crystallized in the Bulk and from Dilute Solution," Macromolecules 2, 266 (1969).

104. Smith, T. L., "Fracture of Polymers in Biaxial and Triaxial Tension," Polymer Sci. Symposium 32, 269 (1971).

105. Smith, T. L., "Physical Properties of Polymers. An Introductory Discussion," Polymer Engineering and Science 13, 161 (1973).

106. Starkweather, H. W. and Brooks, R. E., "Effect of Spherulites of the Mechanical Properties of Nylon 66," J. Applied Poly. Sci. 1, 236 (1959).

BIBLIOGRAPHY (Concluded)

107. Underwood, E. E., Quantitative Stereology; Addison-Wesley Publishing Co.: Reading, Mass., 1970, p. 34.

108. Vadimsky, R. G., Keith, H. D., and Padden, F. J., "Electron Microscopic Studies of Deformation in Polyethylene," J. Polymer Sci. A-2, 17, 1367 (1969).

109. Van Amerongen, G. J., "Diffusion, Solubility, and Permeation of Various Substances," Rubber Chem. and Tech. 37, 1082 (1964).

110. Van Vlace, L. H., Elements of Materials Science, 2nd ed.; Addison-Wesley Publishing Co.: Reading, Mass., 1964, p. 60.

111. Voyutskii, S. S. and Vakula, V. L., "Effects of Self Diffusion and Inter-Diffusion in Polymer Systems," Rubber Chem. and Tech. 37, 1153 (1964).

112. Wunderlich, B. and Cormier, C. M., "Heat of Fusion of Polyethylene," J. Polymer Sci. A-2, 5, 987 (1967).

113. Zhurkov, S. N., Vettegren, V. I., Korsukov, V. E., and Novak, I. I., "Determination of Overstressed Chemical Bonds in Polymers by IR Spectroscopy," Soviet Physics - Solid State 11, 233 (1969).

114. Zhurkov, S. N., Zakrevskii, V. A., Korsukov, V. E., and Kuksenko, V. S., "Mechanism Leading to the Development of Submicroscopic Fissures in Stressed Polymers," Soviet Physics - Solid State 13, 1680 (1972).

115. Thin Sectioning and Associated Techniques for Electron Microscopy, Ivan Sorvall Inc., Norwalk, Conn., 1967.

116. Thermal Analysis Newsletters, No. 1-10, Perkin Elmer Corp., Norwalk, Conn., 1965-1972.

VITA

Roger David Hester was born September 20, 1942, in Iron City, Tennessee to Carmie L. Buttler and James L. Hester. He graduated from Coffee High School, Florence, Alabama and attended Florence University from 1960 to 1962. He received the Bachelor of Science degree in Chemical Engineering after attending Auburn University from 1962 to 1965. Upon graduation he worked as a Technical Engineer for the E. I. DuPont de Nemours and Company in Memphis, Tennessee. In 1967 he left for graduate studies at the Georgia Institute of Technology and received the Master of Science degree in Chemical Engineering there in 1968. From 1968 to 1970, he worked as a Research Engineer for E. I. DuPont de Nemours and Company in Old Hickory, Tennessee. He is a registered Professional Engineer and is a member of Tau Beta Pi, Kappa Mu Epsilon, Phi Lambda Upsilon, and Sigma Xi.